Identification of flow-relevant structural features in history matching

Kahrobaei, Siavash

Important note
To cite this publication, please use the final published version (if applicable).
Please check the document version above.

IDENTIFICATION OF FLOW-RELEVANT STRUCTURAL FEATURES IN HISTORY MATCHING

IDENTIFICATION OF FLOW-RELEVANT STRUCTURAL FEATURES IN HISTORY MATCHING

Proefschrift

ter verkrijging van de graad van doctor
aan de Technische Universiteit Delft,
op gezag van de Rector Magnificus prof. ir. K. C. A. M. Luyben,
voorzitter van het College voor Promoties,
in het openbaar te verdedigen op maandag 4 juli 2016 om 12:30 uur

door

Siavash KAHROBAEI

Master of Science in Applied Earth Sciences,
Delft University of Technology
geboren te Tehran, Iran.

Dit proefschrift is goedgekeurd door de promotor:

Prof. dr. ir. J. D. Jansen
Prof. dr. ir. P. M. J. Van den Hof

Samenstelling promotiecommissie:

Rector Magnificus,	voorzitter
Prof. dr. ir. J. D. Jansen,	Technische Universiteit Delft, promotor
Prof. dr. ir. P. M. J. Van den Hof,	Technische Universiteit Eindhoven, promotor

Onafhankelijke leden:

Prof. dr. ir. A. W. Heemink,	Technische Universiteit Delft,
Prof. dr. ir. S. Weiland,	Technische Universiteit Eindhoven,
Prof. dr. ir. P. L. J. Zitha,	Technische Universiteit Delft,
Dr. ir. S. C. Steele-Dunne,	Technische Universiteit Delft,
Dr. ir. G. M. van Essen,	Shell Global Solutions,
Prof. dr. ir. W. R. Rossen,	Technische Universiteit Delft, reservelid.

To

Nina

and

Ali & Maryam

CONTENTS

LIST OF FIGURES

1

INTRODUCTION

P OROUS rock formations below the earth surface, in some instances, contain oil or natural gas or a combination of both along with water. Such rock formations are called oil or gas reservoirs and are typically several meters thick and several square kilometers wide. Visualization of these rock formations is impossible thus knowledge about the structure and properties of such extensive formations is very limited. Traditionally exploitation of such reservoirs is done through a system of wells which are drilled into the reservoir. Information obtained from these wells is used to develop knowledge about the reservoir formation. Usually, due to economic viability the number of wells drilled into any formation is few and these wells are sparsely spaced. Thus information from such a system of wells is at best very 'local' in nature, hence very little or no information is known about the properties of the reservoir between the wells with any degree of certainty. This lack of knowledge is, by consequence, transferred to the models generated to represent these reservoir formations. As a result of this the reservoir models produce responses which are often inaccurate or not comparable to the responses obtained from the real reservoir. With the advent of technologies it is now technologically and economically feasible to accurately measure and monitor the responses, e.g. phase rates, from a system of wells. Integration of these dynamic responses into the model by adjusting the uncertain model parameters so as to minimize the mismatch between the model responses and actual field measurements is a well-considered inverse problem, called 'history matching' in the petroleum engineering world and 'data assimilation' in the weather forecasting community. In essence the objective of history matching is to employ measurement data to improve knowledge about the model properties so as to enhance the predictability of a model to accurately forecast the production response of a real reservoir.

1

1.1. HISTORY MATCHING

History matching is the process of conditioning reservoir models to the available field observations, such as pressure data, production data, time-lapse seismic data, etc., by adjusting model parameters. The most common data type for history matching is production data, which is a time series of measurements of flow rate or pressure from production or injection wells. The production data has some characteristics that make the history matching more challenging than other inverse problems (Oliver and Chen, 2011):

1. These observations are made at a limited number well locations.

2. The measurements can be repeated frequently, which can result in a large amount of data for a field, but its information content is often relatively low.

3. The relationships between the observed data and the model parameters are generally nonlinear.

Traditionally history matching is performed manually on upscaled reservoir models by adjusting parameters using a trial and error method. Subsequently, manual history matching can be involved with personal judgment and bias, which can result in artificial discontinuities with no geological realism (Datta-Gupta and King, 2007). As an alternative computer-assisted history matching techniques can be used to reduce human bias and judgments. These techniques aim to minimize a predefined mismatch objective function to update the parameters of a numerical model such that the simulated response is more accurate compared with observed data and hopefully gives better predictions of the future system response. Among the different algorithms available to solve this parameter estimation problem, gradient-based optimization is considered to be an efficient method; see Oliver et al. (2008). In this method gradients of the mismatch objective function with respect to the uncertain parameters are calculated. Methods that use numerical gradients, e.g. finite difference gradients, are easy to implement but are computationally inefficient, especially since the number of model parameters is usually in the order of magnitude of 10^6 to 10^8. On the other hand, methods that use analytical gradients are computationally more beneficial. Adjoint-based gradient calculation requires a single forward simulation in conjunction with a single backward simulation to calculate the gradient of any objective function. Thus the gradient calculated with the adjoint technique is independent of the number of optimization variables and the adjoint technique is therefore computationally the most efficient method to solve high-dimensional optimization problems.

1.2. ILL-POSEDNESS OF HISTORY MATCHING PROBLEMS

History matching problems are almost always ill-posed due to the large number of uncertain parameters and limited available observed data (Oliver et al., 2008; Shah et al., 1978). This ill-posedness results in many possible combinations of reservoir parameters, which result in equally good matches to the historical data but may provide different forecasts. A classic way to restore well-posedness is regularization through introducing additional information. This can be done by, e.g., specifying a strong spatial correlation,

zonation, expansion of parameters in terms of a limited number of basis functions, penalizing deviations from a prior model, or a combination of these methods. Penalizing deviations from a prior model forms a natural consequence of applying a Bayesian approach to updating an uncertain prior, using uncertain data, to obtain a less uncertain posterior (Oliver et al., 2008; Tarantola, 2005). The penalty term makes the problem well-posed, restricts the parameter updates to values that keep the posterior values not too far from the prior values, and generally increases the smoothness of the results. Krymskaya et al. (2010) have shown that the information content of the updated model comes mostly from a priori knowledge and to a much lesser extent from the observations.

1.3. UNDER-MODELLING OR UNKNOWN UNKNOWNS

Geo-modeling is the process of populating a reservoir model with properties such as permeabilities, porosities etc., which is a highly uncertain procedure. The uncertainty arises from a lack of knowledge about the reservoir and many times, more importantly, from interpretations of uncertain data sources such as seismic, well logs, core data, etc. Interpretation of any data source is always subject to uncertainty and creativity which can lead to significant bias in the model descriptions. This uncertainty is propagated through a set of models used during the development phase of an oil field. Thus unexpected flow-relevant features that are not captured in the reservoir model may be present in reality. This is known as 'under-modeling'. In such scenarios penalizing deviations from a prior model can be undesirable since it leads to solutions that stay close to the prior. Therefore if a feature is missing in the prior there is almost no chance to capture it since the updated parameters are constrained by incorrect prior knowledge that usually originates from interpretation errors of geological data. On the other hand, attempts to estimate all uncertain parameters from production data without regularization typically lead to very high or low parameter values that have little or no geological realism. Joosten et al. (2011) introduced the 'model maturation' concept and showed through a set of numerical experiments that unrealistic parameter values may have added value. In this thesis we focus on the application of unregularized history matching in finding 'unknown unknowns' and on investigating the theoretical aspects of such unrealistic parameter updates.

1.4. RESEARCH OBJECTIVES

In this thesis we want to show that unregularized history matching may sometimes be used to improve our understanding about the reservoir by identifying problematic areas in the reservoir models or be seen as a way to correct for incorrect interpretations of geological data. In a wider perspective, it is crucial to determine why and under which conditions there is relevant information hidden in the results of unregularized ill-posed inverse problems, since the unrealistic parameter updates can be also caused by the ill-posed nature of the problem. For example if the unrealistic parameters arise in a location or a direction, which does not have a significant influence on the flow in a reservoir it is not reliable to be used as an indicator for under-modelling. Therefore it is essential to investigate the effect of different flow- relevant features on dynamic behaviour of a reservoir such that we can rely on unrealistic parameter updates to indicate problematic

1

areas of our existing reservoir models. Therefore, the main objectives of this research is to

"Investigate the relevant information in the dynamic response of a reservoir system and the possibility of identification of unexpected flow-relevant features that are not captured in the ensemble of prior reservoir models."

For this purpose we will

- Extend the work of Van Essen et al. (2010) to investigate the effect of ill-posedness of history-matched models on reservoir performance prediction.

- Investigate the possibility of model deficiency detection during unregularized parameter updating of subsurface reservoir models.

- Investigate the identifiability of location and magnitude of flow barriers in slightly compressible flow using dynamic data.

- Investigate the possibility of updating of static parameters (structural models) using dynamic data (production and time-lapse seismic data) in a 'big loop' approach, in which parameter updates are performed in the static model in an integrated reservoir modeling workflow.

1.5. THESIS OUTLINE
Below is an executive summary of the different chapters included within this thesis.

1.5.1. EFFECT OF ILL-POSEDNESS OF HISTORY-MATCHED MODELS ON PRODUCTION PREDICTIONS: CHAPTER 2
The main goal of history matching is to produce reservoir models that predict future reservoir performance with more confidence. Ill-posedness of history matching problems can result in many possible reservoir models that produce the same history but different forecast. Van Essen et al. (2010) have proposed a method to determine lower and upper bounds on the predicted production or any other economic objective from history-matched reservoir models through a hierarchical optimization procedure. In this thesis we apply this method to a more realistic reservoir to investigate the effect of ill-posedness of history-matched models on predicted reservoir performance. Moreover, we investigate how this method can be used to indicate the added value of alternative data sources such as time-lapse seismic.

1.5.2. UNDER-MODELING DETECTION: CHAPTER 3
Presence of significant flow-relevant features, e.g. faults or high permeable channels, can strongly affect the dynamic behavior of a reservoir. Therefore, in the case of 'under-modeling', when these features are not captured in the prior, constraining the parameter updates to the prior information is unfavorable. In such a scenario integration of dynamic data without any constraint may help us to detect these flow-relevant features. In this chapter we investigate under which conditions there may be relevant information

hidden in the results of unregularized ill-posed inverse problems by conducting several numerical twin experiments. Moreover to investigate the findings of these numerical experiments, we perform a quantitative identifiability analysis of the examples using the SVD of a dimensionless output sensitivity matrix.

1.5.3. IDENTIFIABILITY OF FLOW-RELEVANT FEATURES: CHAPTER 4

Due to the ill-posedness of history matching problems it is essential to understand which parameters can be estimated with reasonable accuracy from the available data. It is well-known that in incompressible flow only averaged properties of a reservoir can be estimated from production data. On the other hand, from a systems and control theory perspective, the transient response of a dynamic system contains information about dynamics-related properties of a system. Consequently, including compressibility effects (leading to a transient response) can result in a more accurate reservoir parameter estimation than just considering the steady-state response. However certain parameters have a more significant effect on this transient response. Consequently, by investigating the effect of different parameters on the dynamic behavior we can understand which parameters are more identifiable from the available data. On the other hand, the presence of noise in the data may reduce the identifiability of such parameters and can result in unrealistic parameter estimates. Hence, it is important to also investigate the effect of noise on the identifiability of different parameters. In this chapter we extend the classic analysis by including compressibility effects and use two approaches to investigate the identifiability of location and magnitude of flow barriers:

1. A twin-experiment with synthetic production data for use with a time-domain parameter estimation technique,

2. A transfer function formalism in the form of bilaterally coupled four-ports allowing for an analysis in the frequency domain.

Using semi-analytical solutions based on the transfer function formalism we are able to visualize the objective function space and also to investigate the (structural) identifiability of different parameters. These theoretical results appear to support the empirical findings of the second chapter of this thesis, where we have shown that unregularized gradient-based history matching in reservoir models occasionally leads to useful results in the form of model parameter updates having unrealistic magnitudes but indicating the correct location of model deficiencies.

1.5.4. STRUCTURAL MODEL UPDATING USING DYNAMIC DATA: CHAPTER 5

Another source of unfavorable history matching results could result from addressing a wrong uncertainty in the parameter estimation process. In traditional history matching only gridblock parameters are considered to be uncertain, and adjusted to reproduce historical dynamic behavior of a reservoir, while structural parameters of the reservoir model are usually fixed during this process. However the actual uncertainty could be in structural reservoir parameters, such as reservoir thicknesses. This often leads to unlikely or even unfeasible property updates and possibly to a poor predictive capability

1

of the model. In those cases it may be expected that updating of the structural parameters will improve the quality of the history match. In this chapter we use a gradient-based history matching method to update structural properties of the static model using a 'Big Loop' workflow. In the Big Loop workflow the static model and dynamic model are coupled, such that dynamic outcomes can be used to improve the static model. Subsequently, this improved static model is used to improve the dynamic simulation and economic evaluations. The method is tested on a 3D synthetic model, where time-lapse seismic data as well as production data have been used to update the depth of the reservoir's bottom horizon.

2

EFFECT OF ILL-POSEDNESS OF HISTORY-MATCHED MODELS ON PRODUCTION PREDICTIONS

THE main goal of history matching is to produce reservoir models, which predict future reservoir performance with more confidence. Ill-posedness of history matching problems can result in many possible reservoir models which produced the same history but different forecast. Van Essen et al. (2010) proposed a method to determine lower and upper bounds to the predicted production or any other economic objective from history-matched reservoir models. The method consists of two steps: 1) Performing a traditional computer-assisted history match of a reservoir model with the objective to minimize the mismatch between predicted and observed production data through adjusting the grid block permeability values of the model. 2) Performing two optimization exercises to minimize and maximize an economic objective over the remaining field life, for a fixed production strategy, by manipulating the same grid block permeabilities, however without significantly changing the mismatch obtained under step 1. This is accomplished through a hierarchical optimization procedure that limits the solution space of a secondary optimization problem to the (approximate) null-space of the primary optimization problem. We apply this method to a more realistic reservoir to investigate the effect of ill-posedness of history-matched models on predicted reservoir performance. We also investigated how this method can be used as a means to assess the cost effectiveness of acquiring different data types to reduce the uncertainty in the expected NPV.

2

2.1. INTRODUCTION

It is well-known that assimilation of production data into reservoir models is an ill-posed problem; see e.g. Watson et al. (1984), Tavassoli et al. (2004) or Oliver et al. (2008). This is mainly because generally the number of uncertain model parameters largely supersedes the number of measurements. Moreover, the measurements are strongly correlated because they originate from a relatively small number of sources: the wells. As a result, they contain less information about the true value of the model parameters than could be expected based solely on the number of data points. A relevant question in view of the purpose of large-scale, physics-based reservoir models is how much the long-term predictions can vary because of the ill-posedness of the assimilation problem. In other words, what may be the economic consequences of the lack of information about the reservoir in the measurements? In most practical circumstances, this question is addressed by constructing and history-matching low and high case models, besides the nominal model. Alternatively, a set of model realizations can be used in a data-assimilation algorithm to obtain an entire collection of predictions, as is the case with ensemble Kalman filter (EnKF) methods, see, e.g., Evensen (2009) and Aanonsen et al. (2009) . However, in either way the resulting history-matched models are heavily influenced by the prior information that went into the data-assimilation process. Hence, properly answering the question stated above requires either some (heuristic) method to translate static geological properties to flow behavior or economic performance, or requires many forward simulation runs to obtain a proper low or high case prior model. These methods may be either unreliable or impractical to provide a good measure of the economic consequences of the lack of knowledge about the true field. In this chapter a method introduced by Van Essen et al. (2010) is used to search for lower and upper bounds on predicted production (or any other economic objective) over the remaining life of a field, using a history-matched model. The method consists of two steps: 1) Performing a traditional computer-assisted history match of a reservoir model with the objective to minimize the mismatch between predicted and observed production data through adjusting the permeability values of the model. 2) Performing two optimization exercises to minimize and maximize an economic objective over the remaining field life, for a fixed production strategy, by manipulating the same grid block permeabilities, however without significantly changing the mismatch obtained under step 1. To achieve this we make use of the fact that history matching through adjusting grid block parameters is an ill-posed problem such that many combinations of parameter values may result in (nearly) identical mismatch values.

2.2. PROBLEM DEFINITION

The problem of determining a history-matched model that provides either a lower or an upper bound on the predicted economic performance over the life of a reservoir is essentially a multi-objective optimization problem. For a general overview of multi-objective optimization, see, e.g., Marler and Arora (2004). The first objective is to find a certain realization of model parameters that minimizes the error between the measured and simulated production data, which can be expressed through a quantitative objective function J, e.g. mean square difference. The second objective relates to finding a

set of parameter values that – for a certain future production strategy – minimizes or maximizes some economic cost function V, e.g. net present value (NPV). However, the multiple objectives are not of the same importance; priority lies with obtaining a good history-match, while determining a lower or upper bound on predicted economic performance serves as secondary objective. To that end, the multi-objective optimization problem may be cast into a hierarchical optimization problem, as presented in Haimes and Li (1988) and more recently specifically for oil production optimization in Van Essen et al. (2011), Chen et al. (2012) and Fonseca et al. (2014). In this structure, optimization of a (secondary) economic cost function V is constrained by the requirement that the (primary) quantitative history-matching cost function J must remain close to its minimal value $J_{\min}$. This requires solving the following two (hierarchical) optimization problems,

$$J_{\min} \overset{\Delta}{=} \min_{\mathbf{m}} J(\mathbf{m}, \bar{\mathbf{u}}), \tag{2.1}$$

$$s.t. \quad \mathbf{g}_{k+1}(\bar{\mathbf{u}}_k, \mathbf{x}_k, \mathbf{x}_{k+1}, \mathbf{m}) = \mathbf{0}, \quad k = 0, \ldots, K-1, \quad \mathbf{x}_0 = \bar{\mathbf{x}}_0, \tag{2.2}$$

$$\mathbf{c}_{k+1}(\bar{\mathbf{u}}_{k+1}, \mathbf{x}_{k+1}, \mathbf{m}) \leq \mathbf{0}, \tag{2.3}$$

and

$$\max_{\mathbf{m}} V(\mathbf{m}, \bar{\mathbf{u}}) \quad \text{or} \quad \min_{\mathbf{m}} V(\mathbf{m}, \bar{\mathbf{u}}), \tag{2.4}$$

$$s.t. \quad \mathbf{g}_{k+1}(\bar{\mathbf{u}}_k, \mathbf{x}_k, \mathbf{x}_{k+1}, \mathbf{m}) = \mathbf{0}, \quad k = 0, \ldots, K-1, \quad \mathbf{x}_0 = \bar{\mathbf{x}}_0, \tag{2.5}$$

$$\mathbf{c}_{k+1}(\bar{\mathbf{u}}_{k+1}, \mathbf{x}_{k+1}, \mathbf{m}) \leq \mathbf{0}, \tag{2.6}$$

$$J(\mathbf{m}) - J_{\min} \leq \varepsilon, \tag{2.7}$$

where $\bar{\mathbf{u}}$ is the fixed control vector (input vector), $\mathbf{x}$ is the state vector (typically grid block pressures and saturations), $\mathbf{g}$ is a vector-valued function that represents the system equations, $\mathbf{x}_0$ is a vector of the initial conditions of the reservoir, the subscript k indicates discrete time, and K is the total number of time steps. The vector of inequality constraints $\mathbf{c}$ relates to the capacity limitations of the wells. The term ε is an arbitrary small value compared to $J_{\min}$. In order to solve the secondary optimization problem, given in equation (2.4) to equation (2.7), first a (single) optimal solution to the primary optimization problem equation (2.1) to equation (2.3) is required to determine $J_{\min}$. The optimal solution to the primary problem $\mathbf{m}_1^*$ can serve as feasible initial guess for the secondary problem. Note that the second optimization problem is also solved in terms of $\mathbf{m}$, while the values of the control $\bar{\mathbf{u}}$ remain unchanged. The search space of the secondary problem is constrained by the null-space of the primary objective function at a value of $J_{\min}$, through inequality constraint equation (2.7). In other words, the redundant degrees of freedom (DOF) of the primary problem are the DOF of the secondary problem. The motivation for using the constraint equation (2.7) is actually twofold. If ε is arbitrarily small (or even equal to 0) the parameter space that remains is actually the null space within the parameter space, which can be substantial because of the generally

ill-posed nature of the inverse history-matching problem. Any changes of the model parameters within that null-space will have no effect on the value of the used quantitative history-match quality indicator, i.e. the objective function J. For $\varepsilon > 0$ the corresponding parameter space that satisfies equation (2.7) can be given the interpretation of a parameter uncertainty set, with a clear statistical interpretation, in the case of Gaussian noise disturbances on the data. The statistical uncertainty set then results from a hypothesis test based on the so-called likelihood ratio test, and is characterized by level sets of the likelihood function $J(\mathbf{m})$. See e.g. Quinn et al. (2005) for the case of nonlinear models, and den Dekker et al. (2008) for linear models. This implies that under appropriate noise conditions, we can, for every value of $\varepsilon > 0$, connect a probability level to the parameter uncertainty set defined by equation (2.7), and thus account for the variability of the history-matched parameters in the subsequent secondary economic optimization problem.

2.3. METHODOLOGY

In Van Essen et al. (2011), the primary optimization problem is attacked using a gradient-based search algorithm. (Note that in that study the optimization variables were the inputs u, while here they are the model parameters $\mathbf{m}$.) The gradients are obtained using a system of adjoint equations which is solved backwards in time once, regardless of the number of optimization parameters (see Jansen (2011) for an overview of adjoint-based optimization in porous media flow, and Kraaijevanger et al. (2007) for the specific implementation used in this study.). Subsequently, the secondary optimization problem was also attacked using a gradient-based search algorithm. However, the secondary problem was executed with the addition of projecting the search direction onto a second-order approximation of the null-space with respect to the optimality constraint defined in equation (2.7). The second-order approximation was explicitly determined through a forward difference scheme using first-order information obtained with the adjoint. Unfortunately, using this approach the number of forward and backward simulations is proportional to the number of optimization parameters. Hence, for the assimilation of production data this method is in most cases computationally infeasible. In Van Essen et al. (2011), also an alternative method is introduced to solve the hierarchical optimization problem without explicitly calculating the null-space with respect to equation (2.7). It uses an 'on-off' type weighted objective function with weighting functions Ω_1 and Ω_2:

$$W = \Omega_1(J) \cdot J + \Omega_2(J) \cdot V, \tag{2.8}$$

where Ω_1 and Ω_2 are 'switching' functions of J and V that take on values of 1 and 0 ('on' and 'off') or vice versa,

$$\Omega_1(J) = \begin{cases} 1 & \text{if } J - J_{\min} > \varepsilon \\ 0 & \text{if } J - J_{\min} \leq \varepsilon \end{cases} , \qquad \Omega_2(J) = \begin{cases} 0 & \text{if } J - J_{\min} > \varepsilon \\ 1 & \text{if } J - J_{\min} \leq \varepsilon \end{cases} , \tag{2.9}$$

here, ε is the threshold value as defined in inequality constraint equation (2.7). The gradients of W with respect to the model parameters $\mathbf{m}$ for iteration $n+1$ is then simply,

$$\left. \frac{\partial W}{\partial \mathbf{m}} \right|_{n+1} = \Omega_1(J_n) \cdot \left. \frac{\partial J}{\partial \mathbf{m}} \right|_{n+1} + \Omega_2(J_n) \cdot \left. \frac{\partial V}{\partial \mathbf{m}} \right|_{n+1}. \tag{2.10}$$

Solving the secondary optimization problem sequentially, using W as defined in equation (2.8), gives improving directions for either V or J. With each iteration, the value of V either increases while the value of J decreases or the other way around, as the solution moves to and from the feasible region with respect to inequality constraint equation (2.7). If there exist redundant DOF with respect to the primary problem, improvement of V is possible while satisfying equation (2.7) and convergence of the hierarchical optimization will occur in a 'zig-zag' fashion, as schematically represented in Figure 2.1.
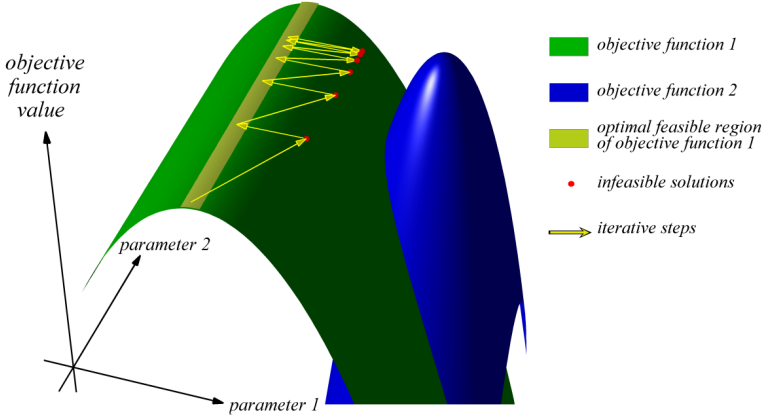
Figure 2.1: Schematic representation of the iterative process of solving a hierarchical optimization problem using a weighted objective function, as described by equation (2.8). The process converges towards a final solution in a zigzag-fashion, moving into and out of the feasible region bounded by the optimal solutions of the primary objective function. (After Van Essen et al. 2011).

To improve convergence speed, as presented above and in Van Essen et al. (2011), a small adaptation to the switching algorithm can be made. By projecting the gradients of secondary objective function V onto the first-order approximation of the null-space of the primary objective function J, the resulting update of $\mathbf{m}$ will keep J closer to $J_{\min}$. Mathematically this becomes,

$$\frac{\partial \tilde{V}}{\partial \mathbf{m}} = \frac{\partial V}{\partial \mathbf{m}} \mathbf{P}_\perp = \frac{\partial V}{\partial \mathbf{m}} \left(\mathbf{I} - \mathbf{P}_{||} \right) = \frac{\partial V}{\partial \mathbf{m}} \left(\mathbf{I} - \frac{\frac{\partial J}{\partial \mathbf{m}}^T \frac{\partial J}{\partial \mathbf{m}}}{\frac{\partial J}{\partial \mathbf{m}} \frac{\partial J}{\partial \mathbf{m}}^T} \right), \tag{2.11}$$

where we use the convention that the derivative of a scalar with respect to a vector is a row vector. $\mathbf{P}_{||}$ is a matrix that projects $\partial V/\partial \mathbf{m}$ on $\partial J/\partial \mathbf{m}$ and $(\partial V/\partial \mathbf{m})\mathbf{P}_\perp$ is the orthogonally complementary projection which ensures that the step towards the secondary objective function is taken in a direction (near-)parallel to the 'ridge' in the primary objective function. Inserting equation (2.11) in equation (2.8) gives an alternative switching search direction $\mathbf{d}$ for solving the hierarchical optimization problem,

$$\mathbf{d}_{n+1} = \Omega_1 \left(J_n \right) \cdot \left. \frac{\partial J}{\partial \mathbf{m}} \right|_{n+1} + \Omega_2 \left(J_n \right) \cdot \left. \frac{\partial V}{\partial \mathbf{m}} \right|_{n+1} \left(\mathbf{I} - \frac{\left. \frac{\partial J}{\partial \mathbf{m}} \right|_{n+1}^T \left. \frac{\partial J}{\partial \mathbf{m}} \right|_{n+1}}{\left. \frac{\partial J}{\partial \mathbf{m}} \right|_{n+1} \left. \frac{\partial J}{\partial \mathbf{m}} \right|_{n+1}^T} \right). \tag{2.12}$$

The switching algorithm using the projected gradient $\mathbf{d}$ was used in the following example to illustrate the performance of the method.

2.4. PRIMARY AND SECONDARY OBJECTIVE FUNCTIONS

Two different reservoir models are used in this chapter with the goal of determining lower and upper bounds on the expected economic performance over the remaining life of the field by changing the permeability field, while the model stays compliant with historic data over the history matching period. Consequently the primary objective function, $J(\mathbf{m})$, is defined as data mismatch between observations and simulated data:

$$J(\mathbf{m}) = (\mathbf{d} - \mathbf{h}(\mathbf{m}))^T \mathbf{P}_d^{-1}(\mathbf{d} - \mathbf{h}(\mathbf{m})), \tag{2.13}$$

where $\mathbf{m}$ is a vector of unknown model parameters, $\mathbf{d}$ is a vector of data (measurements), $\mathbf{h}$ is a vector valued-function that relates the model parameters to the model outputs (i.e. the simulated data), and $\mathbf{P}_d$ is a covariance matrix of data errors.

The secondary objective function, V, is of an economic type, generally NPV,

$$V = \sum_{k=1}^{K}\left(\frac{\sum_{j=1}^{N_{prod}}\left[r_{wp}\cdot\left(y_{wp,j}\right)_k + r_o\cdot\left(y_{o,j}\right)_k\right] - \sum_{j=1}^{N_{inj}}\left[r_{wi}\cdot\left(y_{wi,j}\right)_k\right]}{(1+b)^{\frac{t_k}{\tau_t}}}\Delta t_k\right), \tag{2.14}$$

where $y_{wp,j}$ is the water production rate of well j, $y_{o,j}$ is the oil production rate of well j, $y_{wi,j}$ is the water injection rate of well j, r_{wi}, r_{wp} and r_o are water injection costs, water production costs and oil revenue respectively, Δt_k is the time interval of time step k in days, b is the discount rate for a reference time τ_t, and N_{inj} and N_{prod} are the number of injection and production wells.

2.5. EGG MODEL EXAMPLE

In this example, we consider a three-dimensional oil reservoir model, introduced in Van Essen et al. (2009). The reservoir model consists of 18,553 active grid blocks, as depicted in Figure 2.2, and has dimensions of 480 × 480 × 28 m. Its geological structure involves a network of fossilized meandering channels of high permeability. The average reservoir pressure is 40.0 MPa. All remaining geological and fluid properties used in this example are presented in Table 2.1. The reservoir model contains eight injection wells and four production wells. The near-wellbore flow is modeled using a Peaceman well model.
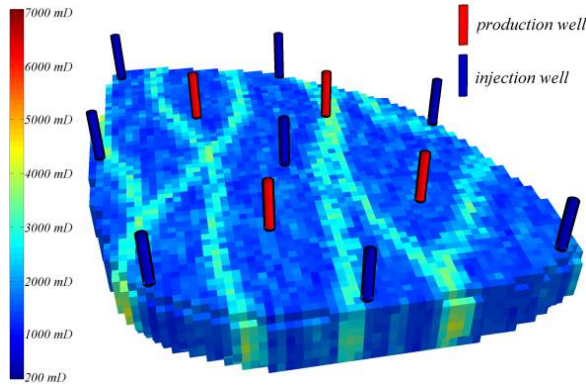
Figure 2.2: Three-dimensional oil reservoir model with eight injection and four production wells, after Van Essen et al., 2009. Its geological structure involves a network of fossilized meandering channels of high permeability in a low-permeability background.

Table 2.1: Geological and fluid properties for the example

Variable	Parameters	Value	Unit
φ	Porosity	0.2	-
ρ_o	Oil density	800	Kg/m^3
ρ_w	Water density	1000	Kg/m^3
c_o	Oil compressibility	1×10^{-10}	1/Pa
c_w	Water compressibility	1×10^{-10}	1/Pa
μ_o	Dynamic oil viscosity	5×10^{-3}	Pa.s
μ_w	Dynamic water viscosity	1×10^{-3}	Pa.s
p_c	Capillary pressure	0	Pa

During the first 1.5 years of production from the reservoir, the bottomhole pressures of the producers are kept at a constant value of 39.5 MPa. During that time, the injection rates of all eight injectors are prescribed to fluctuate monthly with a uniform probability distribution around an average value of 5.52×10^{-4} m^3/s (300 bbl/day) and a maximal offset $\pm 9.2 \times 10^{-4}$ m^3/s (50 bbl/day). Monthly production measurements are taken of the flowing bottomhole pressures of the eight injectors and the oil and water rates of the four producers, on top of which no noise is superimposed. Thus, the total number of measurements is 288.

In this example historic data are available over the first 1.5 years of production and lower and upper bounds on expected economic performance are determined over the remaining life of the field – from 1.5 to 6.0 years – by changing model properties (gridblock permeabilities), while the model stays compliant with historic data over the first 1.5 years of production. In this example the water injection costs r_{wi}, the water production costs

2

r_{wp} and the oil revenue r_o are assumed constant at values of 0 \$/m^3, -1 \$/m^3 and 9 \$/m^3 respectively. The discount rate, b, in this example is zero. The upper and lower bounds of the NPV can only be determined for a given (fixed) control strategy. In this example, a reactive control approach is used that is evaluated on a field level. All injection wells are assumed to continuously operate on their average injection rate of $5.52 \times 10 - 4$ m^3/s and the production wells on their fixed bottomhole pressure of 39.5 MPa. The instant that the field watercut exceeds 0.90, all wells are shut-in. Note that this threshold is related to the ratio between oil revenue r_o and water production costs r_{wp}. To determine the history-matched models that provide the lower and upper bound on NPV for the remaining producing life, two hierarchical optimization procedures are initiated. They terminate when the feasible updates no longer result in a significant change in NPV. Figure 2.3 depicts the measured production data, along with the simulated production data originating from the final lower and upper bound model, resulting from the hierarchical optimization method. It shows that the errors between measured and simulated bottomhole pressures of the injectors and fractional flow rates of the producers are very small for both the lower and upper bound models. Thus, the condition that the updated models maintain a good history match is met. However, in Figure 2.4 it can be observed that the permeability fields of both models are quite different. These differences have a large impact on the predicted production data given the assumed reactive production strategy, as can be observed in Figure 2.5. Moreover the change in permeability in the near-well areas around the injectors has a strong effect on the pressure response of the injectors. Finally, Figure 2.6 shows the actual lower and upper bounds on predicted NPV over time, in terms of NPV for the entire producing reservoir life (6 years), and in terms of incremental NPV for just the remaining (future) producing reservoir life (4.5 years). It can be observed that the upper and lower bounds of the incremental NPV are 63% above and below their average value.
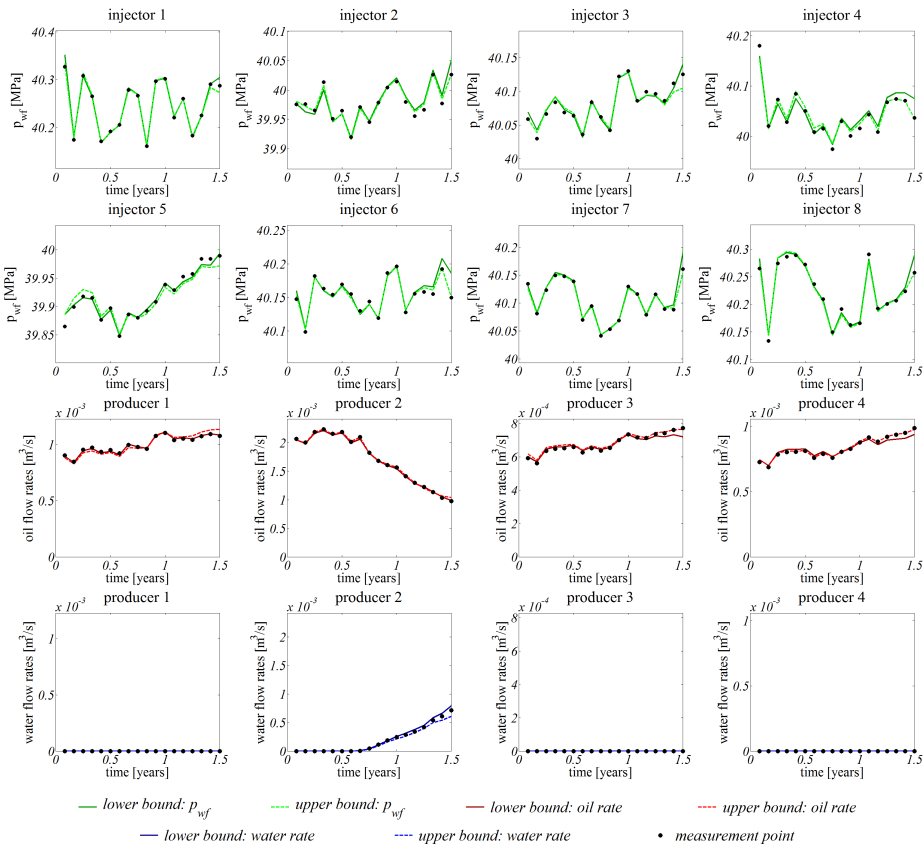
Figure 2.3: Measured production data of the first 1.5 years of production from the (synthetic) 3D reservoir, along with the simulated production data originating from the lower and upper bound models.
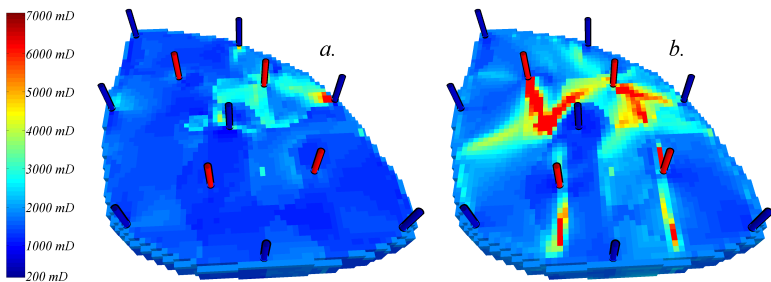
Figure 2.4: Permeability fields of the lower bound 3D reservoir model (a) and upper bound 3D reservoir model (b) determined after the first 1.5 years of production.
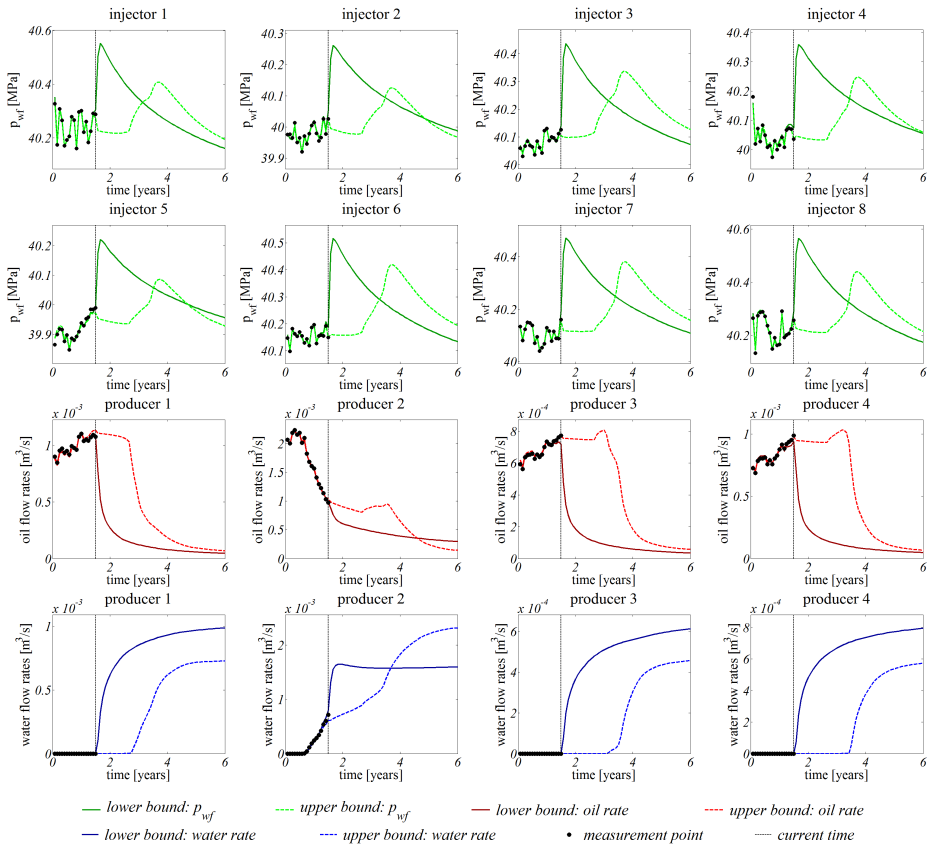
Figure 2.5: Measured production data of first 1.5 years of production from the (synthetic) 3D reservoir, along with the simulated production data for the remaining 4.5 years of production until the end of the field's life, originating from the lower and upper bound models.
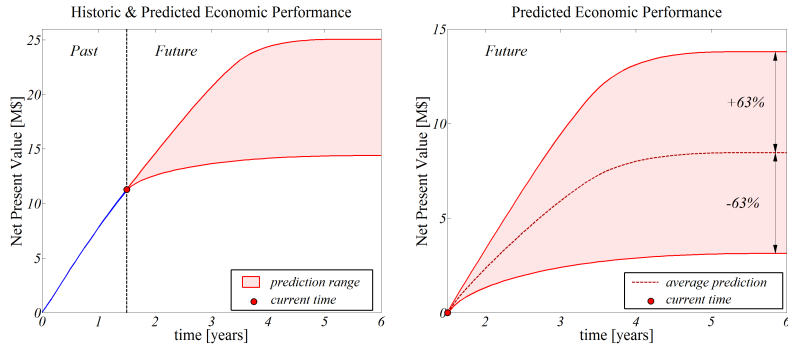
Figure 2.6: NPV over time for the lower and upper bound reservoir models. The plot on the left shows both the historic (first 1.5 year) and future (from 1.5 to 6 years) increase in NPV over time. The plot on the right side only shows the incremental NPV for the remaining (future) 4.5 years of production.

2.6. BRUGGE MODEL EXAMPLE

In the second experiment we use data from the Brugge benchmark workshop organized in 2009 (Peters et al., 2010, 2013). In the original bench mark study, the 'truth' case used to generate the data was not disclosed and therefore, in this work we use a new 'truth' honouring all well logs, geological descriptions distributions of geological model parameters, porosity/permeability relations and the geological structure of the Brugge field. Figure 2.7 depicts the new 'true' Brugge permeability field, which is used to generate synthetic data. Blue and red bars in Figure 2.7 represent injectors and producers respectively. The fluid properties and Corey exponents used in this example are given in Table 2.2.
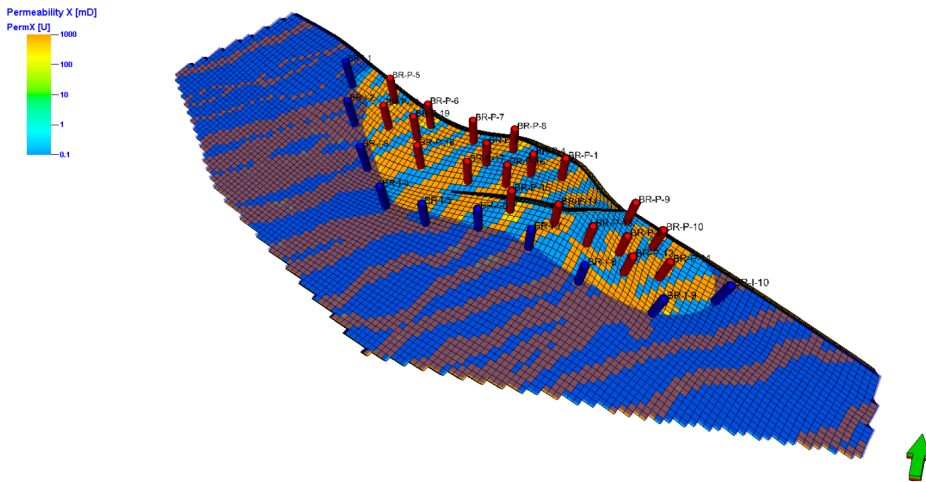
Figure 2.7: Permeability field with 11 injection wells and 20 production wells. The blue surface indicates the oil-water contact.

The reservoir model consists of 60,048 active grid blocks, and has dimensions of 3 km ×10 km×80 m. It contains 11 injection wells located near the rim of the oil-water contact at a depth of 1678 m from the surface and 20 production wells, as depicted in Figure 2.7. Wells are located in the grid block centers, and we use a standard Peaceman well inflow model. During the first 10 years of production (the history matching period) all production wells are constrained to a minimum pressure of 4.9 MPa and a maximum liquid rate of 3.7×10^{-3} m^3/s and all injection wells operate at a constant water flow rate of 7.4×10^{-3} m^3/s. Moreover, production wells are shut-in individually if the water fraction in the produced liquid is above 90%. After the history matching period (10 years), closed wells are reopened. Wells are drilled according to the time scheme presented in the Brugge workshop (Peters, et al., 2009).

2.6.1. HISTORICAL DATA

In this example historical data are available over the first 10 years of production and lower and upper bounds on expected economic performance are determined over the remaining life of the field – from 10 to 30 years – by changing the permeability field,

2

Table 2.2: Fluid properties and Corey exponents for the Brugge field example.

Variable	Parameters	Value	Unit
ρ_o	Oil density	897	Kg/m^3
ρ_w	Water density	1000	Kg/m^3
c_o	Oil compressibility	10.3×10^{-10}	1/Pa
c_w	Water compressibility	4.35×10^{-10}	1/Pa
μ_o	Oil viscosity	1.29×10^{-3}	Pa.s
μ_w	Water viscosity	0.32×10^{-3}	Pa.s
S_{wc}	Connate water saturation	0.266	-
S_{or}	Residual oil saturation	0.15	-
k_{rw}^0	End point water rel perm	0.6	-
k_{ro}^0	End point oil rel perm	0.4	-
n_w	Water Corey exponent	3	-
n_o	Oil Corey exponent	5	-

while the model stays compliant with historic data over the first 10 years of production. Time-lapse seismic data as well as production data are used as historic data. Production data consist of periodic measurements of water and oil rates in the producers. Independent measurement errors are generated from Gaussian distributions with zero mean and standard deviations equal to 10% percent of the original measurements. Negative production rates, after the addition of noise, are reset to zero. Because the measurement errors are independent, the error covariance matrix is diagonal.

2.6.2. MULTI-OBJECTIVE OPTIMIZATION SETTINGS

Using equation (2.13) as the primary objective function and equation (2.14) as the secondary objective function two hierarchical optimization procedures are conducted to determine the history-matched models that provide the lower and upper bounds on NPV for the remaining producing life. The procedures are terminated when the feasible updates no longer result in a significant changes in objective function value. The starting point for the assisted history matching process (primary objective function) is selected randomly out of 104 available prior models in the Brugge data set. The prior model is iteratively conditioned to historical data by adjusting the horizontal gridblock permeability values. In this experiment the water injection cost r_{wi}, the water production cost r_{wp} and the oil revenue r_o are assumed constant at values of 5 \$/bbl, -5 \$/bbl and 80 \$/bbl respectively. The discount rate, b, is set to 10%.

2.6.3. RESULTS: HISTORY MATCHING BASED ON PRODUCTION DATA

In this example, history matching is performed based on production data. We constrain the search space of the secondary problem by choosing the threshold value of equation (2.7) as 0.5% of the minimum of the primary objective function.

Figure 2.8 depicts the historical data and the lower and upper bounds of water produc-

tion in the first eight producers as an example of the typical ranges of the bounds. The history matching and forecasting periods are separated by a dashed line. Blue and red colours represent the lower and upper bounds of oil and water production. Figure 2.9 depicts the injection pressures in the first four injectors. Unlike in the results for the previous example, depicted in Figure 2.5, there is no jump in the pressures at the beginning of the forecasting period because they have already reached their maximum allowable values. Figure 2.10 depicts the historical data and the lower and upper bounds for the cumulative oil and water production of the entire field.
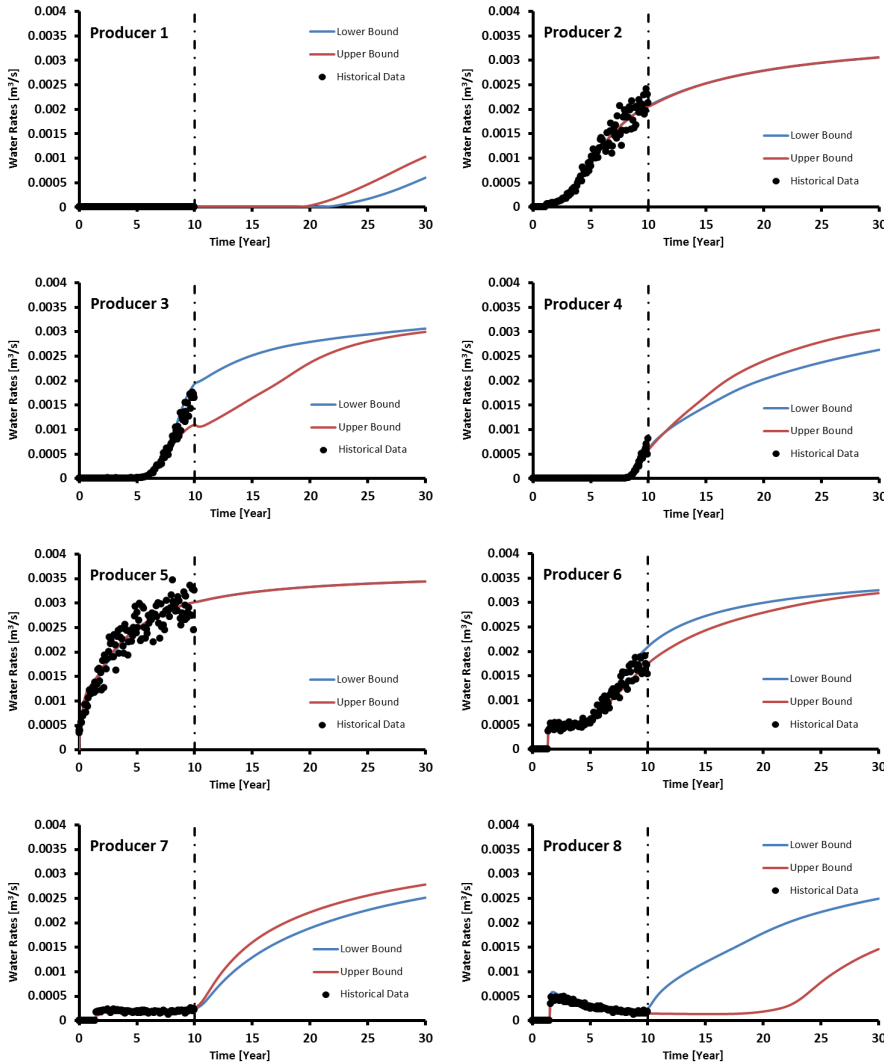
Figure 2.8: Historical and predicted water production over 30 years of production for the first eight producers for the Brugge field example.
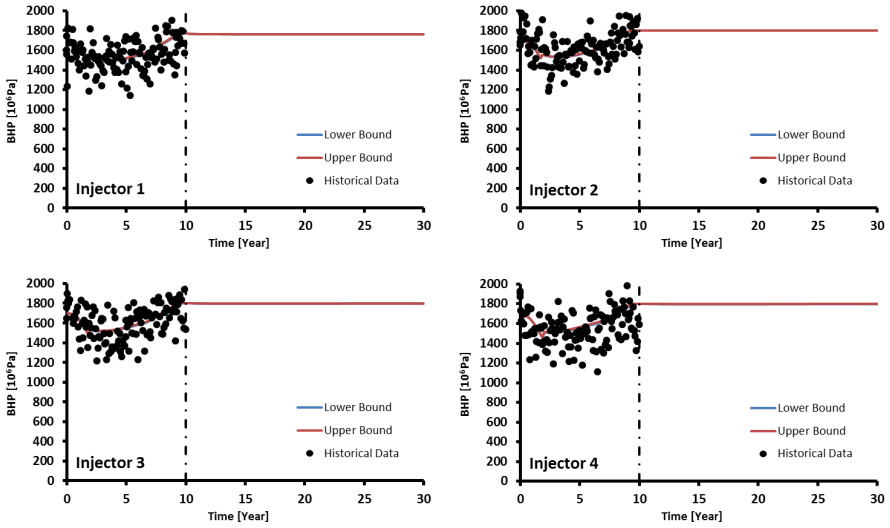
Figure 2.9: Historical and predicted injection pressures over 30 years of production for the first four injectors for the Brugge field example.
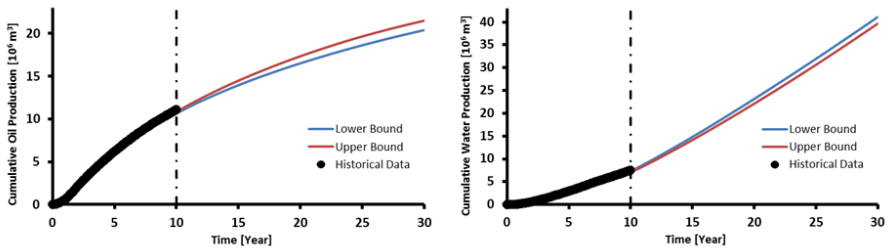
Figure 2.10: Historical and predicted cumulative oil production (left) and water production (right) over 30 years of production.

As can be seen in Figure 2.10 the lower bound and upper bound models produce the same history but different forecast. Moreover Figure 2.11 depicts the economic performance (NPV) of the upper and lower bound models over time for the entire production life, including the history and the prediction. In this experiment the incremental NPV of the upper bound model is 19.5% higher than the incremental NPV of the lower bound model.
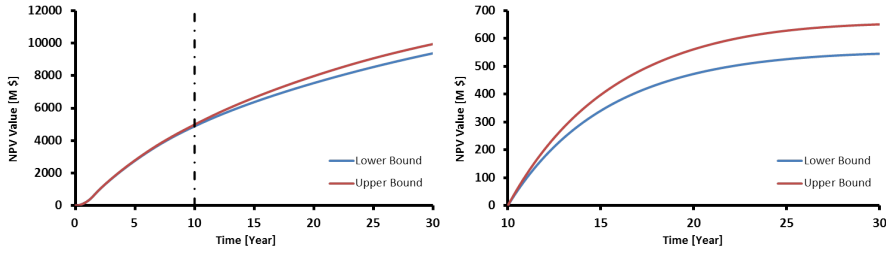
Figure 2.11: NPV over time for the lower and upper bound reservoir models. The plot on the left shows both the historic (first 10 years) and future (from 10 to 30 years) increase in NPV over time. The plot on the right side only shows the incremental NPV for the remaining (future) 20 years of production.Note that the right figure is a blown-up version of a part of the left one.
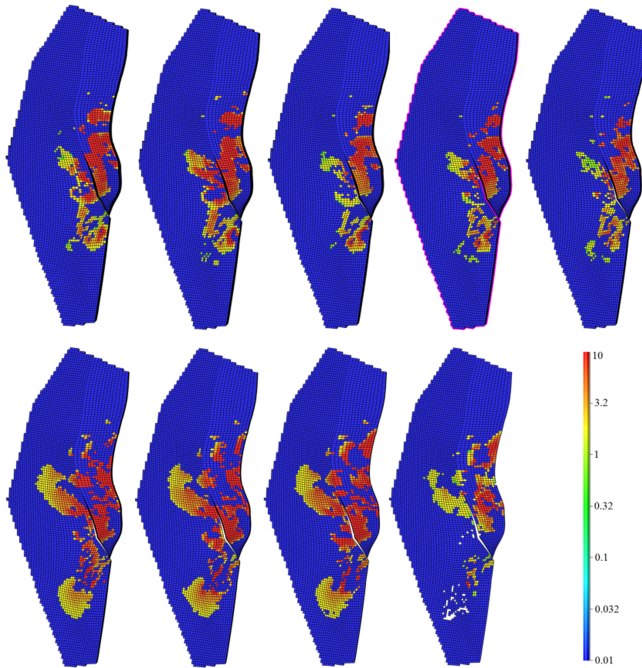
Figure 2.12: Difference between the lower and upper bound permeability fields for Brugge field example. All permeability values are expressed as the natural logarithm of permeability in mD.

Figure 2.12 shows the differences between the lower and upper bound permeability fields for all nine layers of the field. It can be observed in Figure 2.12 that the permeability fields of both models are different, especially in the producing layers. These differences have an impact on the predicted production data while they result in the same production history, as can be observed in Figure 2.10. We note that although the permeability values away from the wells are more likely to be in the null space (i.e. to have room for

2

variation), they also have less of an effect on the output in the wells. Apparently the optimization algorithm did not produce significant changes in these values because that would not have changed the resulting NPV. Computation of these result required 200 pairs of forward and backward (adjoint) simulations, where each pair took, on average, 786 s.

2.6.4. EFFECT OF DATA TYPE
In the previous section we obtained the lower and upper bound models based on production data. In order to investigate the effect of data type on the upper and lower bound models, two more experiments are conducted based on different data types. In the previous experiment the upper and lower bound models are obtained based on interpreted time lapse seismic data (saturation maps) and production data. The saturation maps are generated by simulating the "truth" and adding independent measurement errors by sampling from a Gaussian distribution with zero mean and standard deviations equal to 10% percent of the simulated saturation values. As before, we constrain the search space of the secondary problem by choosing the threshold value of equation (2.7) as 0.5% of the minimum of the primary objective function. The second experiment involves assimilation of both time-lapse seismic and production data while also prior information is added to the primary objective function as a regularization term. Figure 2.13 shows the incremental NPV difference between the lower and upper bound models obtained using different data types. As can be seen in Figure 2.13, the incremental NPV difference decreases by adding more information.
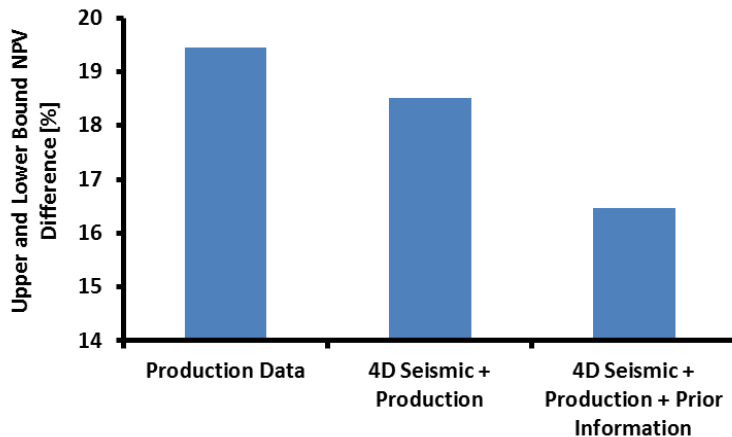
Figure 2.13: Difference between the upper bound and lower bound incremental NPV values for models obtained based on different data types.

2.6.5. EFFECT OF THRESHOLD VALUE
In this section we investigate the effect of the threshold value, ε, in equation (2.7). We constrain the search space of the secondary problem to different extents by choosing a

range of threshold values varying between 0.15% and 1.5% of the minimum of the primary objective function. Interpreted time-lapse seismic data (saturation maps) and production data formed the historical data, and two hierarchical multi-objective optimizations were conducted to find the lower and bounds for the reservoir model for different threshold values. Figure 2.13 shows the incremental NPV difference between the upper and the lower bound models versus the threshold value ε.
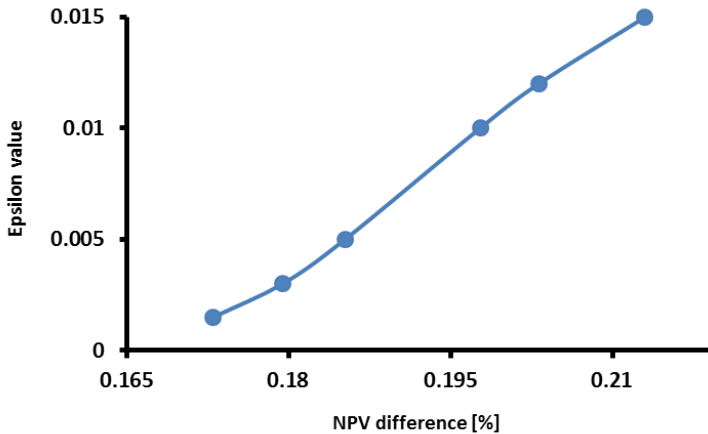
Figure 2.14: Incremental NPV difference between the upper bound and the lower bound model for different epsilon values.

Figure 2.15 depicts how the primary and secondary objective functions change for different values of ε. Figure 2.14 and Figure 2.15 show that as the threshold value in equation (2.7) increases the difference between the lower and upper model values of incremental NPV increases also. However, the effect is not very large and even for the lowest threshold value ($\varepsilon = 0.15\%$), a difference of approximately 17% in incremental NPV is obtained.

We note that the lower and upper bounds have been obtained by a gradient-based optimization technique which may have resulted in local rather than global optima. Lower lower bounds and higher upper bounds may therefore exist. We also note that both the red and the blue curves can be interpreted as parts of (approximate) Pareto curves. Points on a Pareto curve are at the boundary of the feasible set of solutions in the bi-objective space, and recently several studies have been performed to characterise a full Pareto curves for bi-objective flooding optimization; see, e.g., Liu and Reynolds (2014). Such a curve gives the decision maker the opportunity to select between competing objectives, i.e. to achieve a large value of the secondary objective function at the price of a strong drop in the primary objective function value, or a somewhat smaller secondary objective function value without losing much of the primary objective function value.
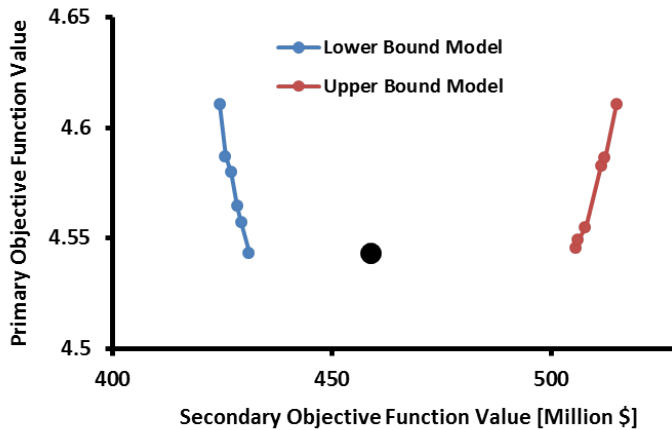
Figure 2.15: Secondary objective function value versus its corresponding primary objective function value, both expressed as incremental NPV.

2.7. DISCUSSION

In this chapter we used gridblock permeabilities as history matching parameters. However the proposed method could equally well be applied using other parameters, e.g. porosities, fault multipliers or aquifer strength. Moreover, other data types than the production data and interpreted time-lapse seismic that we used could be assimilated. We note that the use of gradients with respect to the history matching parameters is an important ingredient in our method. This implies that we need a technique to compute those gradients. We used an adjoint method, which is computationally very efficient. However it is, in theory, also possible to implement our method using approximate gradients obtained with e.g. the simultaneous perturbation stochastic approximation (SPSA) technique, see Spall (1998), or ensemble optimization (EnOpt); see Chen et al. (2009) for the basics of the method and Fonseca et al. (2014) for an implementation in hierarchical optimization. The latter (EnOpt) approach also allows for the inclusion of uncertainty in the reservoir models; see Fonseca et al. (2015). We note that our method has theoretical links to the use of level sets to relax the primary objective function constraint in hierarchical optimization as discussed in the last paragraph of Section 2.2. Moreover, we note that other weak-constrained optimization methods could be applied to solve the hierarchical optimization problem. The current implementation has shown to be robust in various applications using both adjoint-based and ensemble-based techniques (Van Essen et al., 2011; Chen et al., 2012; Fonseca et al., 2014). The determination of lower and upper bounds of future production using different types of data, as performed in the Brugge example, can be interpreted as a means to assess the cost effectiveness of acquiring different data types to reduce the uncertainty in the expected NPV. It is tempting to interpret this as a way to assess the value of information (VOI) of those measurements but because we do not know the statistical properties of the forecasted NPV we can not draw conclusions about the change in expected value

of those forecasts and therefore our method does not truly provide the VOI. (For detailed information about the the concept of VOI see Bratvold et al. (2009) or Eidsvik et al. (2015).)

2.8. CONCLUSIONS

In this chapter, we applied a hierarchical optimization method to determine lower and upper bounds on predicted production from history-matched models. We conclude that:

- The non-uniqueness of history matched models implies that future production can only be predicted within bounds.

- The non-uniqueness implies the presence of remaining degrees of freedom after history matching (i.e. after solving the primary optimization problem) which can be used to determine lower and upper bounds on future production through solving two secondary optimization problems.

- The method proposed in this chapter provides a way to gain more insight in the possible economic consequences of the lack of information in historic data. These consequences can be represented by total production, ultimate recovery, (incremental) NPV or any other economic measure.

- The method is not limited to historic production data. Alternative data sources, e.g. time-lapse seismic data, can be used to determine the impact on the predicted economic performance. Hence, this method may also play a role in the quantification of the value of information.

- Introducing more data sources, e.g. time-lapse seismic or prior information, results in smaller differences in economic performance (incremental NPV) between the lower and upper bound models.

3

UNDER-MODELING DETECTION

I⊤ is well known that parameter estimation of large-scale numerical models for porous-media flow in subsurface oil- and gas reservoirs is an ill-posed inverse problem. The classic solution to this problem is to regularize the unknowns, e.g. by penalizing deviations from a prior model. Attempts to estimate all uncertain parameters from oil production data without regularization typically lead to unrealistically high parameter values. However, it has been suggested by Joosten et al. (2011) that the application of unregularized reservoir parameter estimation may still add value, because it, sometimes, gives an indication of the location of significant missing features in the model. As a first step to investigate this suggestion we conduct numerical experiments and apply regularized parameter estimation as well as unregularized parameter estimation to update uncertain parameters in a simple two-dimensional reservoir model that contains a major deficiency in the form of a missing high- or low-permeability feature. The results show that depending on the noise level in the data, it may indeed be possible to localize the position of such a model deficiency, but generally not the correct magnitude, using an unregularized objective function for history matching purposes. Moreover, we investigate the effect of measurement noise on the results of unregularized history matching. Next, to investigate these findings, we perform a quantitative identifiability analysis of the examples using the SVD of a dimensionless output sensitivity matrix. The results of this identifiability analysis indicate that the closer a flow-relevant model deficiency is located to a production well, the higher the chance to detect it. We conclude that, for the examples considered, the application of unregularized reservoir parameter estimation indeed provides a means to identify the presence and location of significant model deficiencies such that it can improve our understanding about the reservoir model.

3.1. INTRODUCTION

3.1.1. NUMERICAL RESERVOIR SIMULATION

Most oil or gas reservoirs consist of relatively thin slabs of porous rock buried at depths of hundreds to thousands of meters. They are typically in the order of tens of meters thick and cover several square kilometers (Jansen et al., 2008). Generally, the well locations are accurately known, but the reservoir boundaries and its internal geological structure are much more uncertain. The subsurface is very heterogeneous, and the parameters relevant to flow are correlated at different length scales, but often over distances smaller than the inter-well spacing. As a consequence, the uncertainty in the model parameters is very large. During the design phase of an oil field development it is customary to capture this uncertainty by constructing multiple subsurface reservoir models to simulate the multi-phase fluid flow for different geological 'realizations'. Nevertheless, unexpected flow-relevant features may be present in reality that are not captured in the ensemble of reservoir models, and the purpose of this chapter is to investigate to what extent it is possible to identify such model deficiencies.

3.1.2. RESERVOIR PARAMETER ESTIMATION

Estimating reservoir parameters from measured data is usually an ill-posed inverse problem due to the large number of parameters and limited available data. The ill-posed nature of the inverse problem leads to numerical instabilities in the estimated parameters (Shah et al., 1978; Leo et al., 1986). The classic solution to this problem is to regularize the unknowns by introducing additional information. Using prior information is considered as one of the most common solutions for ill-posed nature of the history matching problems. In this approach a term is added to a mismatch objective function to penalize deviations from certain prior information. Therefore, such a penalty term, which restricts the parameter updates to values not too far from the prior values, can be unfavorable in case of wrong prior knowledge. On the other hand, attempts to estimate all uncertain parameters from production data without regularization typically lead to unrealistically high or low parameter values. It is also well known that the estimated parameter values in such unregularized ill-posed problems are extremely sensitive to noise in the data.

3.1.3. MODEL MATURATION

Joosten et al. (2011) have introduced the 'model maturation' concept and have shown that sometimes the application of unregularized reservoir parameter estimation still appears to have added value. They have shown that localized unrealistic parameter values can be used as an indicator of model errors (or 'under-modeling') in the underlying reservoir model. The objective of this chapter is to investigate some of the theoretical aspects of model maturation, i.e. to determine why and under which conditions there is relevant information hidden in the results of unregularized ill-posed inverse problems.

3.1.4. APPROACH

In our approach to investigate the model maturation concept we use 'twin experiments' in which computer-assisted history matching of one or more priors (i.e. reservoir models) is performed using synthetic data, generated with the aid of a 'synthetic truth' (i.e.

another reservoir model). The synthetic truth has a significant flow-relevant feature (e.g. a flow barrier or a high permeability streak) which is missing in the prior models.

3.2. OBJECTIVE FUNCTION

In a Bayesian framework, reservoir history matching can be formulated as a minimization problem. The underlying assumption is usually that the prior model can be characterized by mean values and a covariance matrix of the uncertain parameters (Oliver et al., 2008). The objective function J then consist of a quadratic mismatch term and a term that penalizes deviations of the parameters from their prior mean values:

$$J(\mathbf{m}) = \underbrace{(\mathbf{d} - \mathbf{h}(\mathbf{m}))^T \mathbf{P}_d^{-1} (\mathbf{d} - \mathbf{h}(\mathbf{m}))}_{\text{data mismatch term}} + \underbrace{(\mathbf{m} - \bar{\mathbf{m}})^T \mathbf{P}_m^{-1} (\mathbf{m} - \bar{\mathbf{m}})}_{\text{regularization term}}, \qquad (3.1)$$

where $\mathbf{m}$ is a vector of unknown model parameters and $\bar{\mathbf{m}}$ a vector of the prior estimate of values, $\mathbf{d}$ is a vector of data (measurements), $\mathbf{h}$ is a vector-valued function that relates the model parameters to the model outputs (i.e. the simulated data, which has a size of number of measurement points times number of measurement times), and $\mathbf{P}_d$ and $\mathbf{P}_m$ are covariance matrices of data errors and model parameters respectively. In this study measurements data vector, $\mathbf{d}$, consists of the oil and water rates in the four producers of the 'true' reservoir, which are measured each 30 days for 1500 days.

The unregularized objective function does not contain the regularization term:

$$J(\mathbf{m}) = (\mathbf{d} - \mathbf{h}(\mathbf{m}))^T \mathbf{P}_d^{-1} (\mathbf{d} - \mathbf{h}(\mathbf{m})). \qquad (3.2)$$

Minimization of the objective function is achieved by adjustment of the model parameters $\mathbf{m}$, usually subject to constraints on their values. Various numerical techniques are available to perform this minimization, the most efficient one being gradient-based minimization where the gradient is computed using the adjoint method (Oliver et al., 2008). For the present study we use Shell in-house reservoir simulator with adjoint functionality to calculate the gradients of the objective function (Kraaijevanger et al., 2007). We use the limited-memory Broyden Fletcher Goldfarb Shanno (LBFGS) method to minimize the objective function (Gao and Reynolds, 2006).

3.3. EXPERIMENTAL RESULTS

3.3.1. RESERVOIR MODEL

As a first step we use a simple 2D reservoir model to investigate the model maturation concept. The reservoir is a horizontal square, divided in $21 \times 21 = 441$ grid blocks of size 33.33 m × 33.33 m × 2 m. It is produced with a centrally located water injection well and four production wells in the corners. From a control perspective, the system inputs are the (constant) water rate in the injector and the (constant) bottomhole pressures (i.e. the constant pressures at the bottom of the wells) in the producers which are all assumed to be known. The outputs then consist of the bottomhole pressure in the injector, which is assumed to be unknown, and the oil and water rates in the producers, which are assumed to be measured with random measurement errors. The model parameters of

interest for our study are the 441 grid block permeabilities, i.e. the inverse resistances to flow with units mD ($1\,\text{mD} = 9.87 \times 10^{-16}\text{m}^2$). The porosity of the reservoir is 0.3, the initial water saturation is 0.2, and the initial reservoir pressure is 30 MPa. The four producers, located at the corners, are operated at constant bottomhole pressures of 25 MPa, without rate constraints, and the water injector at the center at a constant water flow rate of $0.002\,\text{m}^3/\text{s}$, without pressure constraints. Oil and water viscosities are $\mu_o = 1.5 \times 10^{-3}$ Pa s, $\mu_w = 1 \times 10^{-3}$ Pa s, oil, rock and water compressibilities are $c_o = 1.0 \times 10^{-9}$ Pa^{-1}, $c_w = 1.0 \times 10^{-10}$ Pa^{-1}, and $c_r = 1.0 \times 10^{-10}$ Pa^{-1}, and relative permeabilities are described with Corey exponents $n_o = n_w = 2$, connate water saturation $S_{wc} = 0.2$, residual oil saturation $S_{or} = 0.2$, and end-point relative permeabilities $k_{ro}^0 = 0.9$ and $k_{rw}^0 = 0.6$. Production is simulated for 1500 days, corresponding to 1.47 moveable pore volumes injected. Wells are located in the grid block centers, and we use a standard Peaceman well inflow model with a well bore radius $r_w = 0.10$ m. The uncertainty in the permeability field is represented with an ensemble of 500 model realizations. The ensemble members are generated by unconditioned sequential Gaussian simulation from a lognormal distribution with a mean of 300 mD and a standard deviation of 100 mD, and a spherical variogram with a nugget of 0.001 and a range of 1000 meters. (For general background information on these geostatistical concepts see, e.g., Caers (2005).) One of the ensemble members is chosen as the 'synthetic truth' after adding a flow-relevant feature, i.e. a flow barrier or a high-perm streak. The mean and covariance of the prior are calculated based on the remaining 499 realizations. The maximum permeability of the true permeability field is 492 mD, the minimum is 205 mD and the average is 387 mD. The synthetic truth is used to generate synthetic historical data in the form of measured oil and water rates in the producers. Independent measurement errors are generated from Gaussian distributions with zero mean and a standard deviation equal to 10% percent of the original measurements. Negative production rates, after the addition of noise, are reset to zero. Because the measurements errors are independent, the error covariance matrix is diagonal. The permeabilities of those grid blocks that contain wells are not updated in the minimization process to avoid localization of the updates in just the well grid blocks. We performed different sets of 'twin experiments', using four 'truth cases', each containing different flow-relevant features, and the two objective functions represented in equation (3.1) and equation (3.2).

3.3.2. EXPERIMENT # 1: TRUTH CASE WITH A FLOW BARRIER | REGULAR-IZED OBJECTIVE FUNCTION

In this experiment the truth contains a flow barrier in the form of a partially sealing fault, which separates production well *prod2* in the bottom-right corner from the rest of the field. The presence of this barrier results in a lower oil production and later water breakthrough in well *prod2* compared to the other wells. Figure 3.1 depicts the true permeability field with the well locations. The black line represents the sealing fault, which is modelled by means of a dimensionless seal factor $0 \le \sigma \le 1$ modifying the inter-grid block transmissibilities T according to

$$T_{eff} = \sigma T, \tag{3.3}$$

where the transmissibility T is a scaled harmonically averaged permeability of the neigh-

boring grid blocks.
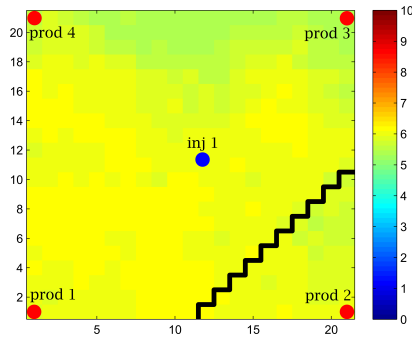
Figure 3.1: True permeability field with well locations for experiment #1. Permeability values are expressed as the natural logarithm of permeability in mD. The black line represents a partially sealing fault.

The fault in the truth is not present in the prior model, which means that we regularize our solution with wrong prior information. We use the regularized objective function, given by equation (3.1), and minimize it by adjustment of the permeability in each grid block. After 137 iterations the objective function mismatch is reduced to about one third of its original value and, because no further reduction occurs, the minimization process is stopped. Figure 3.2 depicts the prior and updated permeability fields. The updated permeability field stays close to the prior and does not show any unphysical updates. Some small adjustment of the permeability close to well *prod2* is visible, but any sign of the flow barrier is absent. Figure 3.3 depicts the oil and water rates in the four producers for the truth, the prior, and the updated model.
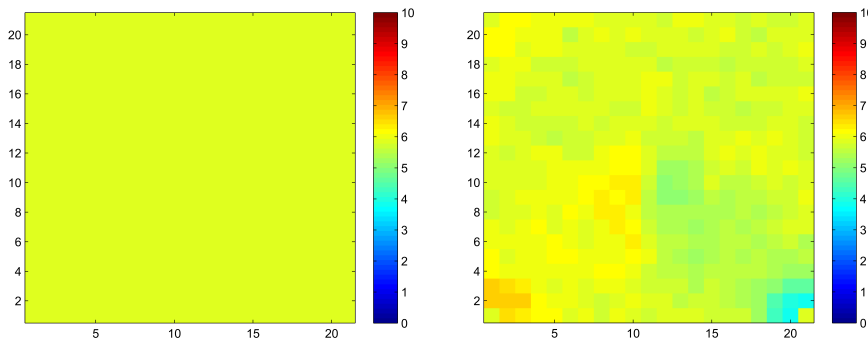
Figure 3.2: Prior permeability field (left), and updated permeability field (right) for experiment #1.

These experiments show that in an under-modeling situations, where an unexpected flow-relevant feature is not captured in the reservoir model, penalizing deviations from
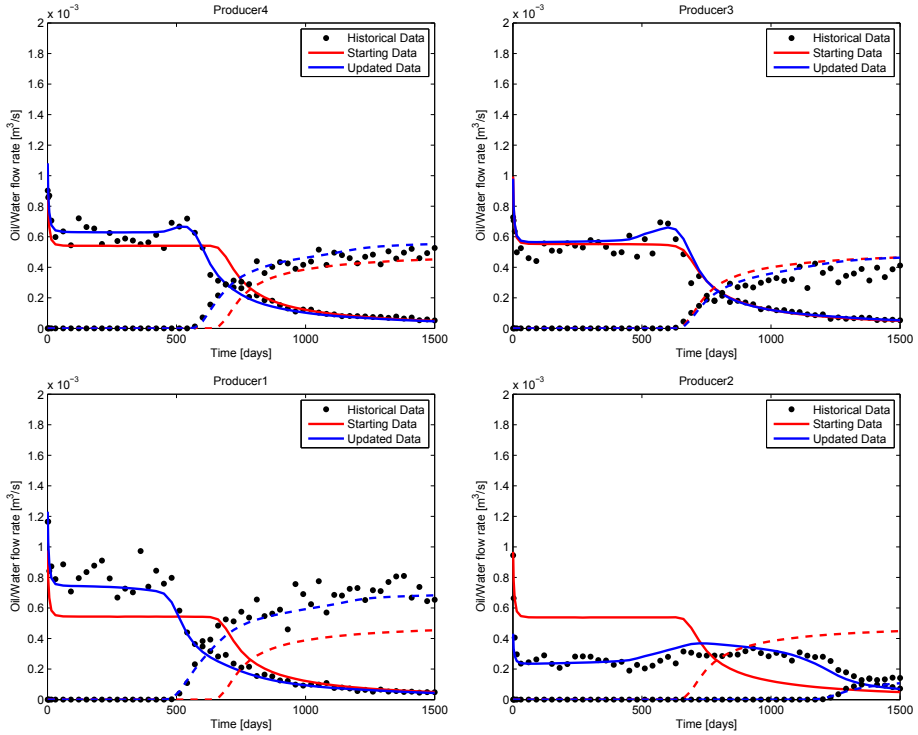
Figure 3.3: Data match in the producers for experiment #1. Black dots indicate the measured oil and water rates. Solid and dashed red lines are the oil and water rates of the prior model. Solid and dashed blue lines are the oil and water rates of the updated model.

a prior model can be undesirable since it leads to the solutions that stay close to the prior. In the other words, if a feature is missing in the prior there is almost no chance to capture it since the updated parameters are constrained by an incorrect prior knowledge that usually originates from interpretation errors of geological data.

3.3.3. EXPERIMENT # 2 - TRUTH CASE WITH A FLOW BARRIER | UNREGU-LARIZED OBJECTIVE FUNCTION

In this experiment we use the same truth as in experiment #1 (see Figure 3.1), but we use the unregularized objective function given by equation (3.2). Different permeability fields, randomly chosen from the ensemble of 499 members, were used as starting values for the iterative minimization procedure. In addition, the mean of the ensemble, i.e. the same model that was used as prior in experiment #1, was also chosen as one of the starting models. The minimizations converged in about 200 to 300 iterations, in which the objective function mismatch reduced with three orders of magnitude. Figure 3.4 shows four different starting models and their updates after history matching. In all four cases a low permeable band, with permeabilities between 1 to 10 mD is visible in the updated permeability fields. This low permeable band is apparently generated in order

to match the production for well *prod2*, which is separated from the other wells through the partially sealing fault in the truth case. The low-permeable band, which has very low permeability values compared to other part of the fields, is apparently indicating that something is missing in our starting models. I.e., in this example, the unrealistic updates resulting from history matching with an unregularized objective function indeed seem to give an indication for under-modeling. Figure 3.5 depicts the oil and water rates in the four producers for the truth, the prior, and the updated model. As can be seen in Figure 3.5, the simulated data for the updated model match the historical data near-perfectly. In the next two experiments we will only use the unregularized objective function given by equation (3.2).
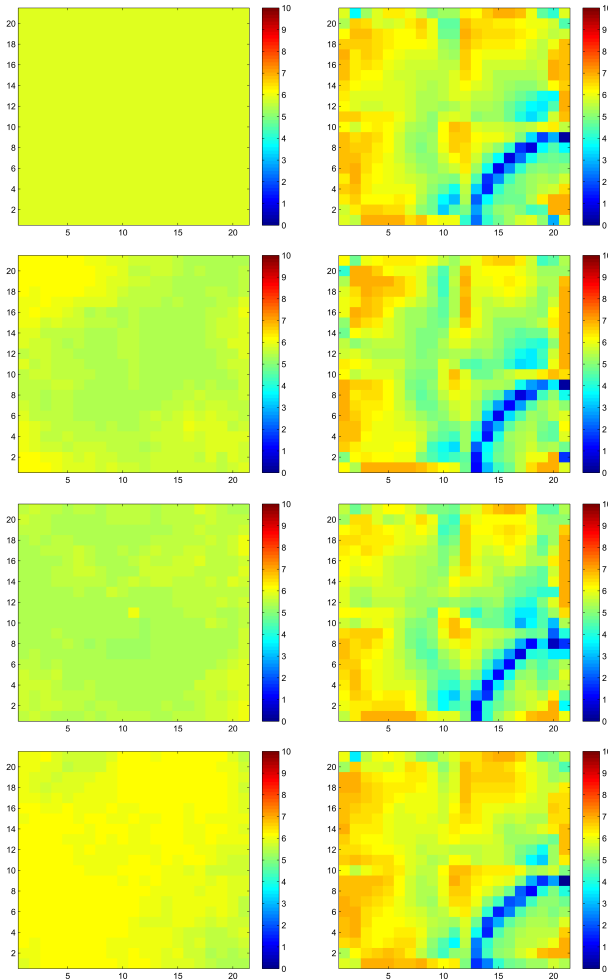
Figure 3.4: Different models used as starting values for the minimization procedure (left), and the updated models (right) for experiment #2. The starting model in the top row is the ensemble average.
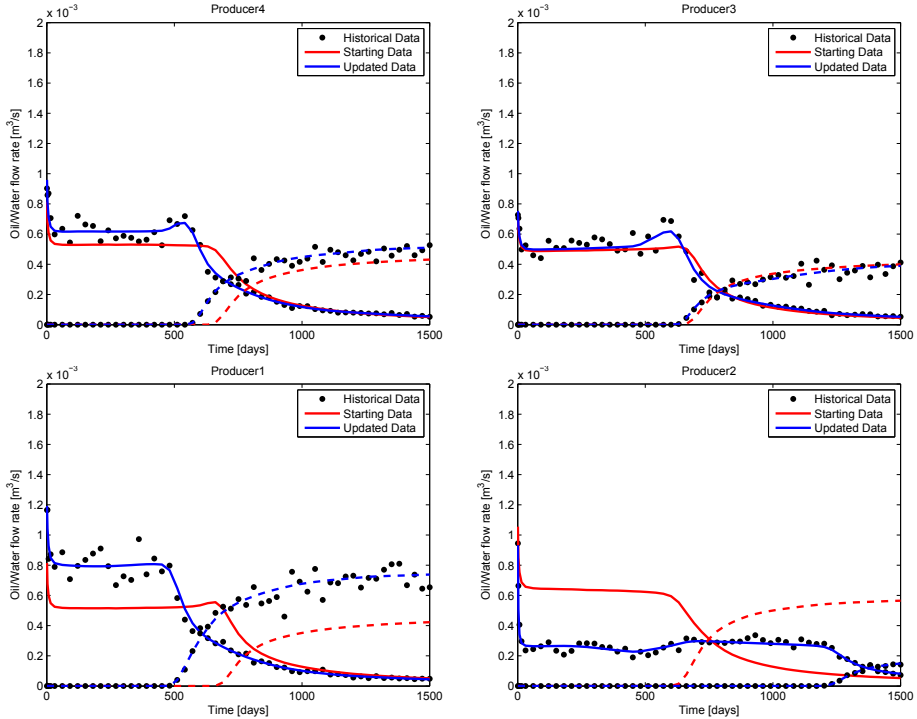
Figure 3.5: Data match in the producers for experiment #2. Black dots indicate the measured oil and water rates. Solid and dashed red lines are the oil and water rates of the prior model. Solid and dashed blue lines are the oil and water rates of the updated model.

3.3.4. EXPERIMENT # 3 - CAPTURING THE POSITION OF A FLOW BARRIER
In this experiment the partially sealing fault in the truth case has a different location than in the previous experiments and is located closer to the well *prod2*. Figure 3.6 depicts the true permeability field together with the location of the fault. Just like in experiment #2, the updated permeability field is obtained by minimization of the unregularized objective function given by equation (3.2). Figure 3.7 shows the starting model and its update after history matching. It can be seen that the low permeable band is now generated closer to well *prod2*, as is the location of the fault in the synthetic truth. In terms of data mismatch the flow rates in the wells are matched near-perfectly. This example indicates that apparently the production information in the wells also carries some information about the location of the flow barrier.

3.3.5. EXPERIMENT #4: TRUTH CASE WITH A HIGH-PERMEABILITY STREAK | REGULARIZED OBJECTIVE FUNCTION
In this experiment the truth case contains a high-permeable streak in the vicinity of production well *prod2* in the bottom-right corner of the field. Figure 3.8 depicts the true permeability field with the well locations. The grid blocks with a red color indicate the
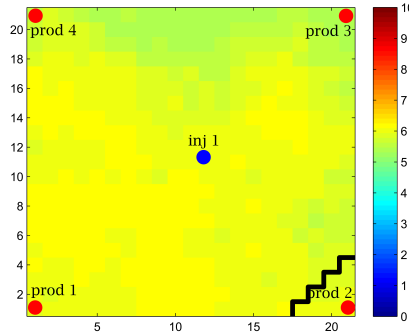
Figure 3.6: True permeability field with well locations for experiment #3. Permeability values are expressed as the natural logarithm of permeability in mD. The black line represents a partially sealing fault.
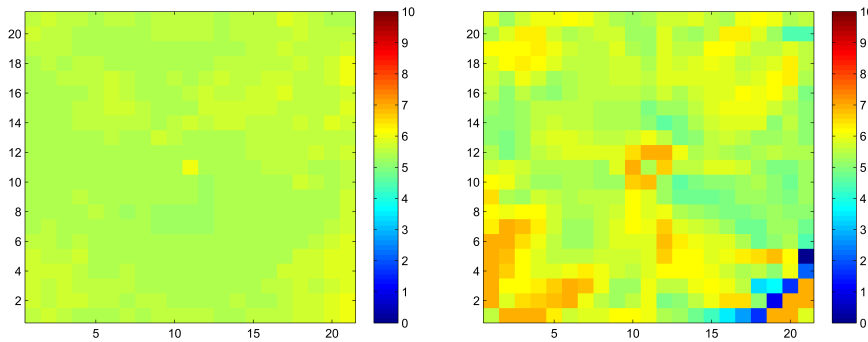
Figure 3.7: Starting permeability field (left) and updated permeability field (right) for experiment #3.

high-perm streak with a permeability of 10000 mD.

The high-perm streak in the truth case is not present in the prior model, which means that we regularize our solution with wrong prior information. We use the regularized objective function, given by equation (3.1), and minimize it by adjustment of the permeability in each grid block. After 310 iterations the objective function mismatch is reduced to about one third of its original value and, because no further reduction occurs, the minimization process is stopped. Figure 3.9 depicts the prior and updated permeability fields. The updated permeability field stays close to the prior and does not show any unexpected updates. Some small adjustment of the permeability close to well *prod2* is visible, but a clear sign of the high-perm streak is absent. Figure 3.10 depicts the oil and water rates in the four producers for the truth, the prior, and the updated model.

Again these experiments show that in an under-modeling situations, where an unexpected flow-relevant feature is not captured in the reservoir model, penalizing deviations from a prior model can be undesirable since it leads to solutions that stay close to the prior. In the other words, if a feature is missing in the prior there is almost no chance
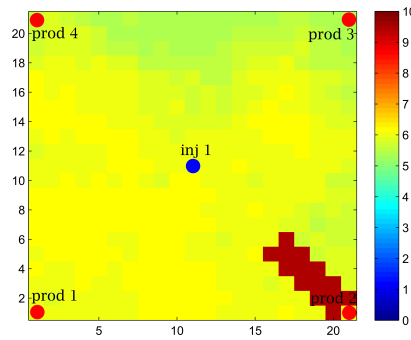
Figure 3.8: True permeability field with well locations for experiment #4. Permeability values are expressed as the natural logarithm of permeability in mD.
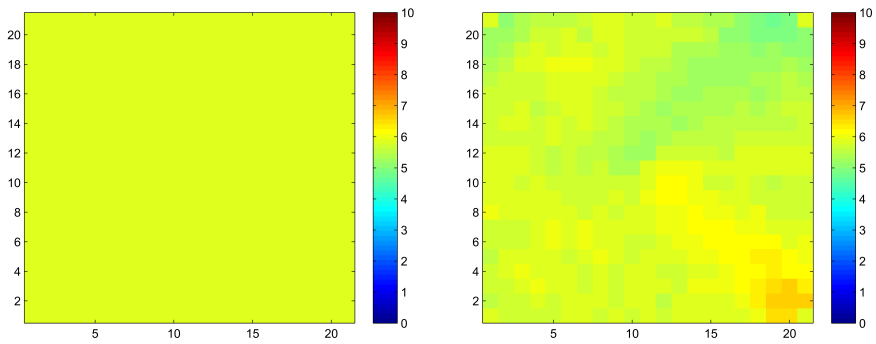
Figure 3.9: Prior permeability field (left), and updated permeability field (right) for experiment #4.

to capture it since the updated parameters are constrained by incorrect prior knowledge that usually originates from interpretation errors of geological data.

3.3.6. EXPERIMENT #5 - TRUTH CASE WITH A HIGH-PERM STREAK | UN-REGULARIZED OBJECTIVE FUNCTION

In this experiment we use the same truth as in experiment #4 (see Figure 3.8), but we use the unregularized objective function given by equation (3.2) for history matching purposes. Figure 3.11 shows the starting model and its updates after 268 iterations in the minimization process. The permeability of the red strip in the updated model in Figure 3.11 is between 2000 to 8000 mD. The high-permeable streak, which has very high permeability values compared to other part of the fields, is apparently indicating that something is missing in our starting models. I.e., also in this example, the unrealistic updates resulting from history matching with an unregularized objective function indeed seem to give an indication for under-modeling. Figure 3.12 depicts the oil and water
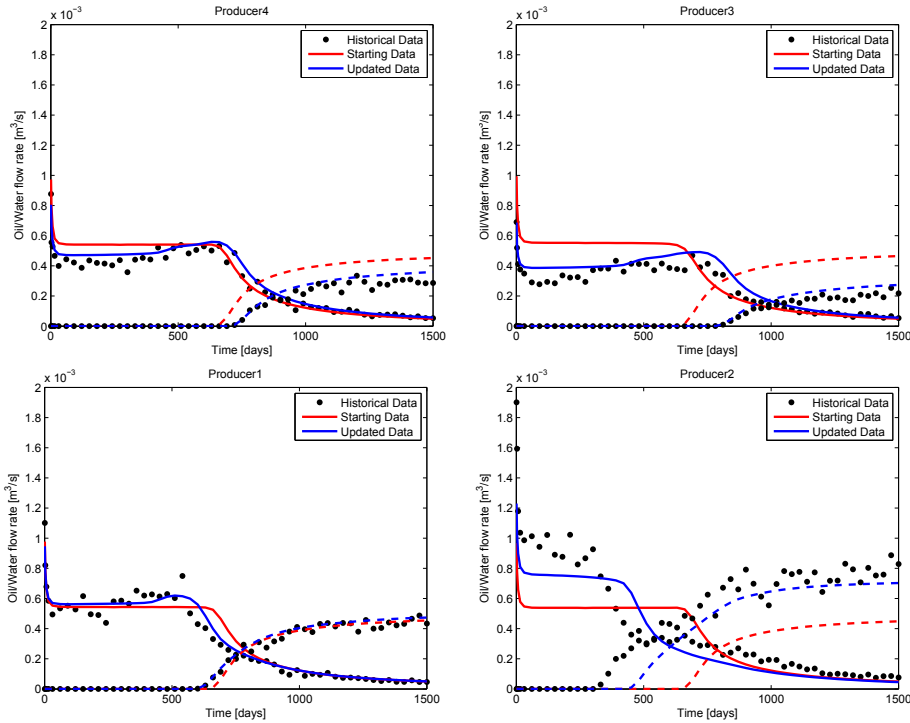
Figure 3.10: Data match in the producers for experiment #4. Black dots indicate the measured oil and water rates. Solid and dashed red lines are the oil and water rates of the prior model. Solid and dashed blue lines are the oil and water rates of the updated model.

rates in the four producers for the truth, the prior, and the updated model.
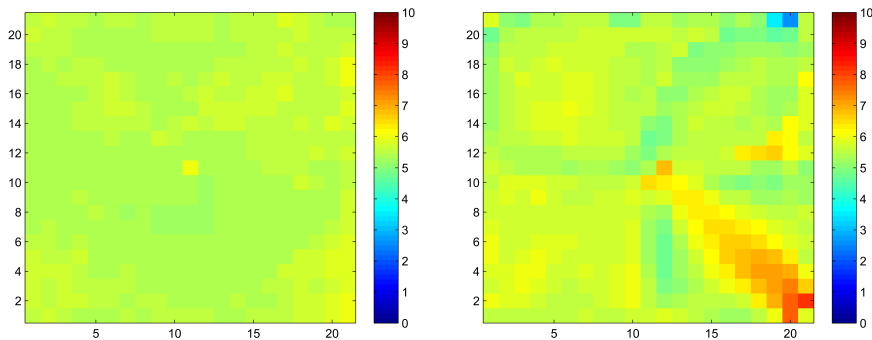
Figure 3.11: Starting permeability field (left) and its update (right) for experiment #5.
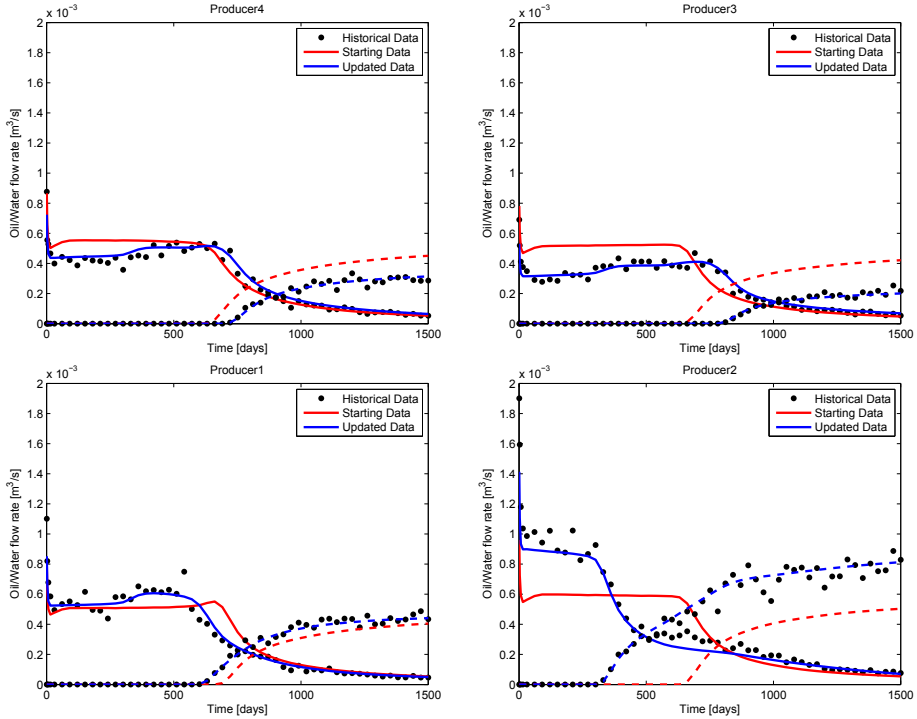
Figure 3.12: Data match in the producers for experiment #5. Black dots indicate the measured oil and water rates. Solid and dashed red lines are the oil and water rates of the prior model. Solid and dashed blue lines are the oil and water rates of the updated model.

3.3.7. EXPERIMENT #6 - CAPTURING THE POSITION OF A HIGH-PERM STREAK

In this experiment the high-perm streak in the truth case has a different location than in experiment #5 and is located closer to the well *inj1*. Figure 3.13 depicts the true permeability field together with the location of the high-perm streak.

Figure 3.14 shows the starting model and its updates after minimization process. The permeability of the red strip in the updated model in Figure 3.14 is 1000 to 3000 mD. Experiment #5 and experiment #6 indicate that, for these examples, the use of unregularized parameter estimation makes it possible to capture the position of a high permeable streak, although the estimated permeability values are not accurate.

3.4. EFFECT OF MEASUREMENT ERRORS

In this set of experiments we investigate the effect of increased measurement errors on the updated parameters. Four truth cases are used to generate synthetic data: two different fault locations (experiment #2 and experiment #3) and two different high-permeable streak locations (experiment #5 and experiment #6). Figure 3.15 shows the experiment results based on the measurements generated with the truth case from experiment #2. The left column of Figure 3.15 depicts the true and prior permeability fields. The right
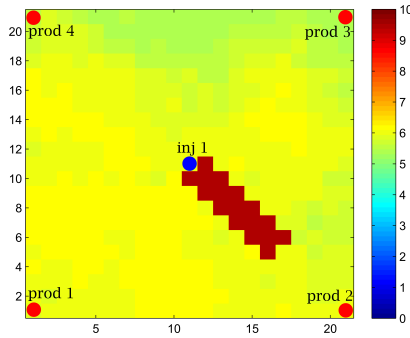
Figure 3.13: True permeability field with well locations for experiment #6. Permeability values are expressed as the natural logarithm of permeability in mD.
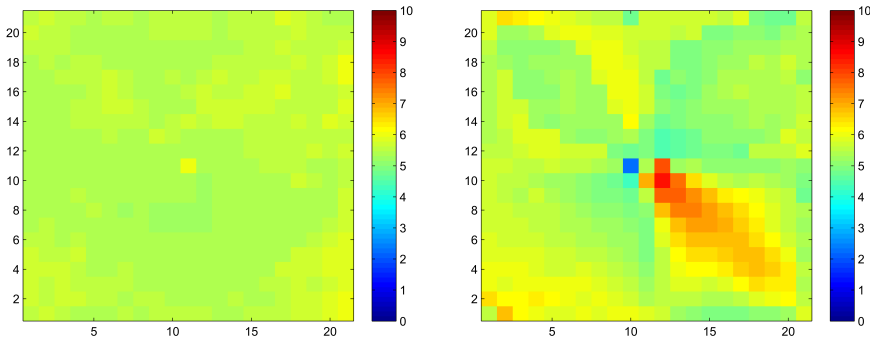
Figure 3.14: Starting permeability field (left) and its update (right) for experiment #6.

column of Figure 3.15 depicts the updated permeability fields for measurements with measurement errors with standard deviations of 10%, 15%, 20% and 25% of the original measured values. It is clear from Figure 3.15 that increasing error levels lead to increasingly worse permeability estimates. For the 25% case the updated model contains completely spurious bands of low-permeability values. Note that these experiments are repeated using different noise realizations and they end up with the same behavior.

Figure 3.16 depicts the experimental results based on the measurements generated with the truth case from experiment #3, which has a partially sealing fault closer to well *prod2*. The left column of Figure 3.16 depicts the true and prior permeability fields and the right column of this figure depicts the updated permeability fields for measurements with measurements having standard deviations of 10%, 15%, 20% and 25% of the original measured values. By comparing Figure 3.15 and Figure 3.16, it can be seen that when the fault is closer to the producer it is possible to capture it, even at higher noise levels compared to the case in which the fault is further away from the producer. Note that these experiments are repeated using different noise realizations and they end up with
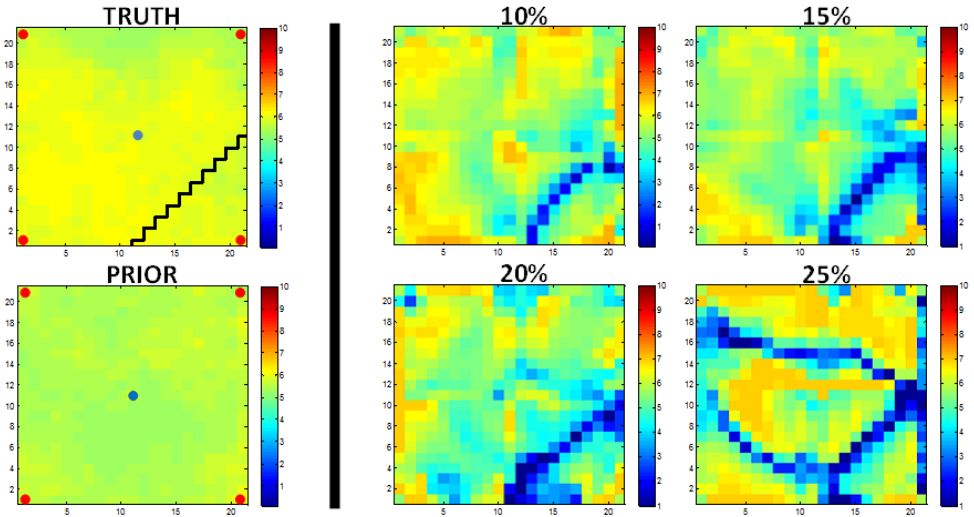
Figure 3.15: Truth and prior permeability field (left) and its updates (right) for different measurement errors.

the same behavior.
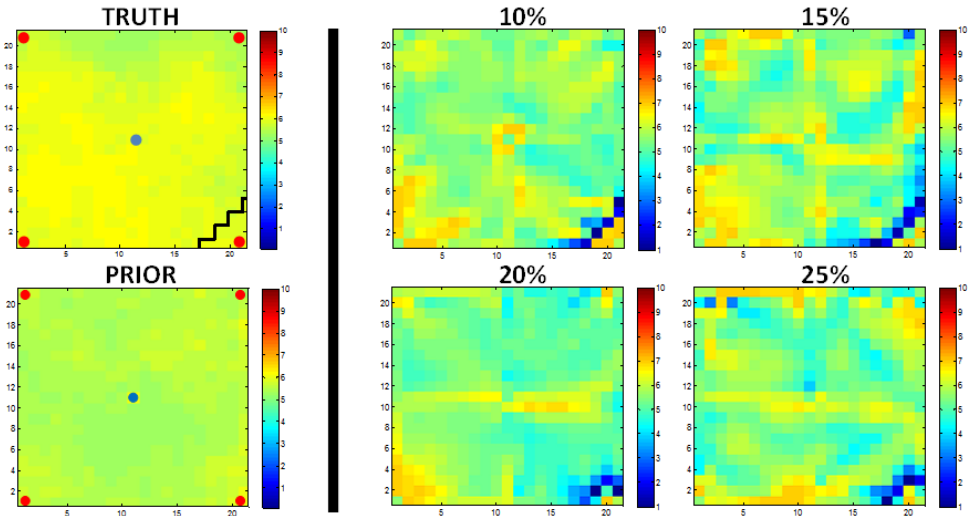
Figure 3.16: Truth and prior permeability field (left) and its updates (right) for different measurement errors.

Figure 3.17 shows the experiment results based on the measurements generated with the truth case from experiment #5, which has a high-perm streak closer to well *prod2*. The left column of Figure 3.17 shows truth and prior permeability fields and the right column of this figure shows the updated permeability fields for measurements with measurement errors with standard deviations of 10%, 15%, 20% and 25% of the original measured

values. Different noise realizations are used to repeat these experiments, which result in the same behavior.
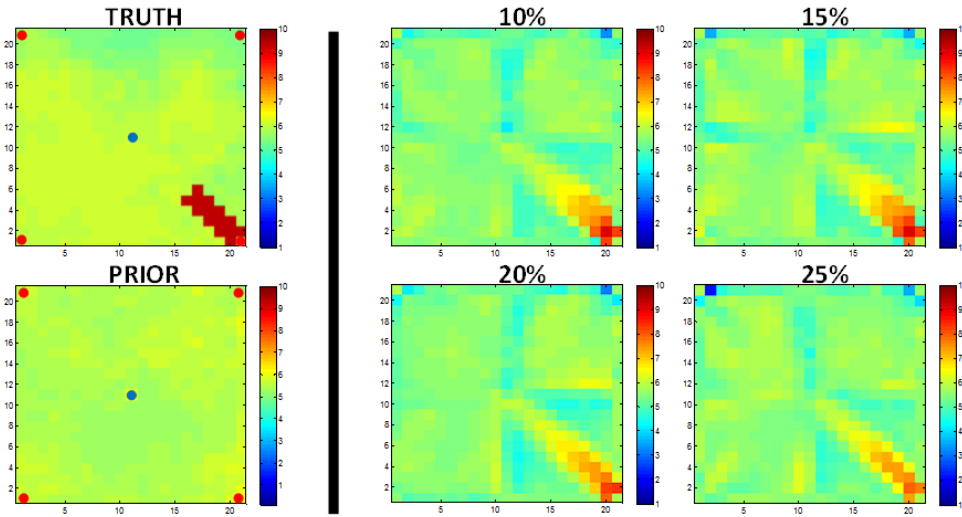
Figure 3.17: Truth and prior permeability field (left) and its updates (right) for different measurement errors.

Figure 3.18 shows the experiment results based on the measurements generated with the truth case from experiment #6, which has a high-perm streak in the vicinity of well *inj1*. The left column of the Figure 3.18 shows truth and prior permeability fields. The right column of this figure shows the updated permeability fields for measurements with measurement errors with standard deviations of 10%, 15%, 20% and 25% of the original measured values. As can be seen in Figure 3.18, increasing error levels lead to increasingly worse permeability estimates. Note that these experiments are repeated using different noise realizations and they end up with the same behavior.

By comparing Figure 3.17 and Figure 3.18, it can be seen that when the high-perm streak is closer to the producer it is possible to capture it, even at higher noise levels compared to the case in which the streak is further away from the producer. Note that we only measure outputs in the producers and not in the injector.

From the experiments described in this section it can be inferred that when a flow-relevant feature is located closer to a producer, the feature can still be retrieved in a history matching process with a higher noise level.

3.5. IDENTIFIABILITY

The system-theoretical analysis of the presence of information in measured data is centered around the concept of identifiability. Roughly speaking the notion of identifiability can refer to the question whether parameter changes can be observed in the model output signal (Zandvliet et al., 2008; Van Doren, 2010). Watson et al. (1984) and Datta-Gupta et al. (1997) address identifiability in steady-state (incompressible) two-phase
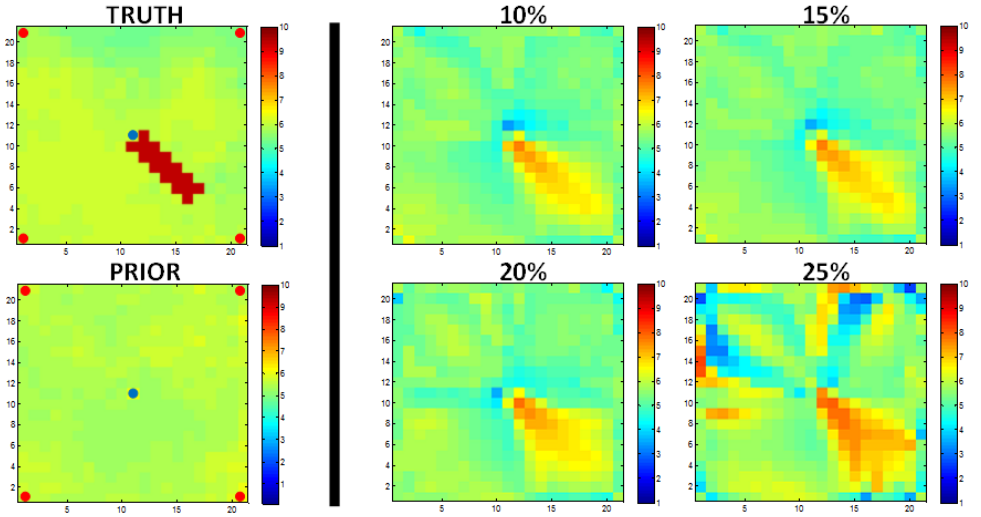
Figure 3.18: Truth and prior permeability field (left) and its updates (right) for different measurement errors.

flow and the authors conclude that identifiability of reservoir properties is limited to
average properties between wells. However, we consider (slightly) compressible flow
and time-varying well rates, and it is well known from classical well testing (pressure
transient analysis), and from related methods such as pulse testing or interference test-
ing, that information about the distance between wells and flow-relevant features (e.g.
reservoir boundaries or sealing faults) is sometimes present in the data, although to a
limited extent due to the diffusive nature of pressure transients; see e.g. Grader and
Horne (1988) and Ahn and Horne (2010). Zandvliet et al. (2008) and Van Doren (2010)
address identifiability in reservoir systems from a system-theoretical point of view. The
authors conclude that the number of identifiable parameters in a reservoir model based
on input-output measurements in wells is very limited, and, moreover, can only be iden-
tified if the input is 'sufficiently exciting'. However, using a singular value decomposition
(SVD) of the sensitivity matrix $\partial \mathbf{h}(\mathbf{m})/\partial \mathbf{m}$, they also show that it is sometimes possible to
identify large-scale flow-relevant features, as captured by the first SVD basis functions.
In this study we first use a dimensionless sensitivity matrix $\boldsymbol{\Psi}$ in order to analyze the
sensitivity of system output (oil and water rates in the wells) to the system parameters
(grid block permeabilities) and characterize the identifiability of different flow-relevant
features in different locations. Moreover, we show how presence of noise in the measure-
ments can affect the history matching results using SVD analysis. The sensitivity matrix,
$\boldsymbol{\Psi}$, is defined as

$$\boldsymbol{\Psi} = \boldsymbol{\Gamma}_m \frac{\partial \mathbf{h}(\mathbf{m})^T}{\partial \mathbf{m}} \mathbf{P}_d^{-\frac{1}{2}}, \tag{3.4}$$

where $\mathbf{h}(\mathbf{m})$ represents system output (oil and water rates in the wells), $\mathbf{m}$ is the param-
eter vector (grid block permeabilities) and $\mathbf{P}_d$ is the covariance matrix of the noise that
is supposed to act on the measured output. $\boldsymbol{\Gamma}_m$ is a scaling matrix which is chosen as

$$\mathbf{\Gamma}_m = \text{diag}\begin{pmatrix} m_1 & \cdots & m_n \end{pmatrix} \tag{3.5}$$

where the elements m_i represent the grid block permeabilities of the model (Van Doren, 2010). In our case scaling can play an important role and can possibly influence the identifiable parameter space, since the magnitudes of the physical parameters differ by several orders of magnitudes (background permeabilities and feature permeabilities). By analyzing the sensitivity matrix we are able to investigate if a feature is identifiable from measured outputs. Moreover by comparing the sensitivity matrices of different model structures with different flow-relevant features we can investigate to what extent the measured outputs are sensitive with respect to a feature location.

Figure 3.19 depicts the sensitivity of the output from well *prod2* with respect to the gird-block properties for two different permeability fields with different fault locations (experiments #2 and #4). As can be seen from Figure 3.19 the measured output of well *prod2* is quite sensitive to a flow barrier (a partially sealing fault), i.e., together with the given input it makes the feature identifiable. Moreover, it can be concluded from Figure 3.19 that the input-output combination for this system is more sensitive to a flow barrier when the barrier is closer to a producer. This confirms our results in section 3.4 where we have shown that it is possible to capture the location of barrier even with higher noise levels in the measured data when it is closer to the producer.
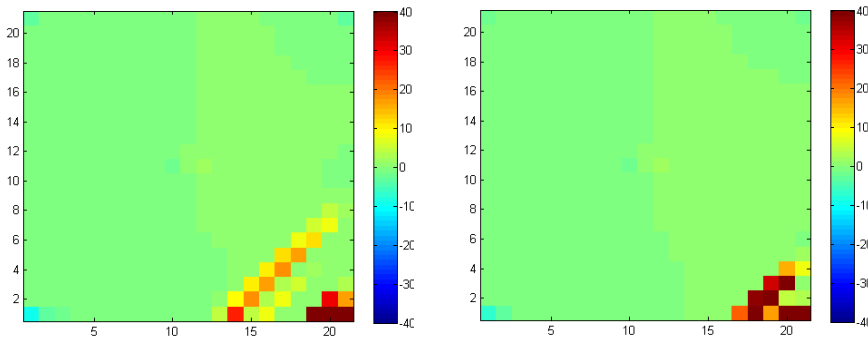
Figure 3.19: Elements of sensitivity matrix, $\mathbf{\Psi}$, of well *prod2* output with respect to the grid block permeabilities for two different models with different fault locations.

Figure 3.20 depicts the sensitivity of the output from well *prod2* with respect to the grid block properties for two different permeability fields with different high-permeable streak locations (experiment #5 and #6). As can be seen from Figure 3.20 the measured output of well *prod2* is quite sensitive to presence of a high-permeable streak, i.e., together with the given input it makes the feature identifiable. Moreover, it can be concluded from 3.20 that the input-output combination for this system is more sensitive to a high-permeable streak when the streak is closer to a producer. This confirms our results in section 3.4 where we have shown that it is possible to capture the location of a high-permeable streak even with higher noise levels in the measured data when it is closer to the producer.
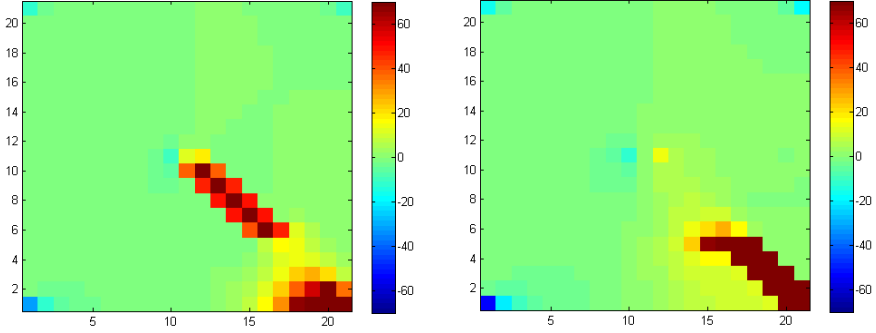
Figure 3.20: Elements of sensitivity matrix, $\boldsymbol{\Psi}$, of well *prod2* output with respect to the grid block permeabilities for two different models with different high-permeable streak locations.

Next, it can be shown how the presence of noise in the measurements can affect the parameter estimation using an SVD analysis of sensitivity matrix $\mathbf{P}_d^{-1/2}\mathbf{h}'(\mathbf{m})$, where $\mathbf{h}'(\mathbf{m})$ is the sensitivity of system output with respect to uncertain parameters (Rodrigues, 2006).

A linear approximation for $\mathbf{h}(\mathbf{m})$ around $\mathbf{m}$ can be expressed as follows,

$$\mathbf{h}(\mathbf{m}) \simeq \mathbf{h}(\mathbf{m}_0) + \mathbf{h}'(\mathbf{m}_0)\,\delta\mathbf{m}, \tag{3.6}$$

where $\mathbf{m}_0$ is the initial guess in the parameter space, $\delta\mathbf{m} = (\mathbf{m} - \mathbf{m}_0)$ and $\mathbf{h}'(\mathbf{m}_0)$ is the sensitivity matrix calculated at $\mathbf{m}_0$. By replacing equation (3.6) in our unregularized objective function given by equation (3.2), we can find an approximation to our objective function,

$$J(\mathbf{m}) \simeq \left[\left(\mathbf{h}(\mathbf{m}_0) + \mathbf{h}'(\mathbf{m}_0)\,\delta\mathbf{m}\right) - \mathbf{d}\right]^T \mathbf{P}_d^{-1}\left[\left(\mathbf{h}(\mathbf{m}_0) + \mathbf{h}'(\mathbf{m}_0)\,\delta\mathbf{m}\right) - \mathbf{d}\right]. \tag{3.7}$$

Equation (3.7) can be rewritten as follows,

$$J(\mathbf{m}) \simeq \left(\mathbf{P}_d^{-\frac{1}{2}}\mathbf{h}'(\mathbf{m}_0)\,\delta\mathbf{m} - \mathbf{P}_d^{-\frac{1}{2}}\mathbf{r}_0\right)^T \left(\mathbf{P}_d^{-\frac{1}{2}}\mathbf{h}'(\mathbf{m}_0)\,\delta\mathbf{m} - \mathbf{P}_d^{-\frac{1}{2}}\mathbf{r}_0\right), \tag{3.8}$$

where $\mathbf{r}_0$ is defined as,

$$\mathbf{r}_0 = \mathbf{d} - \mathbf{h}(\mathbf{m}_0). \tag{3.9}$$

The problem of minimizing equation (3.8) is an under-determined linear least-squares problem and it can be shown that its solution can be expressed in terms of the singular value decomposition of $\mathbf{P}_d^{-1/2}\mathbf{h}'(\mathbf{m}_0)$ (Golub and Van Loan, 2012; Nocedal and Wright, 2006):

The derivative of equation (3.8) can be written as,

$$\frac{\partial J(\mathbf{m})}{\partial \mathbf{m}} = 2\mathbf{P}_d^{-\frac{1}{2}}\mathbf{h}'(\mathbf{m}_0)\left(\mathbf{P}_d^{-\frac{1}{2}}\mathbf{h}'(\mathbf{m}_0)\,\delta\mathbf{m} - \mathbf{P}_d^{-\frac{1}{2}}\mathbf{r}_0\right). \tag{3.10}$$

The optimum of equation (3.8) can be found by choosing a $\delta\mathbf{m}$ which makes equation (3.10) zero, i.e.,

$$\delta\mathbf{m}^* = \left(\mathbf{P}_d^{-\frac{1}{2}}\mathbf{h}'(\mathbf{m}_0)\right)^{-1}\mathbf{P}_d^{-\frac{1}{2}}\mathbf{r}_0. \tag{3.11}$$

Pseudo inverse of the first term of equation (3.11) can be computed by use of singular value decomposition,

$$\mathbf{V}\mathbf{S}^{-1}\mathbf{U}^T = \left(\mathbf{P}_d^{-\frac{1}{2}}\mathbf{h}'(\mathbf{m}_0)\right)^{-1}. \tag{3.12}$$

Substituting equation (3.12) in equation (3.11) results in,

$$\delta\mathbf{m}^* = \mathbf{V}\mathbf{S}^{-1}\mathbf{U}^T\mathbf{P}_d^{-\frac{1}{2}}\mathbf{r}_0, \tag{3.13}$$

where $\mathbf{S}$ is the matrix of singular values, $\mathbf{U}$ is the matrix of left singular vectors and $\mathbf{V}$ is the matrix of right singular vectors of $\mathbf{P}_d^{-1/2}\mathbf{h}'(\mathbf{m}_0)$. Equation (3.13) shows that the largest singular values and corresponding singular vectors contain the most relevant information about the solution, since small singular values tend to amplify noise in the measurements (Hanke and Hansen, 1993; Rodrigues, 2006). In other words, as the singular values decrease the effect of noise on the solution increases.

Figure 3.21 shows first 97 singular values of the sensitivity matrix $\mathbf{P}_d^{-1/2}\mathbf{h}'(\mathbf{m}_0)$ for the truth case of experiment #1 with different noise level. As can be seen from Figure 3.21, as the noise level increases the singular values decrease and therefore the solution to the parameter estimation problem becomes more sensitive to noise. This analysis confirm our findings in section 3.4.

3.6. ALTERNATIVE FORMULATIONS FOR HISTORY MATCHING

Regularization in inverse problems refers to a process of introducing additional information in order to solve an ill-posed problem. This information is usually of the form of a penalty for complexity, such as restrictions for smoothness or bounds on the vector space norm. The main goal of regularizing ill-posed inverse problems is to constrain our solutions to avoid misleading by features that appear in the model, which are not essential in matching the observations (Constable et al., 1987). In conventional reservoir parameter estimation the solution of the inverse problem is usually constrained using regularization based on prior geostatistical knowledge of the reservoir to make the problem solvable. This approach can be promising if the prior information of the reservoir geology is reliable. On the other hand, as it is shown in section 3.3.2, in the case of inaccurate or wrong prior information, the dynamic data cannot be used much to interfere model discontinues (e.g. sealing fault or high-channel) itself. In that sense the parameter search space is limited to a wrong prior knowledge and we do not adequately use the information that dynamic data carries about the reservoir parameters. Moreover, smoothing the solutions as a structural regularization constraint can be useful in a reservoir with gradual heterogeneity, whereas in a reservoir with sudden discontinuities more
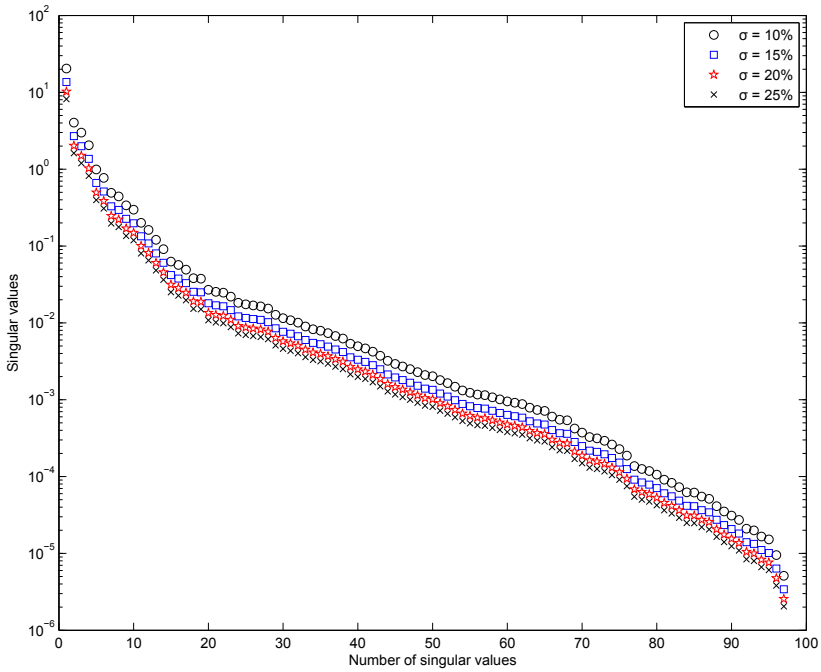
Figure 3.21: First 97 singular values of sensitivity matrix for the truth case of experiment #1 with different noise level.

sophisticated regularization methods have to be used (Li and Jafarpour, 2010). Consequently, proper selection of a regularization method is essential in reservoir parameter estimation problems. Alternatively, it is also possible to reduce the number of uncertain parameters by reparametrization of the problem in such a way that adjustments to the model variables are made in a much lower dimensional space (Oliver and Chen, 2011).

Previously in this section we have shown that penalizing deviations from a prior model in Bayesian framework can be misleading, when we have a wrong prior information. But there are different alternatives to restore well-posedness. The objective of this section is to investigate the possibility of finding "unknown unknowns" by applying different history matching formulations. In this section two alternative objective functions are used for parameter estimation purposes. First, we investigate the possibility of under-modeling detection using the discrete cosine transform as a parameterization technique as proposed by Li and Jafarpour (2010). Secondly, we use a regularized objective function using total variation regularization to investigate to possibility of detecting under-modeling.

3.6.1. DISCRETE COSINE TRANSFORM (DCT)

Li and Jafarpour (2010) proposed a method for reservoir parameter estimation by formulating the solution in a compressive basis. They used compression transform techniques such as the discrete cosine and wavelet transforms for a compact representation of the most significant information in geological formations. In this section we reformulate our objective function in terms of reduced order transformed parameter space using DCT as the sparse bases. Consequently the unregularized objective function in transformed parameter space can be written as,

$$J(\mathbf{z}) = \left[(\mathbf{d} - \mathbf{h}(\mathbf{\Phi z}))^T \mathbf{P}_d^{-1} (\mathbf{d} - \mathbf{h}(\mathbf{\Phi z})) \right], \tag{3.14}$$

where $\mathbf{z}$ is the vector of the expansion coefficients, which represent physical model parameter vector $\mathbf{m}$ in a subspace defined by the basis function $\mathbf{\Phi}$,

$$\mathbf{m}_{n \times 1} = \mathbf{\Phi}_{n \times n} \mathbf{z}_{n \times 1}. \tag{3.15}$$

If the parameter $\mathbf{m}$ has a sparse representation in $\mathbf{\Phi}$, then $\mathbf{m}$ can be approximated by only $s << n$ out of n terms in the basis function (Khaninezhad and Jafarpour, 2014). In this case equation(3.15) can be written as,

$$\mathbf{m}_{n \times 1} \cong \mathbf{\Phi}_{n \times s} \mathbf{z}_{s \times 1}. \tag{3.16}$$

Note that in this study we do not use a regularization term in our formulation in order to only investigate the possibility of under-modeling detection in reduced order parameter space.

3.6.1.1. NUMERICAL EXPERIMENTS

Numerical twin experiments are conducted to test the effect of DCT reparameterization on reservoir parameter estimation in the presence of a missing geological feature (sealing fault). The truth case with a flow barrier as described in section 3.3 is used to generate historical data. Again the flow barrier is missing in our starting model. For parameter estimation purposes we try to minimize equation (3.14). Two different experiments are conducted using 49 and 100 basis elements (out of 441).

The left picture of Figure 3.22 shows the updated permeability field, which is obtained by minimizing equation (3.14) and using 49 basis elements. The right picture of Figure 3.22 shows the updated permeability field using 100 basis elements.

As can be seen from Figure 3.22 in both cases a low permeable band is visible in the updated permeability fields.

3.6.2. TOTAL VARIATION REGULARIZATION

Total variation regularization is defined as integral of the absolute gradient of the signal. Total variation term penalizes highly oscillatory solutions while allowing jumps in the regularized solution (Vogel, 2002). For a discrete parameter space, $\mathbf{m}$ of size of $N_x \times N_y$ where N_x is the number of gridblocks in the X direction and N_y is the number of gridblocks in Y direction, the total variation in two dimensions can be defined as,
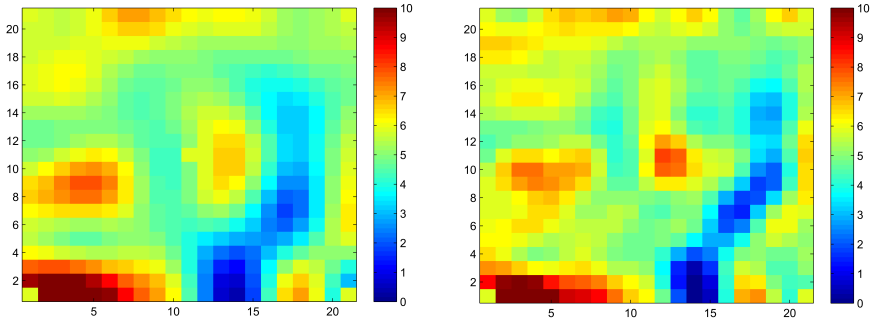
Figure 3.22: Updated permeability field using 49 basis functions (left), updated permeability field using 100 basis functions (right).

$$R(\mathbf{m}) = \sum_{i=1}^{N_x} \sum_{j=1}^{N_y} \sqrt{|m_{i+1,j} - m_{i,j}|^2 + |m_{i,j+1} - m_{i,j}|^2}. \tag{3.17}$$

Subsequently the objective function with a total variation regularization term can be written as,

$$J(\mathbf{m}) = (\mathbf{d} - \mathbf{h}(\mathbf{m}))^T \mathbf{P}_d^{-1} (\mathbf{d} - \mathbf{h}(\mathbf{m})) + \alpha R(\mathbf{m}). \tag{3.18}$$

where α is a regularization parameter that balances the weight given to the regularization term and the data misfit term. In this study we use numerical perturbation to calculate the derivative of the regularization term.

3.6.2.1. NUMERICAL EXPERIMENTS

Numerical twin experiments are conducted to test the effect of total variation regularization on reservoir parameter estimation in the presence of a missing geological feature (sealing fault). The truth case with a flow barrier as described in section 3.3 is used to generate historical data. Again the flow barrier is missing in our starting model. For parameter estimation purposes we try to minimize equation (3.18). Figure 3.23 shows the updated permeability field after minimization process.

As can be seen in Figure 3.23 the low permeable band is better preserved in the updated permeability field compared to the other regularization methods.

3.7. CONCLUSIONS

In this chapter several twin experiments were conducted and unregularized parameter estimation were applied to update uncertain parameters in a simple 2D reservoir model that contained a major flow-relevant deficiency in the form of a missing high- or low-permeability feature. We found that, for these examples,

- Updating in a Bayesian framework results in updates close to the prior, without any indication of the missing feature.
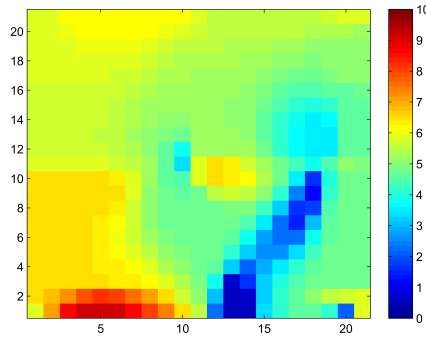
Figure 3.23: Updated permeability field using total variation regularization.

- Updating without regularization enables us to identify the presence and the location of the missing flow-relevant feature in the model, but not the correct magnitude.

- The identifiability of the presence and location deteriorates with increasing noise levels in the data.

- When the flow-relevant feature is located closer to the producer its presence and location seem to become more identifiable.

Next, to investigate these findings, we performed a quantitative identifiability analysis of the examples using a dimensionless sensitivity matrix in order to analyze the sensitivity of the system output (in the form of total flow rates in the wells) to the system parameters (the grid block permeabilities). From the results we conclude that

- The output of these examples is more sensitive to a flow-relevant feature when the feature is closer to a producer.

- As the noise level increases the singular values of the corresponding sensitivity matrix decrease and the parameter estimation solutions become more dominated by noise.

Moreover, discrete cosine transform (DCT) reparameterization and total variation regularization have been used to restore well-posedness in reservoir parameter estimation problems. We have shown that when penalizing the deviations from a prior model can be misleading in an under-modeling situations these two alternative methods are able to restore a missing flow-relevant feature.

We conclude that, for the examples considered, the application of unregularized reservoir parameter estimation provides a means to identify the presence and location of significant model deficiencies, in line with the 'model maturation' concept proposed in Joosten et al. (2011). Further analysis, using larger-scale models and more complex flow-relevant features, will be required to determine the limits of validity of this concept.

4

IDENTIFIABILITY OF FLOW-RELEVANT FEATURES

C LASSIC identifiability analysis of flow barriers in incompressible single-phase flow reveals that it is not possible to identify the location and permeability of low-perm barriers from production data (well bore pressures and rates), and that only averaged reservoir properties in-between wells can be identified. We extend the classic analysis by including compressibility effects. We use two approaches: 1) a twin-experiment with synthetic production data for use with a time-domain parameter estimation technique, and 2) a transfer function formalism in the form of bilaterally coupled four-ports allowing for an analysis in the frequency domain. We investigate the identifiability, from noisy production data, of the location and the magnitude of a low-permeable barrier to slightly-compressible flow in a one-dimensional configuration. We use an unregularized adjoint-based optimization scheme for the numerical time-domain estimation, using various levels of sensor noise, and confirm the results using the semi-analytical transfer function approach. Both the numerical and semi-analytical results show that it is possible to identify the location and the magnitude of the permeability in the barrier from noise-free data. By introducing increasingly higher noise levels the identifiability gradually deteriorates, but the location of the barrier remains identifiable for much higher noise levels than the permeability value. The shape of the objective function surface, in normalized variables, indeed indicates a much higher sensitivity of the well data to the location of the barrier than to its magnitude. These theoretical results appear to support the empirical finding that unregularized gradient-based history matching in large reservoir models, which is well known to be a severely ill-posed problem, may lead to useful results in the form of model parameter updates having unrealistic magnitudes but indicating the correct location of model deficiencies.

4.1. INTRODUCTION

Estimating reservoir parameters from measured data is an ill-posed inverse problem due to the large number of parameters and the limited available data (Shah et al., 1978; Oliver et al., 2008). Consequently, it is important to understand which parameters can be estimated with reasonable accuracy from the available data. This aspect can be addressed as determining the identifiability of the parameters. From a systems and control theory perspective, the transient response of a dynamic system contains information about dynamics-related properties of a system. Consequently, including compressibility effects (leading to a transient response) can result in a more accurate reservoir parameter estimation than just considering the steady-state response. The pressure behavior of a slightly-compressible single-phase fluid in a reservoir can be described accurately by the diffusivity equation. Theoretically, the transient pressure response of every point in a reservoir to, e.g., a step or impulse input may contain information about reservoir boundaries and reservoir heterogeneities (Grader and Horne, 1988; Van Doren, 2010). However certain parameters have a more significant effect on this transient response than others, and in many cases a unique identification of parameters is not possible. Subsequently, by investigating the effect of different parameters on the dynamic behavior we can understand which parameters are more identifiable from the available data. On the other hand, presence of noise in the data may hamper the identifiability of such parameters and can result in unrealistic parameter estimates (Dogru et al., 1977). Hence, it is important to also investigate the effect of noise on identifiability of different parameters.

Identifiability of reservoir heterogeneity has been studied by many authors both from a classic well testing and from a systems and control perspective; see, e.g., Stallman and Brown (1951), Watson et al. (1984), Yaxley (1987), Grader and Horne (1988), Feitosa et al. (1994), Oliver (1996), Van Doren et al. (2008), Zandvliet et al. (2008), Ahn and Horne (2010) and Van Doren (2010). The concept of identifiability as used in systems and control theory can loosely refer to the question whether parameter changes can be observed in the model output signal (Van Doren, 2010). Moreover, the concept of structural identifiability is, loosely speaking, concerned with the question whether it is possible to infer the magnitude of model parameters at all from input-output data, assuming an optimally chosen, 'persistently exciting' input. For a more precise, mathematical definition of (structural) identifiability as applied to porous media flow, see Van Doren (2010). Stallman and Brown (1951) analyzed the pressure response of a constant-rate well and presented a log-log type curves for constant pressure boundaries as well as impermeable linear boundaries. Watson et al. (1984) investigated the identifiability of estimates of two-phase reservoir properties in history matching. They concluded that for single-phase incompressible flow, only the harmonic average of the permeability distribution is identifiable and subsequently the presence of the saturation distribution is essential to identify the absolute permeability spatial distribution. Yaxley (1987) investigated the effects of a partially communicating linear fault on transient pressure behavior. Grader and Horne (1988) and Ahn and Horne (2010) considered (slightly) compressible flow and used well testing related methods such as interference testing and pulse testing to investigate the detectability of reservoir heterogeneities. They showed that there is sometimes

information about the distance between wells and flow-relevant features (e.g. reservoir boundaries, impermeable subregions or permeability distribution) in the data, although to a limited extent due to the diffusive nature of pressure transients.

The objective of this chapter is to investigate the identifiability of location and magnitude of a flow barrier in slightly compressible single-phase flow by analyzing the effect of this heterogeneity on dynamical behavior of the flow. The motivation stems from a paper by Joosten et al. (2011) who showed that sometimes the application of unregularized reservoir parameter estimation still appears to have added value. They argued, based on numerical examples, that localized unrealistic parameter values can be used as an indicator of model errors in the underlying reservoir model, a concept which they named "model maturation". In a follow-up study, Kahrobaei et al. (2014) showed that the application of unregularized reservoir parameter estimation may sometimes indeed give an indication of the location of significant missing features in the model. In this chapter we further analyze this phenomenon by addressing the identifiability of flow-relevant features. In particular, we apply two approaches to study the possibility of detecting a low-permeable barrier from the observations (outputs of the system). In the first approach we conduct three different twin-experiments with synthetic production data contaminated with different noise levels in the time domain. In our twin experiments an unregularized parameter estimation is applied to update uncertain parameters (grid block permeabilities) in a one-dimensional (1D) reservoir model that contains a major deficiency in the form of a missing low permeability feature. In the second approach we develop an analytical method to explain our time-domain findings. In this approach we consider flow through porous media as a linear system and develop a method that gives an analytical expression for the dynamic characteristics of the system as a function of the system's geometric properties, heterogeneity etc. in the frequency domain. This solution is obtained based on a transfer function formalism applied to a series of bilaterally coupled porous media models.

4.2. TIME-DOMAIN TWIN EXPERIMENTS

We perform three 'twin experiments'. They all use the same 'truth model' to generate synthetic data, but the resulting data are contaminated with different noise levels. The first experiment involves the assimilation of noise-free production data, while in the last two experiments we assimilate noisy production data.

4.2.1. SYNTHETIC TRUTH

Consider one-dimensional single-phase flow of a slightly compressible fluid through a porous medium. The domain has a homogenous permeability distribution with a low permeable barrier in between. The size of the reservoir is 500 m × 50 m × 2 m, which is divided into 50 grid blocks. Fluid compressibility is 1×10^{-7} Pa^{-1} and fluid viscosity is 1×10^{-3} Pa s. The reservoir is produced with an injector at the left side and a producer at the right side. A low-permeable barrier with a width of 30 m, is located at 350 m from the injector. The background permeability is 300 mD and the permeability of the barrier is 0.1 mD. The reservoir has a uniform porosity of 0.2. The initial pressure is 300 MPa. The

producer is operating at a bottomhole pressure of 250 MPa and the injector at a constant flow rate of 0.002 m^3/s. The reservoir is simulated for 1000 days and we measure the flow rates in the producer on a daily basis. Figure 4.1 shows the permeability field of the reservoir with its low permeable barrier.

Figure 4.1: Permeability field of a one-dimensional homogenous reservoir model with a low-permeable barrier. Permeability values are expressed as the natural logarithm of permeability in mD. The blue and orange dots indicate the injector and the producer respectively.

4.2.2. Starting Reservoir Model
The low-permeable barrier in the reservoir is missing in the starting model. All remaining parameters in the starting model are identical to those of the 'truth' case. Figure 4.2 depicts the uniform permeability field of the starting model with a constant permeability of 300 mD.

Figure 4.2: Permeability field of the starting model. Permeability values are expressed as the natural logarithm of permeability in mD. The blue and orange dots indicate the injector and the producer respectively.

For parameter estimation purposes we try to minimize an unregularized mismatch objective function, given by equation (3.2). Minimization of the objective function is achieved by adjustment of the model parameters $\mathbf{m}$. For the present study we use an in-house reservoir simulator with adjoint functionality to calculate the gradients of the objective function (Kraaijevanger et al., 2007). We use the limited-memory Broyden Fletcher Goldfarb Shanno (LBFGS) method to minimize the objective function (Gao and Reynolds, 2006).

4.2.3. Experiment #1: Parameter Estimation Based on Noise-Free Measurements
In the first twin experiment, parameter estimation is performed starting from the uniform reservoir model, depicted in Figure 4.2, based on perfect (noise-free) production data. Figure 4.3 shows the updated permeability field after parameter estimation. For this experiment the covariance matrix is chosen as an identity matrix.

Table 4.1 lists the grid block numbers and corresponding permeability values of the low permeable barrier in the 'truth' case and the updated model (Figure 4.1 and Figure 4.3 respectively).

As can be seen in Table 4.1, the grid block numbers and the grid block permeabilities of the low permeable barrier in the updated model are exactly the same as those in the 'truth' case.

Figure 4.3: Updated permeability field of the 1D reservoir model for experiment #1. Permeability values are expressed as the natural logarithm of permeability in mD.

Table 4.1: Grid block numbers and permeabilities of the low permeable barrier in the 'truth' and the updated model.

Model	GB. No.	Permeability [mD]
Truth parameters	36	0.1
	37	0.1
	38	0.1
Updated parameters	36	0.1
	37	0.0997
	38	0.1

4.2.4. EXPERIMENT #2: PARAMETER ESTIMATION BASED ON NOISY MEASUREMENTS: HIGH SIGNAL TO NOISE RATIO

In second twin experiment parameter estimation is performed starting from the same reservoir model as experiment #1 but based on noisy production data. Errors are generated by sampling from a Gaussian distribution with zero mean and a standard deviation equal to 1 m^3/day. Negative production rates, after the addition of noise, are reset to zero. It is assumed that the measurements were affected by independent noise, which results in a diagonal covariance matrix with equal-magnitude elements for the observation errors. The same covariance matrix was used in the objective function defined by equation (3.2). Figure 4.4 depicts the updated permeability field after parameter estimation based on noisy data (with known covariance).

Figure 4.4: Updated permeability field of the 1D reservoir model for experiment #2. Permeability values are expressed as the natural logarithm of permeability in mD.

Table 4.2 lists the grid block numbers and corresponding permeability values of the low permeable barrier in the 'truth' case and the updated model for experiment #2.

As can be seen in Table 4.2, in the experiment with noisy measurements the positions of the low-permeable barriers in the 'truth' case and the updated model are exactly the same but the permeability value of the corresponding grid blocks in the updated model

Table 4.2: Gridblock numbers and permeabilities of the low permeable barrier in the 'truth' and the updated model.

Model	GB. No.	Permeability [mD]
	36	0.1
Truth parameters	37	0.1
	38	0.1
	36	0.1036
Updated parameters	37	0.1206
	38	0.08

are not as accurate as those obtained in the noise-free experiment.

4.2.5. EXPERIMENT #3: PARAMETER ESTIMATION BASED ON NOISY MEASUREMENTS: LOW SIGNAL TO NOISE RATIO

In the third twin experiment the amount of error in the data is increased in comparison with experiment #2. In this case, the errors are generated from a Gaussian distribution with zero mean and a standard deviation equal to 10 m^3/day using the same approach as in the previous experiment. Figure 4.5 depicts the updated permeability field of the 1D reservoir model after parameter estimation.

Figure 4.5: Updated permeability field of the 1D reservoir model for experiment #3. Permeability values are expressed as the natural logarithm of permeability in mD.

Table 4.3 lists the grid block numbers and corresponding permeability values of the low permeable barrier in the 'truth' case and the updated model for experiment #3.

As can be seen in Table 4.3, by increasing the noise level in the measurements, the positions of the grid blocks with the lowest permeabilities in the updated model and the truth case are still identical, but the permeability values of those grid blocks are now significantly different. The harmonic average over all gridblocks based on true permeability distribution is 1.65, and for the noise-free experiment, the low-level noise experiment and the high-level noise experiment they are 1.65, 1.66 and 1.30 respectively. We note that the deviation of our estimates from the true values is caused by random noise in the measurements. Different realizations of the measurement noise are used, in which in all of results the gridblock with lowest permeability magnitude is in the location of the barrier (gridblock 36, 37 and 38). The mean and the standard deviation of the harmonic average over these three gridblocks based on 10 different noise realizations are 0.08 and 0.0035 mD respectively.

Table 4.3: Gridblock numbers and permeabilities of the low permeable barrier in the 'truth' and the updated model.

Model	GB. No.	Permeability [mD]
	36	0.1
Truth parameters	37	0.1
	38	0.1
	36	0.026
Updated parameters	37	19.15
	38	89.6

4.3. TRANSFER FUNCTION REPRESENTATION

To further analyze the behavior that was observed in our 1D twin-experiments in the time-domain, we conduct 1D experiments using a transfer function formalism to characterize the identifiability of the location and magnitude of model deficiencies (absence of flow barriers). We use a two-port network approach which results in a lumped parameter representation of our system (Carslaw and Jaeger, 1959). The structure of the 1D initial-boundary value problem allows for the input to output representation of the system in terms of pressure and flow rate at two points in the spatial domain, mapped by a linear transformation.

4.3.1. MODEL DESCRIPTION

The 1D reservoir model that was described in section 4.2.1 can be considered as a system that consists of three blocks. The total length of the domain and the length of the middle block are known. The length of the first block of the domain is unknown, resulting in an unknown position of the middle block. Note that length of the third block is a function of the length of the first block, since the total length of the domain is constant. The middle block works as a barrier to flow from point 1 to point 4; see Figure 4.6.
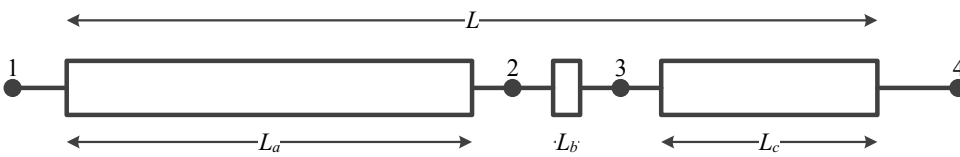
Figure 4.6: Schematic representation of two one-dimensional domains separated by a low permeable barrier.

4.3.2. GOVERNING EQUATIONS

The pressure behavior of a slightly-compressible single-phase fluid in a reservoir can be described by the diffusivity equation. The pressure diffusion equation for linear flow

between two points can be written as

$$\frac{\partial p(x,t)}{\partial t} = \eta \frac{\partial^2 p(x,t)}{\partial x^2}, \tag{4.1}$$

in which η is defined as hydraulic diffusivity,

$$\eta = \frac{k}{\varphi \mu c_t}, \tag{4.2}$$

where k is permeability, φ is porosity, μ is viscosity and c_t is total compressibility. Moreover, the flow rate for linear flow can be written as

$$q(x,t) = -A \frac{k}{\mu} \frac{\partial p(x,t)}{\partial x}, \tag{4.3}$$

where A is the surface area.

Note that wells in Figure 4.6 are to be imagined as (infinite conductivity) fractures fully penetrating a channel of constant cross-section A, and that skin, wellbore storage and near-well radial flow convergence are neglected.

4.3.3. DIMENSIONLESS VARIABLES

To transform equation (4.1) and equation (4.3) into dimensionless equations, the following dimensionless variables are defined:

- Dimensionless length:

$$\xi = \frac{x}{L}, \tag{4.4}$$

where L is total constant length of the first and the last blocks of Figure 4.6.

- Dimensionless pressure:

$$\pi = \frac{p - p_i}{\hat{p}}, \tag{4.5}$$

where $\hat{p}$ is pressure at the outlet boundary and p_i is initial pressure.

- Dimensionless time:

$$\tau = \frac{kt}{\mu c_t \varphi L^2}. \tag{4.6}$$

Using these dimensionless variables, we can rewrite equations (4.1) and (4.3) in dimensionless form:

$$\frac{\partial \pi}{\partial \tau} = \frac{\partial^2 \pi}{\partial \xi^2}, \tag{4.7}$$

$$\theta = -\alpha \frac{\partial \pi}{\partial \xi}, \tag{4.8}$$

where θ is dimensionless flow rate defined as

$$\theta = \frac{q}{\hat{q}},\tag{4.9}$$

and α is a dimensionless number defined as

$$\alpha = \frac{Ak\hat{p}}{L\mu\hat{q}},\tag{4.10}$$

in which $\hat{q}$ is the flow rate at the inlet boundary.

In this study equation (4.7) and equation (4.8) will be applied in three different regions of constant permeability.

4.3.4. TRANSFER FUNCTION DERIVATION

In order to find input-output relations of the system depicted in Figure 4.6, first the transfer functions of each block are derived and then they are coupled together to obtain transfer functions that describe the entire system. In the next subsection we derive the transfer functions for the first block of the system depicted in Figure 6. Similar derivations would apply to the other blocks as well.

4.3.4.1. INPUT-OUTPUT RELATIONS OF ONE BLOCK OF THE SYSTEM

By applying a Laplace transform to equation (4.7) we obtain

$$\frac{\partial^2}{\partial \xi^2}\Pi(\xi, s) - s\Pi(\xi, s) = 0.\tag{4.11}$$

Equation (4.11) has a solution of the form

$$\Pi(\xi, s) = C_1 e^{\xi\sqrt{s}} + C_2 e^{-\xi\sqrt{s}}.\tag{4.12}$$

Moreover, equation (4.8) can also be written in the Laplace domain as follows:

$$\Theta(\xi, s) = -\alpha C_1 \sqrt{s}e^{\xi\sqrt{s}} + \alpha C_2 \sqrt{s}e^{-\xi\sqrt{s}},\tag{4.13}$$

where functions C_1 and C_2 can be determined by requiring the solution to satisfy the boundary conditions which are chosen as flow rate at the left side and pressure at the right side of the block, i.e.,: $\Theta(\xi, s) = \Theta(\xi_1, s)$ at $\xi = \xi_1$ and $\Pi(\xi, s) = \Pi(\xi_2, s)$ at $\xi = \xi_2$. Consequently, solving for C_1 and C_2 leads to:

$$C_1 = \frac{1}{\Lambda(s) + \Lambda^{-1}(s)}\Pi(\xi_2, s) - \frac{1}{\alpha\sqrt{s}}\frac{\Lambda^{-1}(s)}{\Lambda(s) + \Lambda^{-1}(s)}\Theta(\xi_1, s),\tag{4.14}$$

$$C_2 = \frac{1}{\Lambda(s) + \Lambda^{-1}(s)}\Pi(\xi_2, s) + \frac{1}{\alpha\sqrt{s}}\frac{\Lambda(s)}{\Lambda(s) + \Lambda^{-1}(s)}\Theta(\xi_1, s),\tag{4.15}$$

in which

$$\Lambda(s) = e^{\xi_2\sqrt{s}}.\tag{4.16}$$

At the boundaries we have the following output variables:

$$\Pi(\xi_1, s) = C_1 + C_2, \tag{4.17}$$

$$\Theta(\xi_2, s) = -\alpha C_1 \sqrt{s} \Lambda(s) + \alpha C_2 \sqrt{s} \Lambda^{-1}(s). \tag{4.18}$$

Inserting values of C_1 and C_2 from equations (4.14) and (4.15) in equations (4.17) and (4.18) gives the final solutions:

$$\Pi(\xi_1, s) = \frac{2}{\Lambda(s) + \Lambda^{-1}(s)} \Pi(\xi_2, s) + \frac{1}{\alpha\sqrt{s}} \frac{\Lambda(s) - \Lambda^{-1}(s)}{\Lambda(s) + \Lambda^{-1}(s)} \Theta(\xi_1, s), \tag{4.19}$$

$$\Theta(\xi_2, s) = \alpha\sqrt{s} \frac{\Lambda^{-1}(s) - \Lambda(s)}{\Lambda(s) + \Lambda^{-1}(s)} \Pi(\xi_2, s) + \frac{2}{\Lambda(s) + \Lambda^{-1}(s)} \Theta(\xi_1, s). \tag{4.20}$$

4

Subsequently $\Theta(\xi_2, s)$ and $\Pi(\xi_1, s)$ can be written as a function of the boundary conditions:

$$\left[\begin{array}{c} \Theta(\xi_2, s) \\ \Pi(\xi_1, s) \end{array} \right] = \left[\begin{array}{cc} A_{11} & A_{12} \\ A_{21} & A_{22} \end{array} \right] \left[\begin{array}{c} \Theta(\xi_1, s) \\ \Pi(\xi_2, s) \end{array} \right], \tag{4.21}$$

where A_{ij} are the transfer functions of the first block, which explain the input-output relations as a function of model parameters. These transfer functions can be derived as

$$A_{11} = \frac{2}{e^{\xi_2\sqrt{s}} + e^{-\xi_2\sqrt{s}}} = \frac{1}{\cosh(\xi_2\sqrt{s})}, \tag{4.22}$$

$$A_{12} = \alpha\sqrt{s} \frac{e^{-\xi_2\sqrt{s}} - e^{\xi_2\sqrt{s}}}{e^{\xi_2\sqrt{s}} + e^{-\xi_2\sqrt{s}}} = -\alpha\sqrt{s} \tanh(\xi_2\sqrt{s}), \tag{4.23}$$

$$A_{21} = \frac{1}{\alpha\sqrt{s}} \frac{e^{\xi_2\sqrt{s}} - e^{-\xi_2\sqrt{s}}}{e^{\xi_2\sqrt{s}} + e^{-\xi_2\sqrt{s}}} = \frac{1}{\alpha\sqrt{s}} \tanh(\xi_2\sqrt{s}), \tag{4.24}$$

$$A_{22} = \frac{2}{e^{\xi_2\sqrt{s}} + e^{-\xi_2\sqrt{s}}} = \frac{1}{\cosh(\xi_2\sqrt{s})}. \tag{4.25}$$

In this way we can derive the transfer functions for each block of our system.

4.3.4.2. INPUT-OUTPUT RELATIONS OF THE ENTIRE SYSTEM

By coupling the transfer functions of the three blocks we can derive the input-output relations for the entire system. Figure 4.7 depicts the coupled model in block diagram representation for our 1D reservoir model, where we used the letters A, B and C to indicate the three consecutive blocks of Figure 4.6.

Each block of Figure 4.7 has an input-output relation in the form of equation (4.21). Consequently, by performing matrix multiplications, we can find the transfer functions that represent the input-output relations for the entire system. The matrix form of the input-output relations can be written as

$$\left[\begin{array}{c} \Theta(\xi_4, s) \\ \Pi(\xi_1, s) \end{array} \right] = \left[\begin{array}{cc} S_{11} & S_{12} \\ S_{21} & S_{22} \end{array} \right] \left[\begin{array}{c} \Theta(\xi_1, s) \\ \Pi(\xi_4, s) \end{array} \right], \tag{4.26}$$
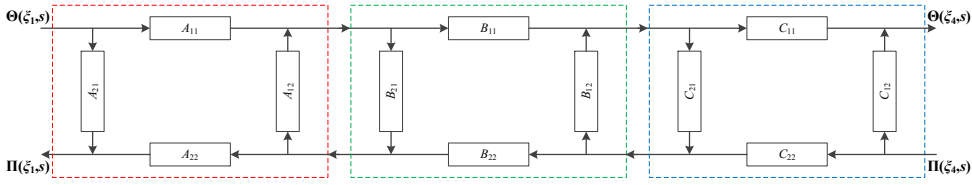
Figure 4.7: Coupled model in block diagram representation for the model depicted in Figure 4.6.

where the elements S_{ij} are given by

$$S_{11} = -\frac{A_{11}B_{11}C_{11}}{C_{21}\left(B_{12} + A_{12}B_{11}B_{22} - A_{12}B_{12}B_{21}\right) + A_{12}B_{21} - 1}, \tag{4.27}$$

$$
\begin{aligned}
S_{12} = &- [C_{12} - A_{12}C_{12}B_{21} + C_{11}C_{22}B_{12} - C_{12}C_{21}B_{12} + \\
&A_{12}C_{11}C_{22}B_{11}B_{22} - A_{12}C_{11}C_{22}B_{12}B_{21} - A_{12}C_{12}C_{21}B_{11}B_{22} + A_{12}C_{12}C_{21}B_{12}B_{21}] \times \\
&[A_{12}B_{21} + C_{21}B_{12} + A_{12}C_{21}B_{11}B_{22} - A_{12}C_{21}B_{12}B_{21} - 1]^{-1},
\end{aligned} \tag{4.28}
$$

$$
\begin{aligned}
S_{21} = &- [A_{21} + A_{11}A_{22}B_{21} - A_{12}A_{21}B_{21} - A_{21}C_{21}B_{12} + \\
&A_{11}A_{22}C_{21}B_{11}B_{22} - A_{11}A_{22}C_{21}B_{12}B_{21} - A_{12}A_{21}C_{21}B_{11}B_{22} + A_{12}A_{21}C_{21}B_{12}B_{21}] \times \\
&[A_{12}B_{21} + C_{21}B_{12} + A_{12}C_{21}B_{11}B_{22} - A_{12}C_{21}B_{12}B_{21} - 1]^{-1},
\end{aligned} \tag{4.29}
$$

$$S_{22} = -\frac{A_{22}C_{22}B_{22}}{A_{12}\left(B_{21} + C_{21}B_{11}B_{22} - C_{21}B_{12}B_{21}\right) + C_{21}B_{12} - 1}, \tag{4.30}$$

where A_{ij}, B_{ij} and C_{ij} are the transfer functions of the three consecutive blocks of Figure 4.6. Consequently the block diagram of the system (Figure 4.7) can be simplified to the configuration depicted in Figure 4.8.
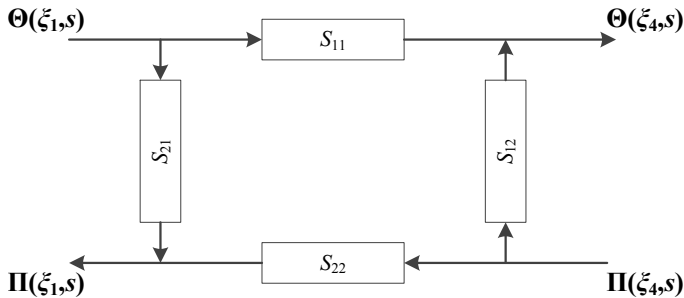
Figure 4.8: Modified block diagram representation for the model depicted in Figure 4.6.

4.4. EFFECT OF LOCATION AND MAGNITUDE OF BARRIER ON DYNAMIC SYSTEM OUTPUT

In the time-domain twin-experiments we have used flow rates in the injector and pressures in the producer as inputs, and flow rates in the producer as outputs. Therefore, we can simplify the configuration depicted in Figure 4.8 in such a way that the single output of our system, $\Theta(\xi_4, s)$, is influenced by two inputs: $\Theta(\xi_1, s)$ and $\Pi(\xi_4, s)$. Consequently the input-output relation of the system is described by the transfer functions S_{11} and S_{12} only; see Figure 4.9.
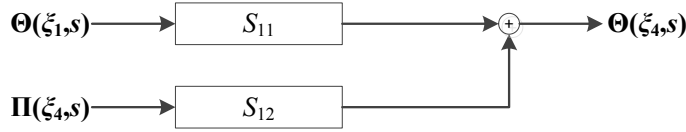
Figure 4.9: Input-output relation in the reservoir system.

With the aid of equation (4.26) we can now write an expression for the system output as follows:

$$\Theta(\xi_4, s) = \Theta(\xi_1, s) S_{11} + \Pi(\xi_4, s) S_{12}. \tag{4.31}$$

Because we have used step inputs in the time-domain twin-experiments, the dimensionless form of our inputs in the Laplace domain can be written as

$$\Theta(\xi_1, s) = \frac{1}{s}, \tag{4.32}$$

$$\Pi(\xi_4, s) = \frac{1}{s}. \tag{4.33}$$

By substituting equation (4.32) and equation (4.33) in equation (4.31) the output of the system can be written as

$$\Theta_{out} = \Theta(\xi_4, s) = \frac{1}{s} S_{11} + \frac{1}{s} S_{12} = \frac{1}{s}(S_{11} + S_{12}). \tag{4.34}$$

Note that all the variables, and therefore the transfer functions, are dimensionless. At this stage we can replace s in equation (4.34) with $j\omega_D$, where j is the imaginary unit and ω_D is dimensionless frequency. The dimensionless sampling frequency is defined according to sampling dimensionless time in our time-domain experiments. This will result in a frequency response description of our system. Now we are able to investigate the effect of location and magnitude of the middle block (the flow barrier) on the output of our system. To perform a sensitivity analysis and a parameter estimation, which are presented in the next sections, we define a 'truth' case, with parameters listed in Table 4.4. The 'truth' parameters are equivalent to the parameters of the time-domain 'truth' case. Moreover, in our experiments the dimensionless frequency range is chosen between 0.6 and 600. The analytical 'truth' case is used to generate synthetic measurements for parameter estimation purposes in section 4.5.

Table 4.4: Truth parameter values

Parameters	Magnitude	Unit
$L_a/L = \xi_2 - \xi_1$	0.7	-
$L_b/L = \xi_3 - \xi_2$	0.06	-
α_a, α_c	0.75	-
α_b	0.0025	-

4.4.1. EFFECT OF LOCATION OF A FLOW BARRIER

In this case we vary the location (ξ_2) of the middle block of the system, while the permeability magnitude of that block is fixed at a small value ($\alpha_b = 0.0025$), and evaluate the corresponding output of the system using equation (4.34). Figure 4.10 depicts the amplitude of the frequency response for different middle block positions at different frequencies. The dashed line in 4.10 is the amplitude of the frequency response in the absence of the flow barrier.
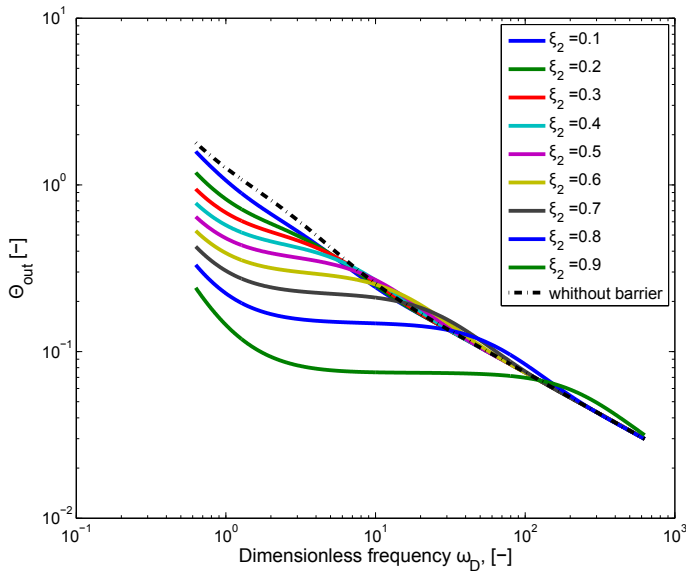
Figure 4.10: Amplitude of the frequency response for different barrier position and a fixed low barrier permeability magnitude.

As can be seen in Figure 4.10, the output of the system is quite sensitive to the location of the middle block when it has smaller magnitudes. In the other words, the location of the low permeable barrier significantly affects the output of our system. Moreover, it can be concluded from Figure 4.10 that as the barrier location is closer to the producer it has

more effect on the output.

4.4.2. EFFECT OF PERMEABILITY MAGNITUDE OF A FLOW BARRIER

In this case we vary the permeability magnitude (α_b) of the middle block of the system while its location is fixed ($\xi_2 = 0.7$). Subsequently we evaluate the corresponding frequency response of the system for different values of the middle block's permeability magnitude. Figure 4.11 depicts the frequency response for these cases. The dashed line in Figure 4.11 is the amplitude of the frequency response in the absence of the flow barrier.
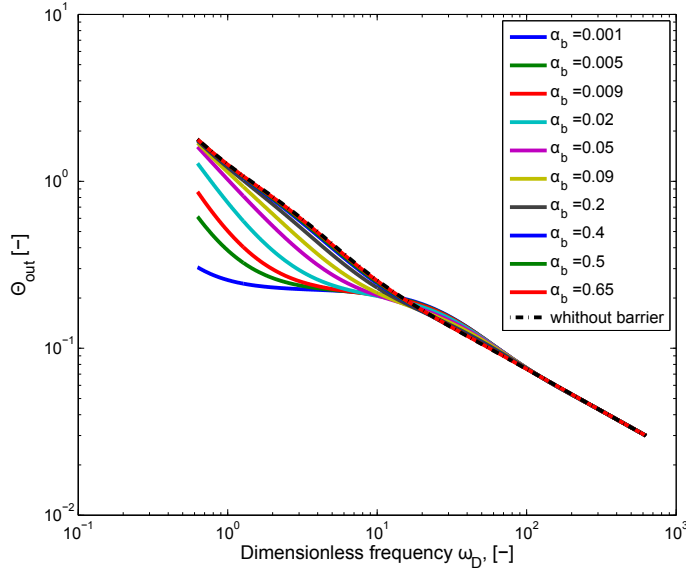
Figure 4.11: Amplitude of the frequency response for different barrier permeability magnitude and fixed location.

It can be clearly seen that as the permeability magnitude of the middle block increases i.e., as the resistance to flow decreases, the frequency response of the system becomes less sensitive to the magnitude variations.

4.5. PARAMETER ESTIMATION IN THE FREQUENCY DOMAIN

In this section we try to estimate uncertain parameters using frequency responses obtained from the transfer function of the system. In this study the location (ξ_2) and magnitude (α_b) of the middle block are considered as unknown parameters; see Figure 4.6. We try to estimate these parameters by minimizing a mismatch objective function defined as

$$V = (\Theta_{observed} - \Theta_{out}(\alpha, \xi))^T \mathbf{P}_\Theta^{-1} (\Theta_{observed} - \Theta_{out}(\alpha, \xi)), \qquad (4.35)$$

where $\Theta_{observed}$ is the 'truth' output vector, which is generated using 'truth' parameters and equation (4.34) at different frequencies by replacing s with $j\omega$. Vector Θ_{out} is the simulated output. The starting model parameters are identical to the 'truth' parameters except for the middle block location and magnitude. $\mathbf{P}_\Theta$ is the measurement error covariance matrix, which is chosen as an identity matrix in this study. Note that the derivative of the objective function can be calculated analytically and we use the limited-memory Broyden Fletcher Goldfarb Shanno (LBFGS) method to minimize the objective function. Moreover, since the data vectors (observed and model output) consist of complex numbers we can make our data real-valued by considering them as 2D data points, i.e. having real and imaginary parts (Blom and Van den Hof, 2010). Following this approach, we define an augmented data vector by stacking the real and imaginary parts of the complex-valued vectors.

4.5.1. Experiment #1: Noise-Free Parameter Estimation

In the first experiment we use noise-free measurements for parameter estimation purposes. Equation (4.35) is minimized by adjustment of the location and the magnitude of the middle block. The minimization converges in 15 iterations. The truth, starting and estimated parameter values for this experiment are listed in Table 4.5.

Table 4.5: Model parameters for experiment #1

Parameters	Truth value [-]	Starting value [-]	Estimated value [-]
ξ_2	0.7	0.4	0.7
α_b	0.0025	0.75	0.0025

It can be concluded from Table 4.5, similar to experiment #1 in time-domain, that in case of noise-free measurements we are able to retrieve the location and the magnitude of a low-perm barrier with 100% accuracy.

4.5.2. Noise Effect on Estimation of Location and Magnitude of a Low-Permeable Barrier

In presence of noise, equation (4.34) can be written as:

$$\Theta_{out} = \frac{1}{j\omega}(S_{11} + S_{12}) + v, \tag{4.36}$$

where v represents noise in the frequency domain. Note that in our experiments noise only affects the output.

4.5.2.1. Experiment #2: High Signal to Noise Ratio

In this experiment we generate white noise from the same distribution as used in section 4.2.4 for the high signal to noise ratio experiment in the time domain, and use a Fourier transform to transform the noise to the frequency domain. Subsequently, we perform

parameter estimation based on this noisy data. The minimization converges in 14 iterations. Ten different noise realizations are used to calculate the mean and the standard deviation for estimated parameters. The truth, starting, mean and standard deviation of the estimated parameter values for this experiment are listed in Table 4.6.

Table 4.6: Model parameters for experiment #2

Parameters	Truth val. [-]	Starting val. [-]	Mean est. val. [-]	Stand. dev. [-]
ξ_2	0.7	0.4	0.69	0.009
α_b	0.0025	0.75	0.0023	0.0003

It can be concluded from Table 4.6, similar to the experiment #2 in the time domain, that for a low amount of noise the location and the magnitude of the low perm barrier can be still retrieved with an acceptable accuracy.

4.5.2.2. Experiment #3: Low Signal to Noise Ratio
In this experiment we increase the amount of noise in the data. Noise is generated from the same distribution as used in section 4.2.5 for the low signal to noise ratio experiment in the time domain. A Fourier transform is used to transform the noise into the frequency-domain. Subsequently, we perform parameter estimation based on this noisy data. The minimization converges in 11 iterations. The truths, starting and mean value of the estimated parameter values for this experiment are listed in Table 4.7. Moreover, ten different noise realizations are used to calculate the standard deviation for estimated parameters.

Table 4.7: Model parameters for experiment #3

Parameters	Truth val. [-]	Starting val. [-]	Mean est. val. [-]	Stand. dev. [-]
ξ_2	0.7	0.4	0.73	0.03
α_b	0.0025	0.75	1×10^{-5}	3.7×10^{-8}

It can be interpreted from Table 4.6 and Table 4.7, that as the noise increases, the accuracy of the estimation of the magnitude parameter becomes worse while the location of the barrier is still accurate. Also these results confirm our twin experiment results in the time domain.

4.6. Visualization of the Objective Function
In this section we consider the objective function, expressed in equation (4.35), which is a function of transfer functions S_{11} and S_{12} and plot it as a function of our two uncertain parameters (location and magnitude of the barrier) in an attempt to visualize

the objective function shape and its spatial dependence on the two parameters. Figure 4.12 depicts the objective function surface in the two-variable space. The red dot in the Figure 4.12 indicates the minimum of the objective function ('truth' parameters).
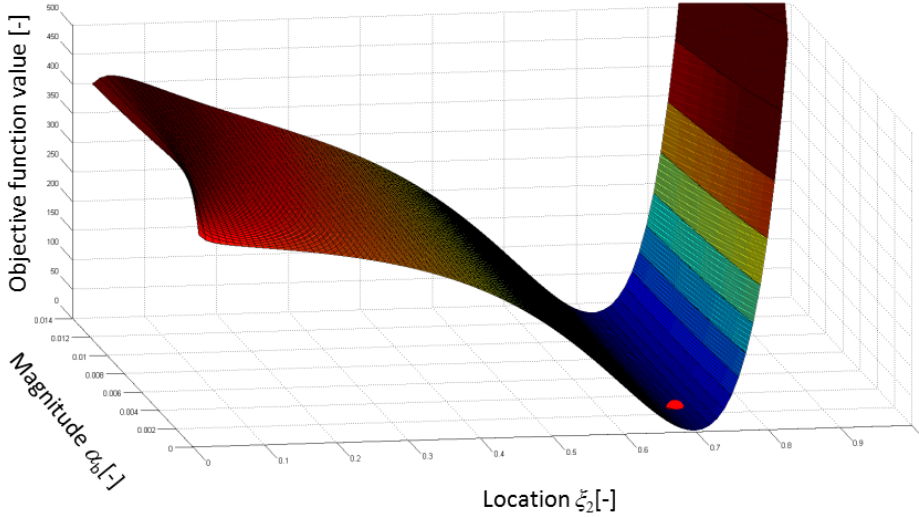
Figure 4.12: Objective function space. The red dot indicates the minimum.

If we zoom in on the vicinity of the minimum of Figure 4.12, we observe that the surface also displays a varying magnitude with a minimum in the α_b direction, see Figure 4.13. Figure 4.12 and Figure 4.13 clearly show that our objective function is more sensitive to the barrier location than to the barrier magnitude, which means that, for the presently chosen input-output configuration and input signals, the barrier location has a higher possibility to be estimated correctly from noisy data than the permeability magnitude. This behavior was indeed observed in our parameter estimation results when the amount of noise in the data was increased.

4.7. STRUCTURAL IDENTIFIABILITY

The question as to whether parameters can be uniquely identified from measured data can be considered in two ways. The first approach considers *identifiability*, i.e. the question whether or not for a specific input-output combination we can distinguish a change in any of the parameters (Van Doren, 2010). Such an identifiability analysis was performed in the previous sections where we considered a specific input-output config-uration with specific inputs and measurement errors. The second approach considers (local) *structural identifiability*., i.e. the question whether or not we can distinguish a change in any of the parameters at all from input-output data, assuming an optimally chosen, 'persistently exciting' input (Glover and Willems, 1974; Van den Hof et al., 2009). Such a structural identifiability analysis is performed in this section by considering the properties of the parameterized transfer functions, which were derived in section 4.3.
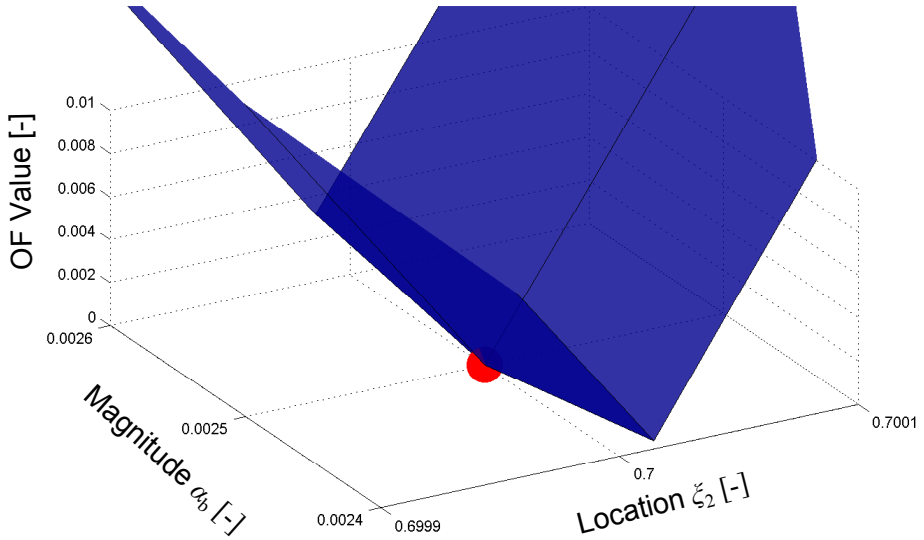
Figure 4.13: Zoomed in objective function space. The red dot indicates the minimum.

To this end we investigate the sensitivity of transfer functions S_{11} and S_{12} with respect to our uncertain parameters (barrier location and barrier magnitude) around the truth parameters. Because the parameters have different orders of magnitude, scaling will influence the identifiable parameter space. Here we scale the sensitivity vectors by the truth parameters:

$$\alpha_b = \frac{\tilde{\alpha}_b}{\alpha_{b,true}}, \tag{4.37}$$

$$\frac{\partial S}{\partial \tilde{\alpha}_b} = \alpha_{b,true} \frac{\partial S}{\partial \alpha_b}, \tag{4.38}$$

where S is the system transfer function, $\tilde{\alpha}_b$ is the scaled magnitude variable and $\alpha_{b,true}$ is the truth case magnitude.

Figure 4.14 depicts the sensitivity of the system transfer functions with respect to barrier location and barrier magnitude. It can be clearly seen that the system transfer functions are more sensitive to the barrier location than to the barrier magnitude for all frequencies considered. This result confirms the findings from the previous sections and, moreover, implies that the difference in identifiability between location and magnitude is not data-dependent but is a structural property of the system.

4.8. DISCUSSION
The time-domain examples presented in this chapter are based on experimental results for a model in which only spatially varying permeabilities are parameterized, while the
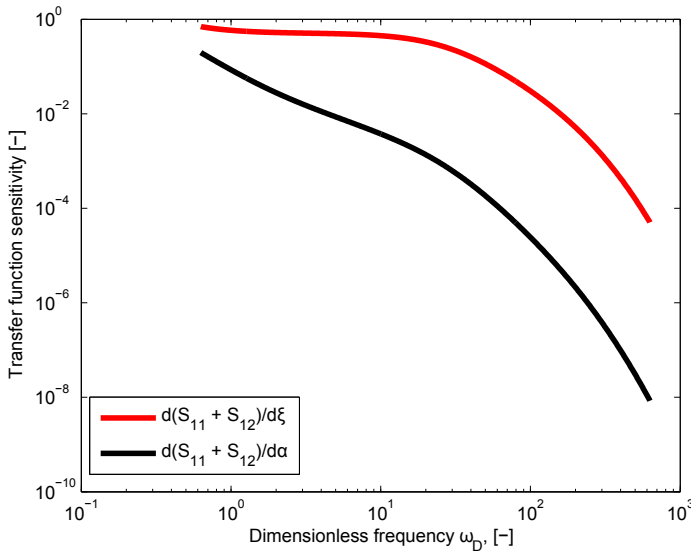
Figure 4.14: Sensitivity of transfer functions with respect to barrier location and barrier magnitude.

frequency domain examples use a model where a structured physics-based approach is applied in terms of location of the barrier, and magnitude of its permeability. We note that there exist techniques to represent the transient response to spatially varying heterogeneities in the Laplace domain with the aid of transformed variables but we did not pursue these (Levitan and Crawford, 2002). In our study the frequency domain approach uses more prior knowledge (the barrier is parameterized) than the time-domain approach (where all permeabilities are estimated separately). Secondly the first approach is really experiment-driven, while the second approach has to the capacity to say something about identifiability independent of the particular experimental data that is used. Moreover, the frequency domain approach could be used to analyze in which particular frequency region the sensitivity of the parameters is largest and to design an experiment by picking, e.g., a sinusoidal signal of that (maximum sensitive) frequency. Similar ideas have been discussed in the well testing community since the early 1970's, for purposes of "harmonic testing"; see, e.g., Hollaender et al. (2002) and references therein.

We note that we could have used the pressure in the injector as an additional output. However, in practice, wellbore pressures in injectors seem to be less frequently available for history matching studies than wellbore (or tubing head) pressures in producers. Moreover, pressures in injectors are strongly influenced by the near-wellbore effects of induced fractures which makes their value for reservoir-wide information inference limited. A similar argument could be made for pressures in the producers, which we used as known inputs, because they may be influenced by the near-wellbore effects of formation damage ("skin"). We expect that including the injector pressure in our analysis (i.e. adding transfer function S_{21} and S_{22} to Figure 4.9) would improve the identifiability whereas leaving out the producer pressure from the inputs (i.e. removing transfer

function S_{12} and only keeping S_{11} in Figure 4.9) will deteriorate the identifiability.

4.9. CONCLUSIONS

- The frequency-domain analytical solution makes it possible to investigate the effect of different parameters on the dynamic behavior of the system.

- It is possible to estimate location and magnitude of a flow barrier from noise-free measurements in slightly compressible single-phase flow.

- When the noise level in the data is increased, the location of the barrier remains relatively more identifiable than its permeability magnitude.

- The presence of noise in the data results in unrealistic permeability magnitude estimates.

- Visualization of the objective function space in the frequency-domain illustrates that the dynamic output of our system is more sensitive to the barrier location than to barrier magnitude

- A structural identifiability analysis using the transfer function approach shows that the difference in identifiability between location and magnitude is not data-dependent but is a structural property of the system.

5

STRUCTURAL MODEL UPDATING USING DYNAMIC DATA

I N spite of large uncertainties in the actual reservoir structure, structural parameters of a reservoir model are usually fixed during history matching and only the flow properties of the model are allowed to vary. This often leads to unlikely or even unfeasible property updates and possibly to a poor predictive capability of the model. In those cases it may be expected that updating of the structural parameters will improve the quality of the history match. Preferably such structural updates should be implemented in the static (geological) model, and not just in the dynamic (flow) model. In this chapter we use a gradient-based history matching method to update structural properties of the static model. We use an adjoint method to efficiently compute the derivatives of the data mismatch with respect to grid block porosities in the dynamic model and convert the corresponding volume changes to structural updates (layer thicknesses) in the static model. The underlying assumption is that the uncertainties in the layer thickness are much larger than the uncertainty in the porosities. This method is suitable for structural updating of large scale reservoir models using production data and/or time-lapse seismic or other spatially distributed data. The method is tested on a 3D synthetic model, where time-lapse as well as production data have been used to update depth of the reservoir's bottom horizon. We obtained significant improvements in the history match quality and the predictive capability of the model.

5.1. INTRODUCTION

The objective of history matching is to improve the predictive capacity of a reservoir simulation model through adjusting the model parameters until the simulated data match the historical data as closely as possible. In spite of large uncertainties in the reservoir structure, in many cases the structural model parameters are fixed during the history matching process and only the flow-related properties (e.g. permeability, porosity and net-to-gross ratio) of the model are allowed to vary. This often leads to either a poor history match or unlikely (or even unfeasible) parameter updates. Structural uncertainties can significantly affect various aspects of the reservoir model such as reservoir bulk volume and well positions and subsequently affect the predictive capability of the model (Thore et al., 2002; Seiler et al., 2010). Consequently, updating of the structural reservoir parameters by assimilation of production data and time-lapse seismic data has the potential to improve the quality of history matched models considerably. In typical computerized modeling workflows, the static (geological) model is built based on seismic interpretations, logs, cores, outcrop data, and geological insight. Subsequently, because the static model contains millions of grid cells, it is upscaled to a coarser grid during export to the dynamic (reservoir flow) model for flow simulations. Thereafter, a set of flow-related uncertain reservoir model parameters is identified and then updated using historical data. There are different disadvantages associated with this workflow. Most importantly, because of the sequential nature of the approach, the history matched reservoir models are often inconsistent with static data and display geologically unrealistic features. Furthermore, in this workflow, modeling is typically based on 'low, medium and high cases' of static reservoir parameters related to stock tank oil initially in place (STOIIP), which are generated before quantifying the dynamic outcomes, such that the flow-related uncertainties are not necessary adequately captured. A related issue is that the geological models and the upscaled flow models often contain many details that are irrelevant to the flow response. In contrast, a 'Big Loop' approach can be used to avoid the disadvantages of the traditional modeling workflow. The Big Loop approach is an integrated reservoir modeling workflow in which parameter updates are performed in the static model. Not only does this ensure more realistic updates, it also facilitates incorporating knowledge from different subsurface disciplines. Moreover, systematic criteria can be derived that help to determine which level of geologic model detail is flow-relevant or business-decision-relevant. Several authors have proposed such an integrated workflow (Chierici, 1992; Caers, 2003; Hamman et al., 2003; Gross et al., 2004; Hoffman et al., 2005; Suzuki and Caers, 2006; Elrafie et al., 2009; Seiler et al., 2009; Kaleta et al., 2012). In this chapter we do not employ a full Big Loop workflow, but, instead, we focus on updating some of the structural aspects of the static model. Such an approach to update structural parameters has been addressed in several studies before (Rivenæs et al., 2005; Suzuki et al., 2008; Schaaf et al., 2009; Seiler et al., 2010; Skjervheim et al., 2012). Rivenæs et al. (2005) generated various fault patterns and ran streamline simulations for the entire set of realizations. Next they performed model selection (rather than history matching) by ranking of the models based on the mismatch between simulated and measured production data. Suzuki et al. (2008) built a large set of models that covered a wide range of possible structural interpretations, and subsequently used stochastic search methods to find those realizations that

matched the historical production data. Schaaf et al. (2009) presented a workflow that updates both geological and simulation models at the same time using two different optimization methods. Synthetic historical production data were assimilated in their workflow. The results showed a reduction in the objective function value (i.e. the averaged mismatch between historic and simulated data) but the data match was relatively poor. Seiler et al. (2010) proposed a method to handle structural uncertainties in the reservoir model and presented a history matching workflow for updating structural model parameters with the ensemble Kalman filter (EnKF) through assimilating production data. To represent structural uncertainty an ensemble of top and bottom reservoir horizons were generated around a base-case representing the most-likely interpretation. The vertical positions of points at the top and bottom horizons were considered as the uncertain parameters which were included in an augmented state vector and updated using the EnKF method. Skjervheim et al. (2012) introduced an integrated workflow in the form of a consistent modeling chain from depth conversion to flow simulation. They also represented the uncertainty with an ensemble of realizations and used various ensemble-based assisted history matching methods such as the ensemble smoother and the EnKF. Leeuwenburgh et al. (2011) also demonstrated the feasibility of an integrated work flow for structural parameter updating using the EnKF. Although, the EnKF is an efficient method for structural surface updating, it has a number of drawbacks. The ensemble and ensemble size in the EnKF need to be selected carefully such that uncertainty is sufficiently captured. In addition, to avoid high computational costs, a relatively small ensemble is generally chosen, i.e., the number of ensemble members (typically hundred) is small compared to the number of unknown parameters (typically in the order of the number of grid blocks). The assimilation of large amounts of data (e.g. as resulting from time-lapse seismic) with relatively small ensembles could lead to spurious correlations which may lead to unphysical updates of state variables and/or model parameters, see e.g. Aanonsen et al. (2009) or Oliver and Chen (2011). Gradient-based history matching is an alternative for structural updating, which does not suffer from these drawbacks. In the studies cited above, only production measurements were assimilated in the history matching workflow. Production data provide localized spatial information about the area around the well locations and only very limited and averaged information about the regions in-between the wells. Consequently, the production data often contain insufficient information for history matching of large-scale structural parameters. On the other hand, time lapse seismic data can provide information on the areal distribution of pressure and saturation changes due to fluid production or injection. Hence, assimilation of time-lapse seismic data to estimate the structural parameters can result in more reliable results, see, e.g., Gosselin et al. (2001) or Van Essen et al. (2012). In this chapter we propose an assisted history matching workflow for structural parameter updating by assimilating time-lapse seismic data and/or production data with a gradient-based history matching method. The methodology is explained in the next section. Thereafter we present and discuss the results of three 'twin experiments' in which the method is tested with the aid of synthetic data.

5.2. Methodology

5.2.1. Adjoint Method for History Matching of Structural Models

Gradient-based history matching is an iterative procedure in which the update of the uncertain parameters is determined with the aid of the gradient vector (i.e. the vector of derivatives) of the mismatch objective function with respect to the uncertain parameters. Typically many iterations are required, and therefore it is essential to choose an efficient way to calculate the gradients. The gradients can be calculated either analytically or numerically. Methods that use numerical gradients are easy to implement but are computationally inefficient, especially when there is a large number of parameters. In the most time-consuming, deterministic, numerical variety one reservoir simulation is required for each uncertain parameter. In stochastic numerical approaches, this number can be somewhat reduced but still becomes prohibitively large for realistically sized reservoir models. On the other hand, methods that use analytical gradients, and in particular the adjoint method, are computationally much more efficient. The computational cost of the adjoint method depends on the number of objective functions and not on the number of variables, because this method provides the gradients of a given objective function with respect to all implemented variables by running a small number of simulations. Hence, among the existing methods for calculating gradients, the adjoint method is the most efficient one. The major disadvantage of the method is the significant amount of programming that is required to implement it in a reservoir simulation code. The adjoint method was first used for history matching by Chen et al. (1974) and Chavent et al. (1975), and thereafter refined by many authors. For detailed overviews, see the book of Oliver et al. (2008) or the review paper by Oliver and Chen (2011). In this study we propose to use the adjoint-method in a Big Loop approach for history matching of structural parameters.

5.2.2. Workflow

We use an in-house reservoir simulator with adjoint-functionality (Kraaijevanger et al., 2007). The simulator can provide the gradient of a mismatch function with respect to grid block parameters (e.g. permeabilities or porosities). However, in order to use gradient information for structural parameter updating we need to integrate static and dynamic modeling. To this end we use a Big Loop workflow in which the in-house dynamic simulator is coupled to commercial geological modeling software (Kaleta et al., 2012). In this workflow all the uncertain parameters are defined in the static domain. After constructing one or more static realizations these are exported to the dynamic domain for reservoir flow simulation, typically after an upscaling step (although the latter is not needed for the example described below). If there is a significant mismatch between the dynamic simulation results and the historical data, the gradients of the mismatch objective function with respect to dynamic grid block parameters are then used to update the static model parameters as will be discussed in detail below. The workflow is shown schematically in Figure 5.1.
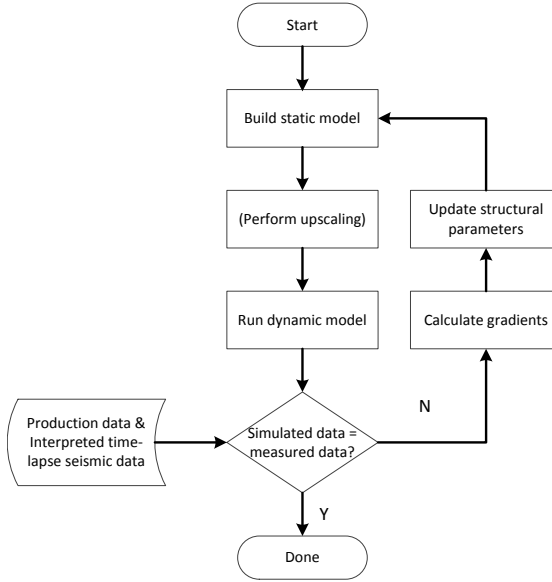
Figure 5.1: Workflow for gradient-based history matching of structural parameters in the static model. Note: upscaling is not performed in our examples.

5.2.3. PARAMETERIZATION

Structural uncertainties may result from different sources such as migration, picking, and time-to-depth conversion errors (Thore et al., 2002). Here we assume that the depths of the top and bottom reservoir horizons are the major uncertainties in the static model, which results in an uncertainty in reservoir thickness. Moreover, in this study the top surface of the reservoir is fixed such that the uncertainty in reservoir thickness is due to the uncertainty in the reservoir bottom depth only. Hence, the reservoir bottom depth is used as history matching parameter. Unfortunately, gradients with respect to grid block heights are not available from our simulator, but gradients with respect to grid block porosity can be interpreted as indications of where the reservoir volume, and thus the bottom depth, needs to be adapted.

5.2.4. MISMATCH OBJECTIVE FUNCTION

We apply the following objective function to represent the mismatch between historical and simulated data:

$$J(\boldsymbol{\varphi}) = (\mathbf{d} - \mathbf{h}(\boldsymbol{\varphi}))^T \mathbf{P}_d^{-1} (\mathbf{d} - \mathbf{h}(\boldsymbol{\varphi})), \tag{5.1}$$

where $\mathbf{d}$ is a vector of measured data, $\mathbf{h}(\boldsymbol{\varphi})$ is a vector of simulated data, $\boldsymbol{\varphi}$ is a vector of grid block porosities, and $\mathbf{P}_d$ is a square positive semi-definite matrix of weight factors which is often chosen as the measurement error covariance matrix. We aim to assimilate production measurements as well as time-lapse seismic data, where we assume that the time lapse seismic results are available in the form of interpreted saturations. Hence, we use two different objective functions: one defined as the mean squared difference between observed and simulated production data, and one defined as the mean squared

difference between observed (i.e. interpreted) and simulated grid block saturations. The gradient of the objective function is defined as the column vector containing the partial derivatives of J with respect to the components of the uncertain grid block porosities:

$$\nabla J_{\boldsymbol{\varphi}} = \left(\frac{\partial J}{\partial \boldsymbol{\varphi}} \right)^T = \left[\frac{\partial J}{\partial \varphi_1} \ \frac{\partial J}{\partial \varphi_2} \ \frac{\partial J}{\partial \varphi_3} \ \cdots \ \frac{\partial J}{\partial \varphi_n} \right], \tag{5.2}$$

where n is the number of grid blocks in the dynamic reservoir model.

5.2.5. STRUCTURAL MODEL UPDATING

The gradient of the objective function is calculated by the adjoint method in the dynamic simulator. Subsequently this gradient information is used to update the position of the reservoir bottom horizon by converting the gradient with respect to porosities to a gradient with respect to bottom depths defined as

$$\nabla J_{\mathbf{b}} = \left(\frac{\partial J}{\partial \mathbf{b}} \right)^T = \left[\frac{\partial J}{\partial b_1} \ \frac{\partial J}{\partial b_2} \ \frac{\partial J}{\partial b_3} \ \cdots \ \frac{\partial J}{\partial b_m} \right], \tag{5.3}$$

where $\mathbf{b}$ is a vector of reservoir bottom depths, and m is the number of grid blocks in the bottom layer of the reservoir model. Using partial derivative of the pore volume of each gridblock with respect to porosity and depth, the relation between the gradients is given by

$$\frac{\partial J}{\partial b_i} = \frac{\partial J}{\partial \varphi_i} \frac{\varphi_i}{\Delta h_i}, \ \ i = 1, \cdots, m, \tag{5.4}$$

where Δh_i is the height of grid block i, and φ_i is the porosity of that gridblock. Note that in our implementation we only use the porosity gradients for the bottom layer of grid blocks such that $n = m$.

We use a simple steepest descent method to update the bottom depth values, i.e. the vertical coordinates (with positive axis pointing downwards) at the centers of the grid blocks in the bottom layer of the reservoir model:

$$\mathbf{b}^{j+1} = \mathbf{b}^j + \beta \left(\frac{\partial J}{\partial \mathbf{b}} \right)^T_j, \tag{5.5}$$

where the positive scalar β is a fixed step length, and j is an iteration counter. The reservoir thickness at the grid blocks corresponding to the well locations is assumed to be known, such that the gradients in those grid-blocks are zero.

5.3. RESULTS AND DISCUSSIONS

5.3.1. TWIN EXPERIMENTS

We perform three 'twin experiments', using the same 'truth' case (used to generate synthetic data) but two different uncertain prior models. The first two experiments involve the assimilation of production data, while in the last one we assimilate time lapse seismic data.

5.3.1.1. TRUTH CASE

The 'truth' case represents a simple three dimensional reservoir with three layers: an impermeable shale layer in between permeable top and bottom zones; see Figure 5.2. The average reservoir thickness is 65 m, the average depth is 4100 m, the water-oil-contact is located at 4085 m and the STOIIP is 1.14×108 bbl. The initial water saturation is 0.1 and the initial reservoir pressure is 40 MPa at the top perforations. The top zone and the bottom zone have a constant permeability of 500 mD and 650 mD and a constant porosity of 0.15 and 0.2 respectively. Corey-type relative permeabilities are used for relperms. The fluid properties and Corey exponents are given in Table 5.1. Eight injectors and four producers, perforated over the entire height of the producing layers, are located in the field. Figure 5.2 shows the permeability field of the 'truth' case together with injector and producer locations. The reservoir model contains three layers of grid blocks with a total number of grid blocks equal to 3888.
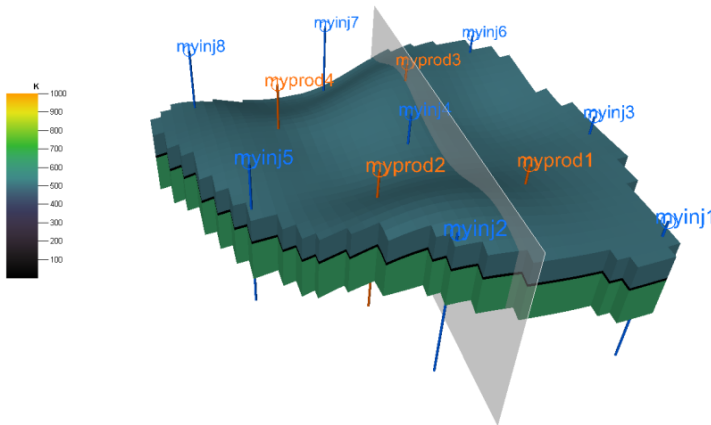
Figure 5.2: The 'truth' case permeability field. Seven injectors are placed around the field and one in the center. Four producers are located in central part of the field. The transparent plane indicates the cross section corresponding to Figure 5.4 and Figure 5.5

At the start of production the injectors operate at a constant flow rate of 300 m^3/day and the producers at a bottomhole pressure of 39 MPa at the top perforations, i.e. 1 MPa below the reservoir pressure. This 'truth' case is used to create synthetic production data over a period of 12 years. The measurements (oil rate, water rate per well) are taken monthly. After eight years of production one seismic survey is conducted. Interpreted time-lapse seismic data is represented as saturation changes per grid block. Figure 5.3 shows the oil saturation in the bottom layer of the truth model after eight years of production. No measurement errors are added to the data.

Table 5.1: Fluid properties and Corey exponents

Variable	Parameters	Value	Unit
ρ_w	Water density	1009	Kg/m^3
ρ_o	Oil density	880	Kg/m^3
μ_w	Water viscosity	1×10^{-3}	Pa.s
μ_o	Oil viscosity	4×10^{-3}	Pa.s
S_{wc}	Connate water saturation	0.2	-
S_{or}	Residual oil saturation	0.1	-
k_{rw}^0	End point water rel perm	0.9	-
k_{ro}^0	End point oil rel perm	0.8	-
n_w	Water Corey exponent	3	-
n_o	Oil Corey exponent	4.75	-
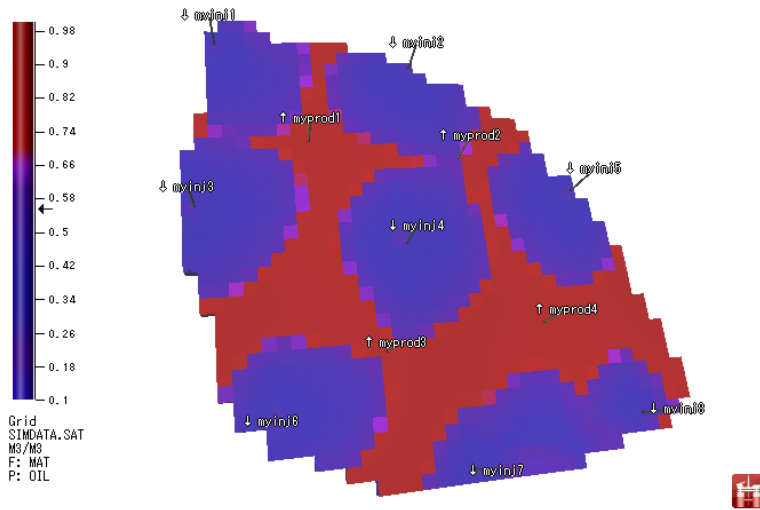
Figure 5.3: Oil saturation in the bottom layer of the 'truth' case after 8 years of production.

5.3.1.2. PRIOR MODELS

In this study, the true bottom horizon is assumed to be unknown. The bottom horizon of the prior models is obtained by stochastic manipulation of the bottom horizon of the 'truth' case. Two different prior models are chosen: prior #1 represents a reservoir structure that is relatively close to the truth case, and prior #2 a structure that displays significant differences compared to the truth. All remaining parameters in the prior models are chosen identical to those of the 'truth' case and assumed to be known. Figure 5.4 and Figure 5.5 show cross sections of the prior models and the 'truth' for prior #1 and prior #2 respectively. The blue line represents the bottom of the 'truth' case, the red line repre-

sents the bottom of the prior model, and the black line represents the top of the bottom layer (i.e. the bottom of the shale layer).
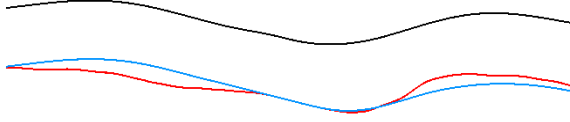
Figure 5.4: A cross section of the 'truth' case and prior #1. This prior is close to the truth. Red represents the bottom of the prior model, blue represents the bottom of the truth, and the black represents the bottom of the shale layer.
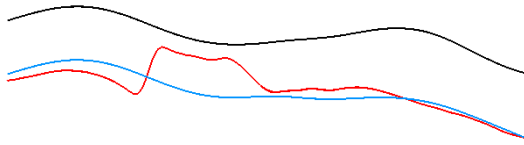
Figure 5.5: A cross section of the truth model and the prior #2. This prior is significantly different from the truth. Red represents the bottom of the prior model, blue represents the bottom of the truth, and the black represents the bottom of the shale layer.

5.3.2. EXPERIMENT #1: ASSIMILATION OF PRODUCTION DATA STARTING FROM PRIOR #1

In the first twin experiment the history match is performed starting from prior #1 by assimilating production data. We do not use any scaling of the data. After some trial and error we selected a step size $\beta = 7.5 \times 10^{-4}$ m^2, while a relative convergence of 0.005 is used a stopping criterion. Figure 5.6 shows the convergence of the objective function after eleven iterations.

Figure 5.7 depicts a cross section of bottom horizons of the 'truth' case (blue), the prior model (red) and the updated model (green) after eleven iterations. Figure 5.8 depicts the prior and updated residual maps of the bottom horizon, where the residual is defined as the difference in depth between the 'truth' and the model. The colors represent the residuals (in m) and the contour lines indicate the shape of the true bottom horizon (without scale). The black line indicates the cross section corresponding to Figure 5.7. In this experiment, which starts from a prior that is close to the truth, updating the reservoir bottom depth by assimilation of production data leads to an improved posterior.
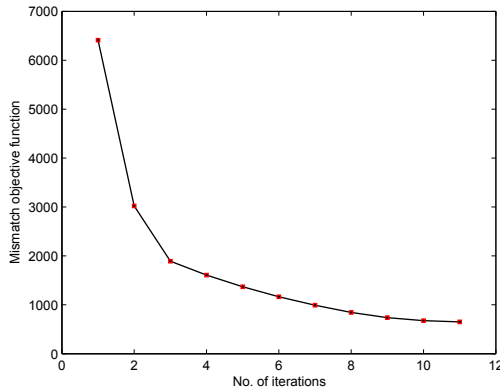
Figure 5.6: Mismatch objective function for experiment #1
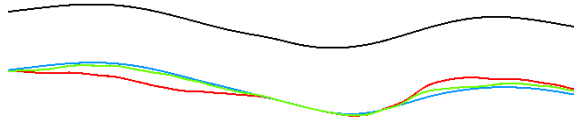
Figure 5.7: Cross section through the bottom layer of the reservoir for experiment #1. Blue represents the truth, red represents prior #1, and green represents the updated model.
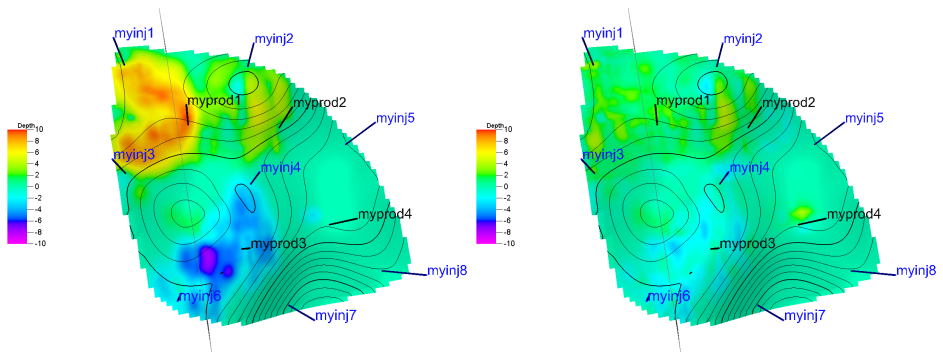
Figure 5.8: Prior (left) and updated (right) residual maps for experiment #1. Colors represent the residuals in m. Contour lines indicate the true bottom depth (without scale).

5.3.3. EXPERIMENT #2: ASSIMILATION OF PRODUCTION DATA STARTING FROM PRIOR #2

Experiment #2 involves the assimilation of production data starting from prior #2 which is further from the truth than prior #1. With a step length $\beta = 7.5 \times 10^{-6}$ m^2, the objective

function converged after 50 iterations but did not show a large drop in value; see Figure 5.9. Note that the small increase in the objective function value in 21st iteration is due to the fact that we used a fixed step length without line search. The updated model does not show a good match with the truth; see Figure 5.10. The same message is conveyed by Figure 5.11 which depicts the prior and updated residual maps of the bottom horizon. Except for minor changes close to some of the well locations (myprod3, myprod4 and myinj4), the updated model has not changed significantly with respect to the prior model. This example illustrates that production data often do not contain enough information to reduce uncertainties in areas that are not in the immediate vicinity of the wells, and that the results of history matching using production data are dependent on the quality of the prior model.
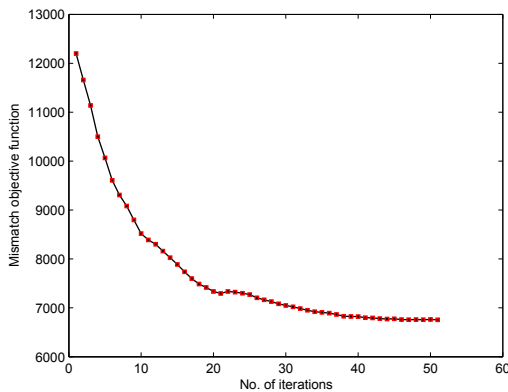
Figure 5.9: Mismatch objective function for experiment #2.
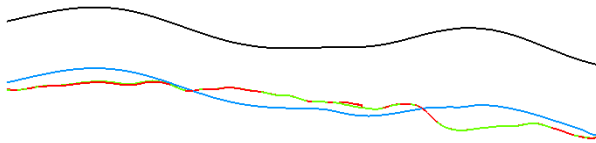
Figure 5.10: Cross section through the bottom layer of the reservoir for experiment #2. Blue represents the truth, red represents prior #2, and green represents the updated model.

5.3.4. EXPERIMENT #3: ASSIMILATION OF TIME-LAPSE SEISMIC DATA START-ING FROM PRIOR #2

Just like experiment #2, experiment #3 starts from the 'poor' prior #2, but now involves the assimilation of time-lapse seismic data instead of production data. The step length is chosen as $\beta = 3.5$ and after 30 iterations the value of the objective function is reduced
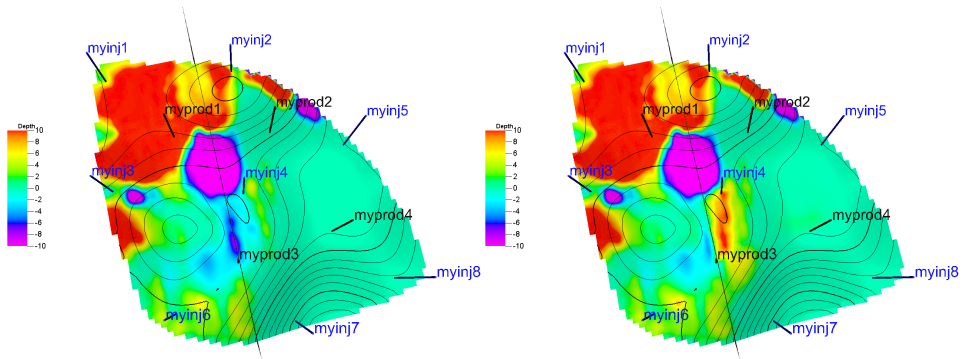
Figure 5.11: Prior (left) and updated (right) residual maps for experiment #2. Colors represent the residuals in m. Contour lines indicate the true bottom depth (without scale).

5

by a factor of ten; see Figure 5.12.
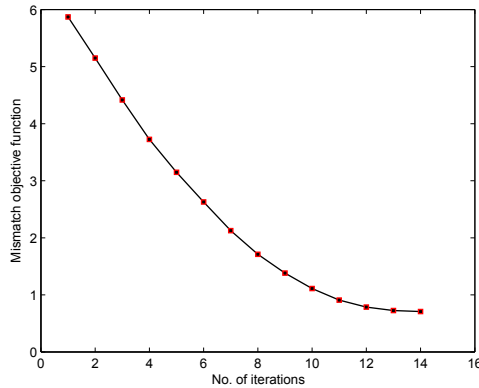
Figure 5.12: Mismatch objective function for experiment #3.

Figure 5.13 depicts the prior and updated depths of the bottom horizon and Figure 5.14 the corresponding residual maps. In contrast with the previous example, history matching of the bottom horizon by assimilation of time-lapse seismic data results in an acceptable mismatch objective function value as well as a good match between the updated model and the truth.

Figure 5.15 depicts the oil flow rates of each of the four production wells during 15 years of production for experiment #3. Production starts in 2004 and after eight years, in 2012, a time lapse seismic survey is conducted and the interpreted results are assimilated. The curves thereafter represent predictions of the future oil production. It can be observed that not only the simulated oil flow rates of the updated model are in a good agreement with the measured rates, but that also the predicted flow rates are much closer to the
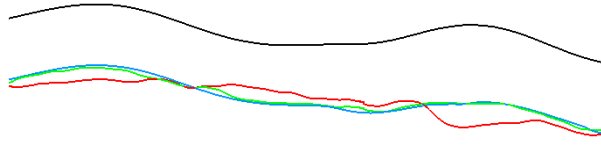
Figure 5.13: Cross section through the bottom layer of the reservoir for experiment #3. Blue represents the truth, red represents prior #2, and green represents the updated model.
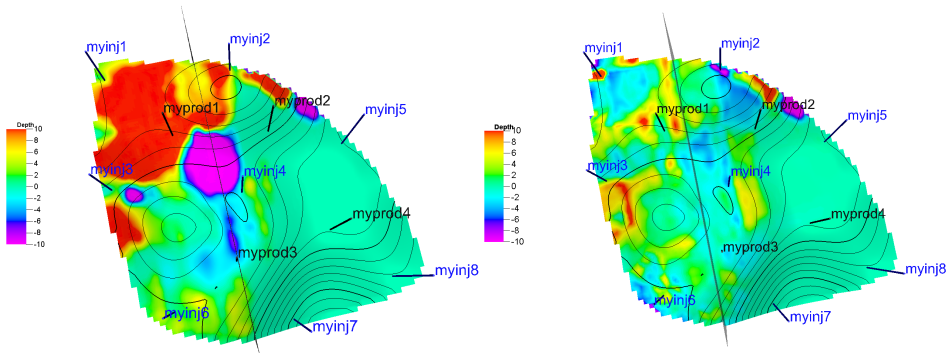
Figure 5.14: Prior (left) and updated (right) residual maps for experiment #3. Colors represent the residuals in m. Contour lines indicate the true bottom depth (without scale).

truth than those simulated with the prior model.

5.4. DISCUSSION

In this study the uncertain parameters are updated without constraints. Moreover, the objective function does not contain a term that penalizes deviations from the prior parameter values, as is required in a Bayesian framework (see e.g. Oliver et al. (2008)). Such a penalty term makes the problem well posed, restricts the parameter updates to values that keep the posterior values not too far from the prior values, and generally increases the smoothness of the results. Assimilation of production data to update the bottom depth of prior #2 showed that production data do not provide sufficient information for reliable updates away from the wells whereas time lapse seismic provides much more spatially distributed information, leading to improved updates and improved predictions. Similar conclusions, but then for updating flow properties instead of structural properties have been reported before, see e.g. Walker and Lane (2007).
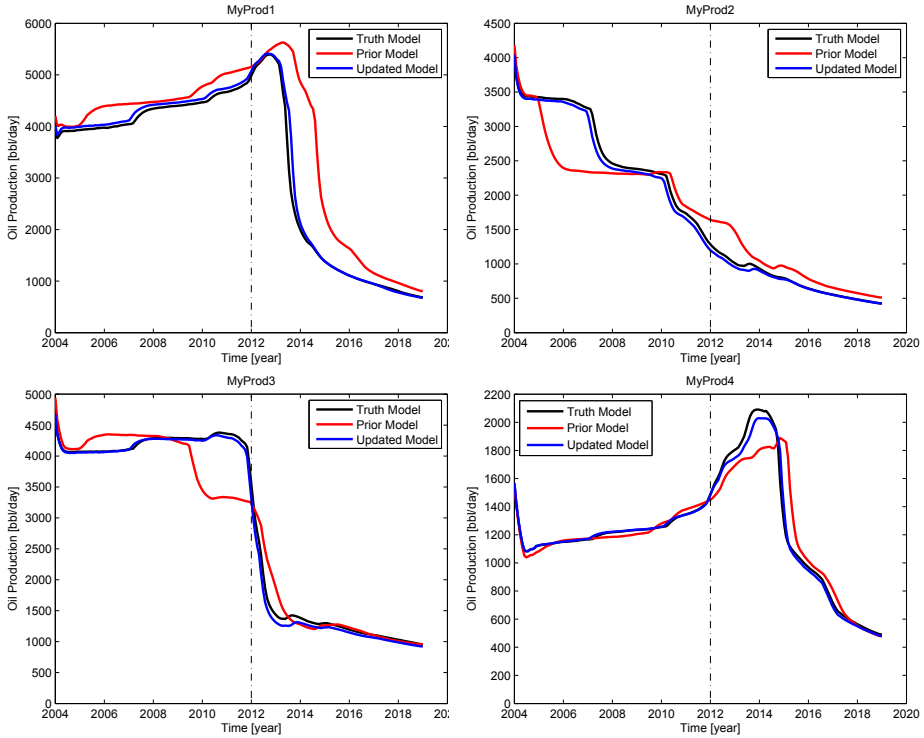
Figure 5.15: Oil flow rates of each of the four production wells for experiment #3. Red curves represent the rates of the prior model simulation, blue curves represent the rates of the updated model, and black curves represent the true rates. The vertical dashed line indicates the moment that the history match is performed.

5.5. CONCLUSIONS

In this chapter we proposed a new method for updating uncertain structural reservoir parameters by combining static and dynamic reservoir models in a 'Big Loop' history matching workflow using gradient-based history matching. In particular we assumed the parameters defining the bottom horizon of the static reservoir model to be uncertain and updated them by assimilation of production data or time-lapse seismic data using the adjoint method. We tested the method on three simple 3D synthetic examples in which the bottom depth was the only uncertain parameter while the measurements were assumed to be error free. We conclude that for these examples:

- The adjoint method is a computationally efficient method for history matching of the structural model parameters.

- Gradients of the mismatch objective function with respect to grid block porosities can serve as an acceptable approximation for gradients with respect to bottom depths and can thus be used to update the reservoir thickness, or in case of uncertain porosities, the product of porosity and reservoir thickness.

- Production data contain mostly localized information from the near-well bore area and are therefore of limited value to update structural reservoir parameters in areas away from the wells. As a result the updated results are strongly dependent on the prior model.

- Time-lapse seismic data (in the form of interpreted saturations) contain much more spatially distributed information and are therefore a much better source of information to update structural reservoir parameters in areas away from the wells.

- Updating the structural parameters of the static reservoir model significantly improves the predictive capacity of the correspondingly updated dynamic reservoir model.

5

6

CONCLUSIONS

I N this chapter we first provide general conclusions and observations from this thesis followed by specific conclusions of each chapter of the thesis.

6.1. GENERAL CONCLUSIONS

One of the key elements of history matching using the Bayesian framework is "regularization" which essentially aims to find an updated model constrained to the prior information. In reality it is highly likely that this prior knowledge is incorrect due to the presence of a large number of uncertainties. In this thesis we show that updating models constrained by the prior knowledge may lead to suboptimal results in the presence of incorrect prior knowledge. To solve this problem, in this thesis we show that using an unregularized update during the history matching procedure leads to unrealistic updates of the model parameters. While these unrealistic updates may seem undesirable, we show in this thesis that these unrealistic parameter updates can actually provide very significant information about flow relevant features present in reality which were missing in the prior knowledge. The information content from these unrealistic parameter updates obtained using dynamic flow data is used to improve the fundamental understanding of the static/geological model by incorporating the 'missing' geological/structural features. In this way, through a multi-disciplinary approach, we are able to improve the understanding of our reservoir, and the associated updated reservoir models will be able to provide more robust results within a decision making context. The information content in dynamic data can be investigated within a theoretical framework using a transfer function formalism which has been introduced and investigated in detail in this thesis. This transfer function formalism provides a new and unique perspective to assess the identifiability of different parameters and provides insights into the physical characteristics of a system. Through this transfer function formalism we have shown that we are able to identify the position of the 'missing' features using dynamic data. We have shown that the location of the 'missing' feature has a more pronounced effect on the data compared to the magnitude of the 'missing' feature. For the examples considered in this thesis we have shown that the transfer function formalism provides a theoretical explanation for the behavior observed for unregularized history matching. In addition to using unregularized updates during history matching we have also investigated the impact of a variety of different regularization techniques. These regularization techniques aim to restore well-posedness in the problem. These techniques are also able to retrieve the 'missing' features which were non-existent in the prior knowledge and provide smoother parameter updates compared to the unregularized updates. In this thesis, building on an earlier work, we have shown the impact of non-uniqueness of history matched model due to the inherent ill-posedness in such inverse problems which provides a methodology to determine upper and lower bounds on future production predictions. Such upper and lower bounds for the predictions give vital insights into possible consequences for a variety of objectives, economic or recovery based. This information can play a role in the quantification of the value of information through history matching. The specific conclusions of each chapter of this thesis are provided in the following sections.

6.2. CHAPTER TWO: EFFECT OF ILL-POSEDNESS OF HISTORY-MATCHED MODELS ON PRODUCTION PREDICTIONS

In this chapter, we applied a hierarchical optimization method, proposed by Van Essen et al. (2010), to determine lower and upper bounds on predicted production to inves-

tigate the effect of ill-posedness of history-matched models on reservoir performance prediction. We conclude that:

- The non-uniqueness of history matched models implies that future production can only be predicted within bounds.

- The non-uniqueness implies the presence of remaining degrees of freedom after history matching (i.e. after solving the primary optimization problem) which can be used to determine lower and upper bounds on future production through solving two secondary optimization problems.

- The method proposed in this chapter provides a way to gain more insight in the possible economic consequences of the lack of information in historic data. These consequences can be represented by total production, ultimate recovery, (incremental) NPV or any other economic measure.

- The method is not limited to historic production data. Alternative data sources, e.g. time-lapse seismic data, can be used to determine the impact on the predicted economic performance. Hence, this method may also play a role in the quantification of the value of information.

- Introducing more data sources, e.g. time-lapse seismic or prior information, results in smaller differences in economic performance (incremental NPV) between the lower and upper bound models.

6.3. CHAPTER THREE: UNDER-MODELING DETECTION

In this chapter several twin experiments were conducted and unregularized parameter estimation was applied to update uncertain parameters in a simple 2D reservoir model that contained a major flow-relevant deficiency in the form of a missing high- or low-permeability feature. We found that, for these examples,

- Updating in a Bayesian framework results in updates close to the prior, without any indication of the missing feature.

- Updating without regularization enables us to identify the presence and the location of the missing flow-relevant feature in the model, but not the correct magnitude.

- The identifiability of the presence and location deteriorates with increasing noise levels in the data.

- When the flow-relevant feature is located closer to the producer its presence and location seem to become more identifiable.

Next, to investigate these findings, we performed a quantitative identifiability analysis of the examples using a dimensionless sensitivity matrix in order to analyze the sensitivity of the system output (in the form of total flow rates in the wells) to the system parameters (the grid block permeabilities). From the results we conclude that

- The output of these examples is more sensitive to a flow-relevant feature when the feature is closer to a producer.

- As the noise level increases the singular values of the corresponding sensitivity matrix decrease and the parameter estimation solutions become more dominated by noise.

Moreover, discrete cosine transform (DCT) reparameterization and total variation regularization have been used to restore well-posedness in reservoir parameter estimation problems. We have shown that while penalizing the deviations from a prior model can be misleading in an under-modeling situations other alternative methods are able to restore a missing flow-relevant feature.

We conclude that, for the examples considered, the application of unregularized reservoir parameter estimation provides a means to identify the presence and location of significant model deficiencies, in line with the 'model maturation' concept proposed in Joosten et al. (2011). Further analysis, using larger-scale models and more complex flow-relevant features, will be required to determine the limits of validity of this concept.

6.4. CHAPTER FOUR: IDENTIFIABILITY OF FLOW-RELEVANT FEATURES

6

In this chapter we have investigated the possibility of detecting the location and the magnitude of flow barriers in a 1D reservoir for slightly compressible single-phase flow from the observations (outputs) under different noise conditions. To this end we have conducted different twin-experiments in the time domain and the frequency domain. For the latter we have developed an analytical expression for the dynamical characteristics of the system as a function of system properties based on a transfer function formalism in the form of bilaterally coupled porous media models. We conclude that:

- The frequency-domain analytical solution makes it possible to investigate the effect of different parameters on the dynamic behavior of the system.

- It is possible to estimate location and magnitude of a flow barrier from noise-free measurements in slightly compressible single-phase flow.

- When the noise level in the data is increased, the location of the barrier remains relatively more identifiable than its permeability magnitude.

- The presence of noise in the data results in unrealistic permeability magnitude estimates.

- Visualization of the objective function space in the frequency-domain illustrates that the dynamic output of our system is more sensitive to the barrier location than to barrier magnitude

- A structural identifiability analysis using the transfer function approach shows that the difference in identifiability between location and magnitude is not data-dependent but is a structural property of the system.

6.5. CHAPTER FIVE: STRUCTURAL MODEL UPDATING USING DYNAMIC DATA

In this chapter we proposed a new method for updating uncertain structural reservoir parameters by combining static and dynamic reservoir models in a 'Big Loop' history matching workflow using gradient-based history matching. In particular we assumed the parameters defining the bottom horizon of the static reservoir model to be uncertain and updated them by assimilation of production data or time-lapse seismic data using the adjoint method. We tested the method on three simple 3D synthetic examples in which the bottom depth was the only uncertain parameter while the measurements were assumed to be error free. We conclude that for these examples:

- The adjoint method is a computationally efficient method for history matching of the structural model parameters.

- Gradients of the mismatch objective function with respect to grid block porosities can serve as an acceptable approximation for gradients with respect to bottom depths and can thus be used to update the reservoir thickness, or in case of uncertain porosities, the product of porosity and reservoir thickness.

- Production data contain mostly localized information from the near-well bore area and are therefore of limited value to update structural reservoir parameters in areas away from the wells. As a result the updated results are strongly dependent on the prior model.

- Time-lapse seismic data (in the form of interpreted saturations) contain much more spatially distributed information and are therefore a much better source of information to update structural reservoir parameters in areas away from the wells.

- Updating the structural parameters of the static reservoir model significantly improves the predictive capacity of the correspondingly updated dynamic reservoir model.

REFERENCES

Aanonsen, S. I., Nævdal, G., Oliver, D. S., Reynolds, A. C., and Vallès, B. (2009). The ensemble kalman filter in reservoir engineering–a review. *SPEJ*, **14**(03):393–412. DOI: 10.2118/117274–PA.

Ahn, S. and Horne, R. N. (2010). Estimating permeability distributions from pressure pulse testing. Paper SPE-134391-MS presented at the SPE Annual Technical Conference and Exhibition, Florence, Italy. DOI: 10.2118/134391-ms.

Blom, R. S. and Van den Hof, P. M. (2010). Multivariable frequency domain identification using iv-based linear regression. pages 1148–1153. Paper presented at the Decision and Control (CDC). DOI: 10.1109/CDC.2010.5717297.

Bratvold, R., Bickel, J., and Lohne, H. (2009). Value of information in the oil and gas industry: Past, present, and future. *SPEREE*, **12**(04):630–638. DOI: 10.2118/110378–PA.

Caers, J. (2003). History matching under training-image-based geological model constraints. *SPEJ*, **8**(03):218–226. DOI: 10.2118/74716–PA.

Caers, J. (2005). *Petroleum Geostatistics*. Society of Petroleum Engineers, Richardson.

Carslaw, H. S. and Jaeger, J. C. (1959). *Conduction of heat in solids, 2nd ed.* Oxford University Press.

Chavent, G., Dupuy, M., and Lemmonier, P. (1975). History matching by use of optimal theory. *SPEJ*, **15**(01):74–86. DOI: 10.2118/4627–pa.

Chen, C., Li, G., and Reynolds, A. (2012). Robust constrained optimization of short-and long-term net present value for closed-loop reservoir management. *SPEJ*, **17**(03):849–864. DOI: 10.2118/141314–PA.

Chen, W. H., Gavalas, G. R., Seinfeld, J. H., and Wasserman, M. L. (1974). A new algorithm for automatic history matching. *SPEJ*, **14**(6):593–608. DOI: 10.2118/4545–pa.

Chen, Y., Oliver, D., and Zhang, D. (2009). Efficient ensemble-based closed-loop production optimization. *SPEJl*, **14**(04):634–645. DOI: 10.2118/112873–PA.

Chierici, G. L. (1992). Economically improving oil recovery by advanced reservoir management. *JPSE*, **8**(3):205–219. DOI: 10.1016/0920–4105(92)90034–X.

Constable, S. C., Parker, R. L., and Constable, C. G. (1987). Occam's inversion: A practical algorithm for generating smooth models from electromagnetic sounding data. *Geophysics*, **52**(3):289–300. DOI: 10.1190/1.1442303.

Datta-Gupta, A. and King, M. J. (2007). *Streamline simulation: theory and practice.* Society of Petroleum Engineers, Richardson.

Datta-Gupta, A., Vasco, D., and Long, J. (1997). On the sensitivity and spatial resolution of transient pressure and tracer data for heterogeneity characterization. *SPEFE*, **12**(02):137–144. DOI: 10.2118/30589–PA.

den Dekker, A., Bombois, X., and Van den Hof, P. (2008). Finite sample confidence regions for parameters in prediction error identification using output error models. Proceedings of the 17th IFAC World Congress, Seoul, Korea, 6-11-July, pp. 5024-5029.

Dogru, A., Dixon, T., and Edgar, T. (1977). Confidence limits on the parameters and predictions of slightly compressible, single-phase reservoirs. *SPEJ*, **17**(01):42–56. DOI: 10.2118/4983–pa.

Eidsvik, J., Mukerji, T., and Bhattacharjya, D. (2015). *Value of Information in the Earth Sciences: Integrating Spatial Modeling and Decision Analysis.* Cambridge University Press, Cambridge.

Elrafie, E. A., Agil, M. A., Abbas, R. T., Idroos, B. E., and Colomar, F.-M. (2009). Innovated simulation history matching approach enabling better historical performance match and embracing uncertainty in predictive forecasting. Paper 120958-MS presented at the EUROPEC/EAGE Conference and Exhibition, Amsterdam, The Netherlands, 8-11 June. DOI: 10.2118/120958-MS.

Evensen, G. (2009). *Data assimilation: the ensemble Kalman filter.* Springer Science & Business Media.

Feitosa, G., Chu, L., Thompson, L., and Reynolds, A. C. (1994). Determination of permeability distribution from well-test pressure data. *JPT*, **46**(07):607–615. DOI: 10.2118/26047–PA.

Fonseca, R., Leeuwenburgh, O., Della Rossa, E., Van den Hof, P., and Jansen, J. (2015). Ensemble-based multiobjective optimization of on/off control devices under geological uncertainty. *SPEREE*, **18**(04):554–563. DOI: 10.2118/173268–PA.

Fonseca, R., Leeuwenburgh, O., Van den Hof, P., and Jansen, J. (2014). Ensemble-based hierarchical multi-objective production optimization of smart wells. *Computational Geosciences*, **18**(3-4):449–461. DOI: 10.1007/s10596–013–9399–2.

Gao, G. and Reynolds, A. (2006). An improved implementation of the lbfgs algorithm for automatic history matching. *SPEJ*, **11**(1):5–17. . DOI: 10.2118/90058–PA.

Glover, K. and Willems, J. C. (1974). Parametrizations of linear dynamical systems: canonical forms and identifiability. *Automatic Control, IEEE Transactions on*, **19**(6):640–646. DOI: 10.1109/tac.1974.1100711.

Golub, G. H. and Van Loan, C. F. (2012). *Matrix computations*, volume **3**. JHU Press.

Gosselin, O., van den Berg, S., and Cominelli, A. (2001). Integrated history-matching of production and 4d seismic data. Paper SPE 71599 presented at the SPE Annual Technical Conference and Exhibition, New Orleans, Louisiana, 30 September-3 October. DOI: 10.2118/71599-ms.

Grader, A. S. and Horne, R. N. (1988). Interference testing: Detecting a circular impermeable or compressible subregion. *SPEFE*, **3**(02):420–428. DOI: 10.2118/15585–PA.

Gross, H., Thiele, M., Alexa, M., Caers, J., and Kovscek, A. (2004). Streamline-based history matching using geostatistical constraints: Application to a giant, mature carbonate reservoir. Paper 90069-MS presented at the SPE Annual Technical Coference and Exhibition, Houston, Texas, 26-29 September. DOI: 10.2118/90069-MS.

Haimes, Y. Y. and Li, D. (1988). Hierarchical multiobjective analysis for large-scale systems: Review and current status. *Automatica*, **24**(1):53–69. DOI: 10.1016/0005–1098(88)90007–6.

Hamman, J., Buettner, R., and Caldwell, D. (2003). A case study of a fine scale integrated geological, geophysical, petrophysical, and reservoir simulation reservoir characterization with uncertainty estimation. Paper SPE 84274-MS presented at the SPE Annual Technical Conference and Exhibition Denver, Colorado, 5-8 October. DOI: 10.2118/84274-MS.

Hanke, M. and Hansen, P. C. (1993). Regularization methods for large-scale problems. *Survey on Mathematics for Industry*, **3**(4).

Hoffman, B. T., Wen, X.-H., Strebelle, S. B., and Caers, J. K. (2005). Geologically consistent history matching of a deepwater turbidite reservoir. Paper SPE 95557-MS presented at the SPE Annual Technical Conference and Exhibition, Dallas, Texas, 9-12 October. DOI: 10.2118/95557-MS.

Hollaender, F., Hammond, P. S., and Gringarten, A. C. (2002). Harmonic testing for continuous well and reservoir monitoring. Paper SPE 77692 presented at the SPE Annual Technical Conference and Exhibition, San Antonio, USA, 29 September-2 October. DOI: 10.2118/77692-MS.

Jansen, J. (2011). Adjoint-based optimization of multi-phase flow through porous media–a review. *Computers & Fluids*, **46**(1):40–51. DOI: 10.1016/j.compfluid.2010.09.039.

Jansen, J.-D., Bosgra, O. H., and Van den Hof, P. M. (2008). Model-based control of multiphase flow in subsurface oil reservoirs. *Journal of Process Control*, **18**(9):846–855. DOI: 10.1016/j.jprocont.2008.06.011.

Joosten, G. J., Altintas, A., and De Sousa, P. (2011). Practical and operational use of assisted history matching and model-based optimisation in the salym field. Paper SPE-146697-MS presented at the SPE Annual Technical Conference and Exhibition, Denver, 30 October-2 November. DOI: 10.2118/146697-MS.

Kahrobaei, S., Mansoori, M., Joosten, G., Van den Hof, P., and Jansen, J. (2014). Hidden information in ill-posed inverse problems. Paper presented at the 14th European Conference on the Mathematics of Oil recovery (ECMOR XIV), Catania, Italy, 8-11 September. DOI: 10.3997/2214-4609.20141825.

Kaleta, M., Van Essen, G., Van Doren, J., Bennett, R., van Beest, B., Van Den Hoek, P., Brint, J. F., and Woodhead, T. J. (2012). Coupled static/dynamic modeling for improved uncertainty handling. Paper SPE 154400-MS presented at the SPE EUROPEC/EAGE Annual Conference, Copenhagen, Denmark, 4-7 June. DOI: 10.2118/154400-MS.

Khaninezhad, M. and Jafarpour, B. (2014). Prior model identification during subsurface flow data integration with adaptive sparse representation techniques. *Computational Geosciences*, **18**(1):3–16. DOI: 10.1007/s10596–013–9378–7.

Kraaijevanger, J., Egberts, P., Valstar, J., and Buurman, H. (2007). Optimal waterflood design using the adjoint method. Paper SPE-105764 presented at the SPE Reservoir Simulation Symposium, Houston, Texas, U.S.A., 26-28 February 2007. DOI: 10.2118/105764-MS.

Krymskaya, M., Hanea, R., Jansen, J., and Heemink, A. (2010). Observation sensitivity in computer-assisted history matching. Paper presented at 72nd Europec/EAGE Annual Conference and Exhibition, Barcelona, Spain, 14-17 June. DOI: 10.3997/2214-4609.201400961.

Leeuwenburgh, O., Peters, E., and Wilschut, F. (2011). Towards an integrated workflow for structural reservoir model updating and history matching. Paper SPE-143576 presented at the SPE EUROPEC/EAGE Annual Conference and Exhibition, Vienna, Austria, 23-26 May 2011. DOI: 10.2118/143576-MS.

Leo, T.-y., Kravaria, C., and Seinfeld, J. H. (1986). History matching by spline approximation and regularization in single-phase areal reservoirs. *SPERE*, **1**(05):521–534. DOI: 10.2118/13931–pa.

Levitan, M. and Crawford, G. (2002). General heterogeneous radial and linear models for well-test analysis. *SPEJ*, **7**(02):131–138. DOI: 10.2118/78598–PA.

Li, L. and Jafarpour, B. (2010). Effective solution of nonlinear subsurface flow inverse problems in sparse bases. *Inverse Problems*, **26**(10):105016. DOI: i:10.1088/0266–5611/26/10/105016.

Liu, X. and Reynolds, A. (2014). Gradient-based multi-objective optimization with applications to waterflooding optimization. pages 8–11. Paper presented at the 14th European Conference on the Mathematics of Oil recovery (ECMOR XIV), Catania, Italy, 8-11 September. DOI: 10.3997/2214-4609.20141892.

Marler, R. T. and Arora, J. S. (2004). Survey of multi-objective optimization methods for engineering. *Structural and Multidisciplinary Optimization*, **26**(6):369–395. DOI: 10.1007/s00158–003–0368–6.

Nanba, T. and Horne, R. (1989). Estimation of water and oil relative permeabilities from pressure transient analysis of water injection well data. Paper SPE-19829-MS presented at SPE Annual Technical Conference and Exhibition, San Antonio, Texas, 8-11 October 1989. DOI: 10.2118/19829-MS.

Nocedal, J. and Wright, S. (2006). *Numerical optimization*. Springer Science & Business Media.

Oliver, D. S. (1996). Multiple realizations of the permeability field from well test data. *SPEJ*, **1**(02):145–154. DOI: 10.2118/27970–PA.

Oliver, D. S. and Chen, Y. (2011). Recent progress on reservoir history matching: a review. *Computational Geosciences*, **15**(1):185–221. DOI: 10.1007/s10596–010–9194–2.

Oliver, D. S., Reynolds, A. C., and Liu, N. (2008). *Inverse theory for petroleum reservoir characterization and history matching*. Cambridge University Press.

Peters, E., Chen, Y., Leeuwenburgh, O., and Oliver, D. (2013). Extended brugge benchmark case for history matching and water flooding optimization. *Computers & Geosciences*, **50**:16–24. DOI: 10.1016/j.cageo.2012.07.018.

Peters, L., Arts, R., Brouwer, G., Geel, C., Cullick, S., Lorentzen, R. J., Chen, Y., Dunlop, N., Vossepoel, F. C., and Xu, R. (2010). Results of the brugge benchmark study for flooding optimization and history matching. *SPEREE*, **13**(03):391–405. DOI: 10.2118/119094–PA.

Quinn, S. L., Harris, T. J., and Bacon, D. W. (2005). Accounting for uncertainty in control-relevant statistics. *Journal of Process Control*, **15**(6):675–690. DOI: 10.1016/j.jprocont.2005.01.002.

Rivenæs, J. C., Otterlei, C., Zachariassen, E., Dart, C., and Sjøholm, J. (2005). A 3d stochastic model integrating depth, fault and property uncertainty for planning robust wells, njord field, offshore norway. *Petroleum Geoscience*, **11**(1):57–65. DOI: 10.1144/1354–079303–612.

Rodrigues, J. R. P. (2006). Calculating derivatives for automatic history matching. *Computational Geosciences*, **10**(1):119–136. DOI: 10.1007/s10596–005–9013–3.

Schaaf, T., Coureaud, B., and Labaune, F. L. (2009). Joint structural and petrophysical history matching leads to global geological stochastic reservoir models. Paper SPE 121899-MS presented at the EUROPEC/EAGE Conference and Exhibition, Amsterdam, the Netherlands, 8-11 June. DOI: 10.2118/121899-MS.

Seiler, A., Aanonsen, S. I., Evensen, G., and Rivenæs, J. C. (2010). Structural surface uncertainty modeling and updating using the ensemble kalman filter. *SPEJ*, **15**(04):1062–1076. DOI: 10.2118/125352–PA.

Seiler, A., Evensen, G., Skjervheim, J.-A., Hove, J., and Vabo, J. G. (2009). Advanced reservoir management workflow using an enkf based assisted history matching method. Paper SPE 118906-MS presented at the SPE Reservoir Simulation Symposium, The Woodlands, Texas, USA, 2-4 February. DOI: 0.2118/118906-MS.

Shah, S., Gavalas, G., and Seinfeld, J. (1978). Error analysis in history matching: The optimum level of parameterization. *SPEJ*, **18**(03):219–228. DOI: 10.2118/6508–pa.

Skjervheim, J., van Lanen, X., Hulme, D., Stenerud, V. R., Zachariassen, E., Liu, S., Hove, J., and Evensen, G. (2012). Integrated workflow for consistent model building from depth conversion to flow simulation-north sea field case. Paper presented at the 74th EUROPEC/EAGE Annual Conference, Copenhagen, Denmark, 4-7 June. DOI: 10.3997/2214-4609.20148221.

Spall, J. (1998). Implementation of the simultaneous perturbation algorithm for stochastic optimization. *IEEE Transactions on Aerospace and Electronic Systems*, **34**(3):817–823. DOI: DOI 10.1109/7.705889.

Stallman, R. and Brown, R. (1951). Nonequilibrium type curves modified for two-well systems. Technical report.

Suzuki, S. and Caers, J. K. (2006). History matching with an uncertain geological scenario. Paper SPE 102154-MS presented at the SPE Annual Technical Conference and Exhibition, San Antonio, Texas, 24-27 September. DOI: 10.2118/102154-MS.

Suzuki, S., Caumon, G., and Caers, J. (2008). Dynamic data integration for structural modeling: model screening approach using a distance-based model parameterization. *Computational Geosciences*, **12**(1):105–119. DOI: 10.1007/s10596–007–9063–9.

Tarantola, A. (2005). *Inverse problem theory and methods for model parameter estimation*. siam.

Tavassoli, Z., Carter, J. N., and King, P. R. (2004). Errors in history matching. *SPEJ*, **9**(03):352–361. DOI: 10.2118/86883–pa.

Thore, P., Shtuka, A., Lecour, M., Ait-Ettajer, T., and Cognot, R. (2002). Structural uncertainties: Determination, management, and applications. *Geophysics*, **67**(3):840–852. DOI: 10.1190/1.1484528.

Van den Hof, P. M., Van Doren, J. F., and Douma, S. G. (2009). Identification of parameters in large scale physical model structures, for the purpose of model-based operations. In *Model-Based Control:*, pages 125–143. Springer.

Van Doren, J. F., Van den Hof, P. M., Jansen, J. D., and Bosgra, O. H. (2008). Determining identifiable parameterizations for large-scale physical models in reservoir engineering. Paper presented at the Proceedings of the 17th IFAC World Congress, Seoul. DOI: 10.3182/20080706-5-KR-1001.01935.

Van Doren, J. F. M. (2010). *Model Structure Analysis of Model-based Operation of Petroleum Reservoirs*. TU Delft, Delft University of Technology.

Van Essen, G., Jansen, J., and Van den Hof, P. (2010). Determination of lower and upper bounds of predicted production from history-matched models. Paper presented at the 12th European Conference on the Mathematics of Oil recovery (ECMOR XII), Oxford, United Kingdom, 6-9 September. DOI: 10.3997/2214-4609.20144982.

Van Essen, G., Jimenez, E., Przybysz-jarnut, J. K., Horesh, L., Douma, S. G., van den Hoek, P., Conn, A., and Mello, U. T. (2012). Adjoint-based history-matching of production and time-lapse seismic data. Paper SPE 154375-MS presented at the SPE EUROPEC/EAGE Annual Conference, Copenhagen, Denmark, 4-7 June. DOI: 10.2118/154375-MS.

Van Essen, G., Van den Hof, P., and Jansen, J.-D. (2011). Hierarchical long-term and short-term production optimization. *SPEJ*, **16**(01):191–199. DOI: 10.2118/124332–PA.

Van Essen, G., Zandvliet, M., Van den Hof, P., Bosgra, O., and Jansen, J.-D. (2009). Robust waterflooding optimization of multiple geological scenarios. *SPEJ*, **14**(01):202–210. DOI: 10.2118/102913–PA.

Vogel, C. R. (2002). *Computational methods for inverse problems*, volume 23. Siam.

Walker, G. J. and Lane, H. S. (2007). Assessing the accuracy of history-match predictions and the impact of time-lapse seismic data: A case study for the harding reservoir. Paper SPE-106019 presented at the SPE Reservoir Simulation Symposium, Houston, Texas, U.S.A., 26-28 February. DOI: 10.2118/106019-MS.

Watson, A., Gavalas, G., and Seinfeld, J. (1984). Identifiability of estimates of two-phase reservoir properties in history matching. *SPEJ*, **24**(06):697–706. DOI: 10.2118/12579–PA.

Yaxley, L. (1987). Effect of a partially communicating fault on transient pressure behavior. *SPEFE*, **2**(04):590–598. DOI: 10.2118/14311–pa.

Zandvliet, M., Van Doren, J., Bosgra, O., Jansen, J., and Van den Hof, P. (2008). Controllability, observability and identifiability in single-phase porous media flow. *Computational Geosciences*, **12**(4):605–622. DOI: 10.1007/s10596–008–9100–3.

LIST OF PUBLICATIONS

Journal Publications

1. **Kahrobaei, S.**, Mansoori, M., Joosten, G.J.P, Van den Hof, P.M.J. and Jansen, J.D. (2015), *Identifiability of Location and Magnitude of Flow Barriers in Slightly Compressible Flow*. Accepted for publication in *SPE Journal*.

2. Van Essen, G.M., **Kahrobaei, S.**, van Oeveren, H., Van den Hof, P.M.J. and Jansen, J.D. (2016), *Determination of Lower and Upper Bounds of Predicted Production from History-Matched Models*. Accepted for publication in *Computational Geosciences*.

3. Fonseca, R.M., **Kahrobaei, S.**, Gastel, L.J.T., Leeuwenburgh, O. and Jansen, J.D. (2015), *Quantification of the Impact of Ensemble Size on the Quality of an Ensemble Gradient Using Principles of Hypothesis Testing*. Under review at *SPE Journal*. .

4. Jansen, J.D., Fonseca, R.M., **Kahrobaei, S.**, Siraj, M., Van Essen, G.M. and Van den Hof, P.M.J. (2013), *The Egg Model- A Geological Ensemble for Reservoir Simulation. Geoscience Data Journal*.

5. **Kahrobaei, S.**, Farajzadeh, R., Suicmez, V.S. and Bruining, J. (2012), *Gravity-Enhanced Transfer Between Fracture and Matrix in Solvent-Based Enhanced Oil Recovery. Ind. Eng. Chem. Res.*

Conference Proceedings

1. **Kahrobaei, S.**, Mansoori, M., Joosten, G.J.P, Van den Hof, P.M.J. and Jansen, J.D. (2015), *Identifiability of Location and Magnitude of Flow Barriers in Slightly Compressible Flow*, Proc. SPE Reservoir Simulation Symposium, Houston, Texas, USA.

2. Fonseca, R.M., **Kahrobaei, S.**, Gastel, L.J.T., Leeuwenburgh, O. and Jansen, J.D. (2015), *Quantification of the Impact of Ensemble Size on the Quality of an Ensemble Gradient Using Principles of Hypothesis Testing*, Proc. SPE Reservoir Simulation Symposium, Houston, Texas, USA.

3. **Kahrobaei, S.**, Mansoori, M., Joosten, G.J.P, Van den Hof, P.M.J. and Jansen, J.D. (2014), *Hidden Information in Ill-Posed Inverse Problems*, Proc. ECMOR XIV, Catania, Italy.

4. **Kahrobaei, S.**, Van Essen, G.M., Van Doren, J.F.M., Van den Hof, P.M.J., Jansen, J.D. (2013), *Adjoint-Based History Matching of Structural Models Using Production and Time-Lapse Seismic Data*, Proc. SPE Reservoir Simulation Symposium, The Woodlands, Texas, USA.

5. **Kahrobaei, S.**, Farajzadeh, R., Suicmez, V.S. and Bruining, J. (2012), *Gravity-Enhanced Transfer Between Fracture and Matrix in Solvent-Based Enhanced Oil Recovery*, Proc. SPE Improved Oil Recovery Symposium, Tulsa, Oklahoma, USA.

SUMMARY

Subsurface reservoir models, which are used to simulate and predict the fluid flow through the porous media below the earth surface, are associated with uncertainties. These uncertainties in the reservoir models, which result from limited knowledge about the reservoir and also from interpretation errors, may lead to responses which are often inaccurate or not comparable to the responses obtained from the real reservoir. This discrepancy can significantly affect long-term predictions and decisions. Therefore it is essential to constantly improve and correct the reservoir models by integration of dynamic responses from the real reservoir field. The objective of this process, which is called history matching, is to employ measurements to improve knowledge about the model properties so as to enhance the predictability of a model to accurately forecast the production response of a real reservoir. Due to a large number of uncertain parameters and limited available data, history matching problems are ill-posed, which results in many possible combinations of reservoir parameters. A most common way to restore well-posedness in history matching problems is to regularize the problem by adding an extra term to the objective function, which penalizes deviation from a prior model. This regularization term constrains the parameters values to values not too far from the prior model. In an under-modeling situation, where some unexpected features are not captured in the prior reservoir model due to interpretation errors of geological data, such a penalty term is undesirable since the updated parameters are constrained by an incorrect prior knowledge. In such scenarios integration of dynamic data of a reservoir system without any regularization can be more insightful. Unregularized integration of dynamic data may result in unrealistic parameter updates, but these unrealistic parameters may compensate for a flow-relevant feature that is not modeled. Therefore, it can serve as a tool to indicate the geological interpretation errors. In this thesis the relevant information in the dynamic response of a reservoir system and the possibility to identify unexpected flow-relevant features that have not been modeled are investigated.

Chapter 2 employs a hierarchical optimization procedure, proposed by Van Essen et al. (2010), to show the ill-posed nature of history-matched models by determining lower and upper bounds of the predicted production. This chapter illustrates through a detailed set of numerical experiments the impact of ill-posedness inherently present in history matching problems, which can result in reservoir models that equally match the historical data but provide different forecasts. Additionally, chapter 2 investigates how this method can be used to indicate the added value of alternative data sources such as time-lapse seismic.

Chapter 3 provides a numerical experimental analysis which aims to investigate the information content in unregularized ill-posed inverse problems. Different flow-relevant features are considered in different locations under different noise conditions to inves-

tigate their influence on the dynamic of a reservoir system. This chapter shows that integration of dynamic data without any constraint may be helpful to detect some flow-relevant features that are not captured in the prior model. Chapter 3 also provides a quantitative identifiability analysis to further analyse the numerical findings. Moreover, different alternative formulations rather than penalizing deviations from a prior model are used to restore well-posedness and to capture the missing features. Chapter 3 illustrates that the discrete cosine transform reparameterization and total variation regularization are able to retrieve missing features in the reservoir models.

Chapter 4 explores the conditions under which a flow barrier can be determined from the dynamic response of a reservoir system. Both numerical and analytical techniques are employed to address this question. Chapter 4 develops an analytical method based on a transfer function formalism of a series of bilaterally coupled porous media models. This has been done by using the Laplace transforms of the diffusivity equation and Darcy's law and therefore the analytical input/output relations of the system are derived through sets of transfer functions. The frequency response of the system makes it possible to investigate the effect of the barrier location and the barrier permeability on the system output. Chapter 4 also provides a structural identifiability analysis, which makes it possible to investigate whether or not we can distinguish a change in any of the parameters at all without considering a specific input-output configuration.

Chapter 5 considers another source of unfavorable history matching results, which is addressing a wrong uncertainty in the parameter estimation process. Chapter 5 provides an approach in which parameter updates are performed in the static model rather than the dynamic model in an integrated reservoir modeling workflow. In this chapter historical dynamic data of a reservoir is employed to update structural parameters of the reservoir. Moreover, chapter 5 investigates the effect of different data types on the quality of structural parameter updating.

The results from this thesis provide a quantitative analysis along with a new transfer function-based analytical formulation to assess the impact of unregularized history matching of realistic reservoir models for different data types and geological attributes.

SAMENVATTING

Modellen van ondergrondse reservoirs die gebruikt worden om vloeistofstroming in poreuze media te simuleren en voorspellen worden geassocieerd met onzekerheden. Deze onzekerheden worden veroorzaakt door een beperkte kennis over het reservoir en fouten in de interpretatie daarvan, waardoor het stromingsgedrag vaak inaccuraat is of niet met de daadwerkelijk gemeten stroming overeenkomt. Deze discrepantie kan op de lange termijn een grote invloed hebben op voorspellingen en beslissingen. Het is daarom essentieel om reservoirmodellen constant te verbeteren en te corrigeren door de dynamische respons van het daadwerkelijke reservoir erin te integreren. Het doel van dit proces, de zogenaamde 'history matching', is om de meetgegevens te gebruiken teneinde de kennis van gemodelleerde eigenschappen te verbeteren waardoor het model de vloeistofstroming in het reservoir preciezer kan voorspellen. Door het grote aantal onzekere parameters en beperkte meetgegevens zijn problemen met history matching slecht gedefinieerd, waardoor oplossingen bestaan uit meerdere mogelijke combinaties van reservoirparameters. De gebruikelijke manier om dit soort problemen beter te definiëren is door een extra term aan de doelfunctie toe te voegen waarmee het afwijken van een voorgaand model tegengegaan wordt. Deze zogenaamde regularisatieterm beperkt de parameters tot waarden die niet teveel afwijken van het eerdere model. Bij situaties waarin het model een oversimplificatie van de werkelijkheid is en onverwachte geologische reservoireigenschappen niet of verkeerd gemodelleerd worden is een regularisatieterm onwenselijk omdat hij parameters beperkt tot waarden die uit incorrecte voorgaande kennis voortvloeien. In zulke gevallen kan integratie van dynamische reservoirmetingen zonder regulatieterm tot betere inzichten leiden. Deze ongeregulariseerde integratie van dynamische metingen kan resulteren in onrealistische aanpassingen van de parameters, maar die kunnen ook gegenereerd worden om een niet-gemodelleerde eigenschap die relevant is voor vloeistofstroming te compenseren. Het kan daarom gebruikt worden als een manier om de fouten in de geologische interpretatie op te merken. Dit proefschrift behandelt de achtergrond van de dynamische productierespons van een reservoirsysteem en de mogelijkheid om de onverwachte en niet-gemodelleerde eigenschappen die relevant zijn voor vloeistofstroming te identificeren.

Hoofdstuk 2 gebruikt een hiërarchische optimalisatiemethode, zoals ontwikkeld door Van Essen et al. (2010), om het slecht gedefinieerde karakter van history matching modellen aan te tonen. Het hoofdstuk illustreert middels een aantal numerieke experimenten hoe dit kan resulteren in verschillende reservoirmodellen die even goed voldoen aan de historische reservoirgegevens. Verder onderzoekt het hoofdstuk hoe deze methode gebruikt kan worden om de toegevoegde waarde van alternatieve gegevensbronnen zoals timelapse seismiek aan te tonen.

Hoofdstuk 3 behandelt een numeriek-experimentele analyse die de verborgen informa-

tie in ongeregulariseerde en slecht gedefinieerde inverse problemen onderzoekt. Verschillende eigenschappen die relevant zijn voor vloeistofstroming worden in overweging genomen op uiteenlopende locaties en met verschillende ruiscondities om hun invloed op het dynamische gedrag van een reservoirsysteem te onderzoeken. Dit hoofdstuk toont aan dat onbeperkte integratie van dynamische gegevens kan helpen bij het detecteren van eigenschappen die relevant zijn voor vloeistofstroming, maar die niet voorkomen in eerdere modellen. Het hoofdstuk geeft ook een kwantitatieve identificeerbaarheidsanalyse om de uitkomsten van de numerieke experimenten verder te analyseren. Verder worden alternatieve formuleringen voor het beter definiëren van reservoirmodellen en het meenemen van ontbrekende eigenschappen gebruikt. Dit hoofdstuk laat zien dat herparametrisatie van de discrete cosinustransformatie en regularisatie van de totale variatie de ontbrekende eigenschappen in een reservoirmodel kunnen herstellen.

Hoofdstuk 4 verkent de omstandigheden waaronder een stromingsbarrière kan worden herleid uit de dynamische respons van een reservoirsysteem. Zowel numerieke als analytische technieken worden ingezet om deze vraag te beantwoorden. Het hoofdstuk ontwikkelt een analytische methode gebaseerd op transferfunctieformalisme van een serie bilateraal-gekoppelde modellen van poreuze media. Dit is gedaan met een Laplacetransformatie van de diffusiviteitsvergelijking en de Wet van Darcy, waardoor de analytische invoer/uitvoer-relaties van het systeem afgeleid worden middels reeksen van transferfuncties. De frequentierespons van het systeem maakt het mogelijk het effect van de locatie en permeabiliteit van de stromingsbarrière op de systeemuitvoer te onderzoeken. Het hoofdstuk geeft ook een structurele identificeerbaarheidsanalyse die het mogelijk maakt om te onderzoeken of er een verandering in het systeem te onderscheiden is zonder een specifieke invoer/uitvoer configuratie in acht te nemen.

Hoofdstuk 5 behandelt een andere bron van onwenselijke history matching resultaten die een verkeerde onzekerheid in het parameterinschattingsproces in ogenschouw neemt. Het hoofdstuk stelt een geïntegreerde werkwijze voor waarin parameteraanpassingen worden uitgevoerd in het statische- in plaats van in het dynamische reservoirmodel. In dit hoofdstuk worden de historische dynamische gegevens van een reservoir gebruikt om structurele parameters van het reservoir aan te passen. Verder onderzoekt dit hoofdstuk de invloed van verschillende gegevenstypen op de kwaliteit van deze aanpassing.

ACKNOWLEDGEMENTS

First and foremost I would like to offer my sincerest gratitude to my supervisor Professor Jan Dirk Jansen who has earnestly supported me throughout my PhD. Jan Dirk, I really appreciate your guidance during the past four years. I would also like to thank you for helping me to be more professional and to develop my critical thinking.

I would like to thank Professor Paul Van den Hof for his valuable guidance and encouragement during my PhD. Paul, many thanks for helping me to learn how to formulate the problems in a structured way and also how to think out of the box.

I am also deeply indebted to Dr. Mehdi Mansoori for the brilliant discussions and comments and also for helping me to learn systems and control concepts.

My special thanks to the people at Shell: Paul Gelderblom who gave me the opportunity to work in the Shell's office. I also would like to thank Gerard Joosten for his invaluable and generous supports also his precious comments and guidance during the past four years. Gerard, many thanks for all the encouragements and motivations as well as the brilliant and constructive discussions that we had. A big thank you to Gijs van Essen, Jorn Van Doren and Gosia Kaleta for helping me to initiate my work and their valuable comments. One simply could not wish for a better environment or friendlier supervisors and colleagues.

A special thank you to the administrative side of the Geosciences and Engineering department, Anke, Marlijn, Lydia, Margot, Ralf and Hannie for their compassionate supports.

I want to truly appreciate all my friends and colleagues at the petroleum engineering department. Rahul, for his wise advices, encouragements and also endless supports. Rahul! You were not only a friend to me, you were my real twin brother! Roozbeh, for listening to my endless naggings about everything and being always available whenever I felt alone! Jakolien and Koen, for all helps and translations in this thesis. Ehsan, for all scientific and philosophical discussions. Eduardo, for all encouragements and also his innovative thoughts for designing the cover of my thesis. Durgesh, Rafael, Anna, Nikita, Christian, Chris, Negar, Jiakun, Daniel, Amin, Maryam, Matei, Amin Fatemi, Mojtaba, Matei, Matteo, Jinyu, Bander, Rodrigo, Ahmed, Mohammad and Kevin for making our working environment as a unique place.

My grateful thanks to my old friends, Jamshid and Azin, for their compassionate helps in designing my thesis cover.

I also would like to thank Nina, who always tried to keep me motivated in different and unique ways. Nina, I never forget your patience, your magnificent smile, your passion and your optimistic attitude in this period of my life and also your two-days intercontinental travels for making me happy.

Last but not least, I shall express my deepest gratitude to my parents without whose unconditional, selfless and perpetual supports I would not be even close to where I am now.

ABOUT THE AUTHOR

Siavash Kahrobaei was born on September 2, 1985 in Tehran, Iran. He received his Bachelor degree in Mining Engineering with a specialization in Rock Mechanics from University of Tehran. Hereafter he moved to the Netherlands to pursue a Masters in Applied Earth Sciences with a specialization in Petroleum Engineering at Delft University of Technology, from which he graduated, *cum laude*. Upon graduation he continued his academic education in Reservoir Systems and Control group at the department of Geoscience & Engineering of Delft University of Technology, as a PhD. During the PhD project he did several internships at Shell Global Solutions International. In September 2015, he started a post-doctoral research, sponsored by Shell Global Solutions International, in the area of Enhanced Oil Recovery at Delft University of Technology.